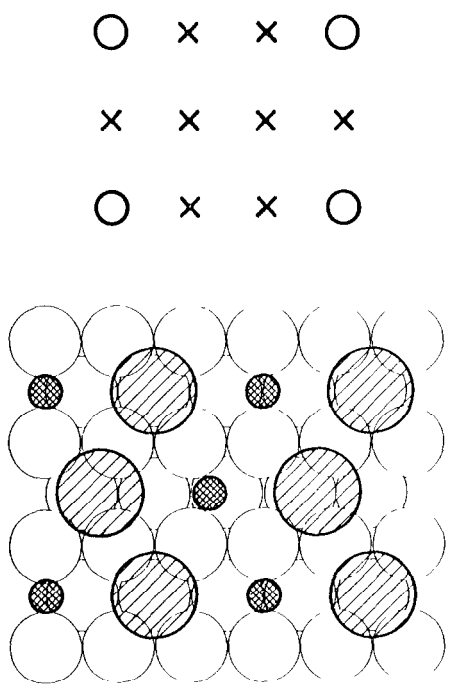

Fig 57. LEED pattern (top) and structural model (bottom) for water (~ 1 L exposure) and bromide ($\theta_{Br} = 0.15$) coadsorbed on Cu(110) In the top frame, the open circles represent substrate-related spots and the ×'s show the adsorbate-induced spots In the bottom panel, the open circles are the Cu atoms, the small shaded circles are the water molecules, and the large shaded circles are the adsorbed bromine atoms From Sass et al. [231]

removal of ideally polarizable electrodes from solution under potential control in what has been defined as a dry or hydrophobic state, i.e., without a liquid film or droplets on the surface. The results have been interpreted to indicate that such electrodes retain their compact double layer (perhaps, a water bilayer) intact after the emersion operation, allowing the use of spectroscopic techniques to characterize the interface without the bulk electrolyte present. The most detailed measurements involve the surface concentrations of Cs^+ and Br^- on gold electrodes, derived from ESCA signals for emersed gold electrodes as a function of emersion potential, from a 0.02M CsBr solution. In light of the foregoing discussion, it is extremely unlikely that the H_2O double layer would survive intact following emersion and transfer *to UHV* at ~ 300 K. As we have seen, for H_2O + Br on Ag and Cu surfaces, H_2O desorption is *complete* at ~ 250 K. *In the presence of H_2O vapor* at 300 K, the double layer *might* exist on a Br or Cs doped Au electrode as a result of dynamic adsorption–desorption processes, and work function measurements indicate

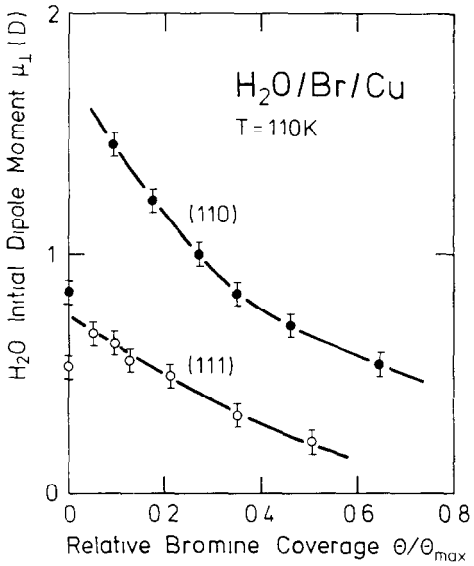

Fig 58 Perpendicular component, $\mu_{\perp}$, of the initial dipole moment of H_2O adsorbed on Cu(110) and Cu(111) as a function of bromine coverage Taken from Sass et al. [121]

that this is the case [239]; but in ultrahigh vacuum, the double layer would almost certainly desorb before spectroscopic characterization could be achieved. Indeed, Neff and Kötz have used UPS to show that no water is retained on an emersed Au electrode at room temperature in UHV [240].

Recently, Wagner and Moylan have described an important study of the interaction between hydrogen fluoride and water on Pt(111) [116]. This has provided the most complete picture to date of the chemical interactions which may actually occur at an electrode surface in situ, based on work done in UHV. We must defer discussion of the hydronium (H_3O^+) ion which is identified in that work until section 6.2.3; here we note that anhydrous HF *does not* dissociate, but in the presence of water, HF *does* dissociate [116]. The stoichiometries of the fully-hydrated phases indicate that each pair of fluorine and hydronium ions in the chemisorbed layer is hydrated by *five* water molecules, whereas in the multilayer they are each linked to *eight* water molecules [116]. There is no evidence for dissociation of H_2O. Although the results of Wagner and Moylan are somewhat reminiscent of the data just described for hydration of Br on Cu and Ag [120,136,231], they are different in that the range of coverages of coadsorbed molecules is greatly extended. This allows Wagner and Moylan to conclude that "even such classically 'non-specifically' adsorbed ions such as H^+ and F^- interact sufficiently strongly with Pt surfaces to displace some water from their inner solvation shells", i.e.

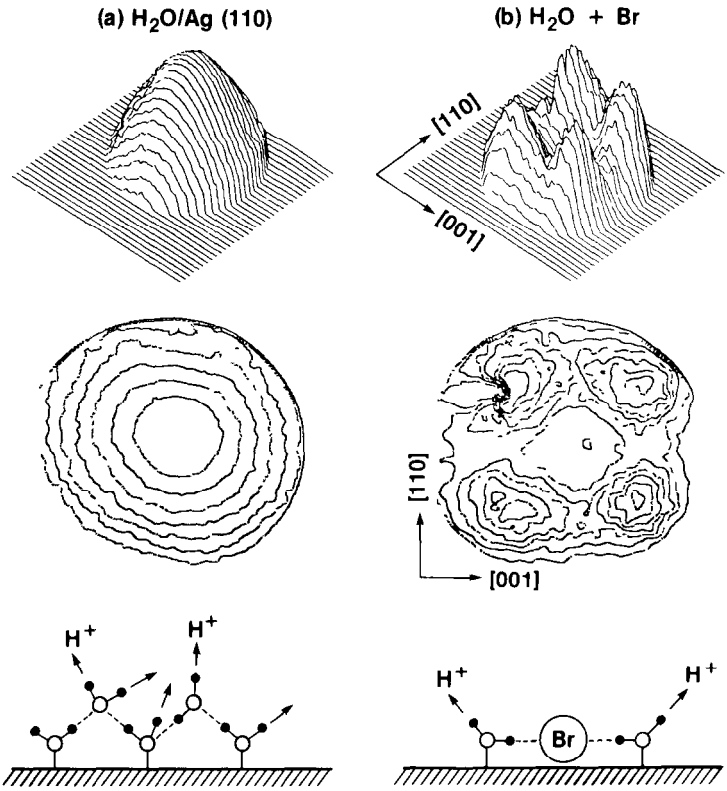

Fig 59. H^+ ESDIAD patterns and schematic models illustrating the effect of Br on the local structure of H_2O on the Ag(110) surface The top row contains perspective plots of the H^+ ion desorption intensity displayed on a fluorescent screen The second row contains contour plots of the same measurements The third row contains schematic models. Column (a) H^+ ESDIAD and model for H_2O on clean Ag(110). Column (b) H^+ ESDIAD and model for H_2O + Br on Ag(110). $\theta_{Br} < 0.2$ monolayers Taken from Bange et al [136] and Madey [181]

they have been able to distinguish between hydration of the H^+ and F^- ion *at* the metal surface and hydration of the ions in the solvent-like multilayer [116].

Evidence for the strongest interactions between H_2O and electronegative additives involves H_2O + oxygen on metals (i.e., the desorption temperature/binding energy of molecular H_2O appears highest in the presence of oxygen). The most well-documented example is H_2O + O/Ru(001). The EELS data of Thiel et al. [241] show clearly that adsorption and desorption of H_2O in the presence of varying oxygen predoses on Ru(001) proceeds *without* H_2O dissociation. Under all conditions, the scissors mode at ~ 1600 cm^{-1} accompanies an OH stretch at ~ 3500 cm^{-1}, so that the adsorbed species are dominated by molecular H_2O; see fig. 60 [241]. The appearance of a strong

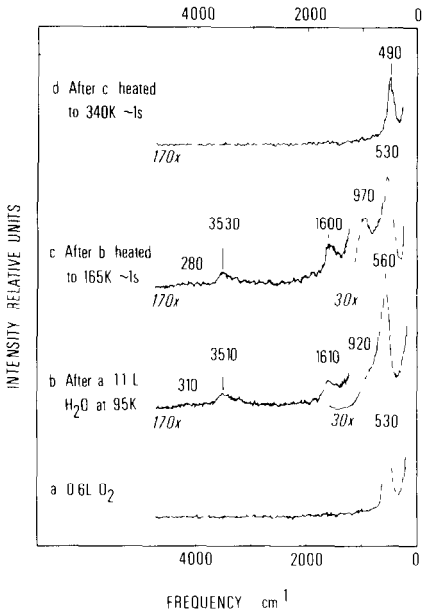

Fig. 60 Coadsorption of water and oxygen on Ru(001) at 95 K, followed by sequential heating as indicated The peak positions and halfwidths are noted in inverse centimeters From Thiel et al [241]

peak at 970 cm^{-1} (H_2O libration) corresponding to an annealed (165 K) $H_2O + O$ layer is due to a thermally induced change in the intermolecular structure of the mixed H_2O–O adlayer. Doering and Madey suggest [79] that the 970 cm^{-1} EELS feature could be related to water–oxygen bonding configurations having preferred molecular H_2O orientations which can be generated under conditions similar to the EELS experiments, as shown in fig. 61 [79]. The TDS data of Doering and Madey [79] show that the presence of preadsorbed oxygen causes an increase in the binding energy (increased T_p) of adsorbed H_2O on Ru(001), but that desorption is essentially complete by ~ 260 K. The unique long-range order and local bonding geometries in H_2O on *clean* Ru(001) are discussed extensively in section 3.4. The main influence of oxygen is to *destroy* both long-range order and preferred molecular orientation upon adsorption at $T < 150$ K. Apparently, the H_2O–O interaction is strong enough to overcome the ordering introduced by the H_2O–H_2O hydrogen bonds; the H_2O is pulled away from the ideal lattice sites by oxygen and the surface layer disorders. (The only exception, as indicated above, occurs when a mixed $H_2O + O$ layer with a particular stoichiometry is heated, which results in a layer with short-range order.)

Further evidence that oxygen influences the H_2O clustering process (i.e.,

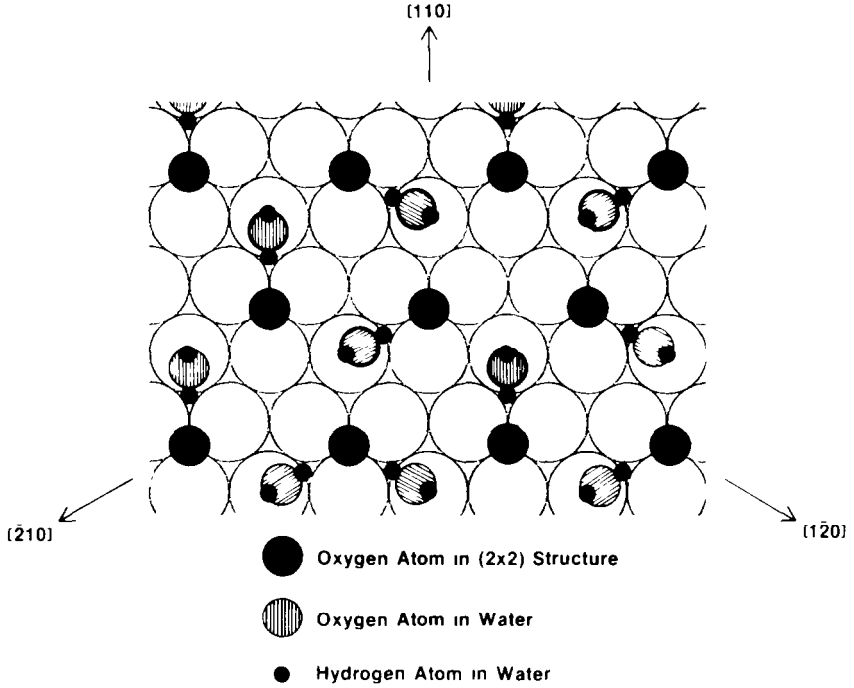

Fig 61. A model for isolated water molecules on Ru(001) with a saturated (2×2) oxygen coverage ($\theta_O = 0.25$) after heating to 190 K which would produce a hexagonal ESDIAD pattern rotated 30° relative to that from a clean surface Taken from Doering and Madey [79]

delays the formation of H_2O–H_2O hydrogen bonds) is reported by Kretzschmar et al. [170]. Using infrared reflection-absorption spectroscopy, they find that H_2O forms hydrogen bonds immediately on the clean Ru(001) surface, but that the presence of preadsorbed oxygen delays this process: the first H_2O molecules on the surface interact strongly with isolated O atoms. Only at higher H_2O coverage, when O atoms are fully "saturated" by surrounding H_2O, do IR bands appear in the region expected for ν(OH). In an interesting vibrational-dynamics sidelight to the above experiments, Thiel et al. [241] compare their EEL measurements with the IR data [170]: they report that the surface dipolar selection rule applies in an infrared but not in an electron energy-loss measurement.

Water adsorption has also been examined on an oxygen-predosed Re(001) surface. Preadsorption of oxygen *prevents* the H_2O decomposition which is observed on clean Re(001) at $T > 180$ K. Fig. 62 [141] illustrates the role of oxygen in blocking H_2O decomposition: The TDS yield of H_2 from H_2O decomposition *decreases* with increasing oxygen coverage, θ_O, while the yield of molecular water *increases* with increasing θ_O. As for H_2O on other additive dosed surfaces, desorption is essentially complete at ~ 250 K. The *deactivat-*

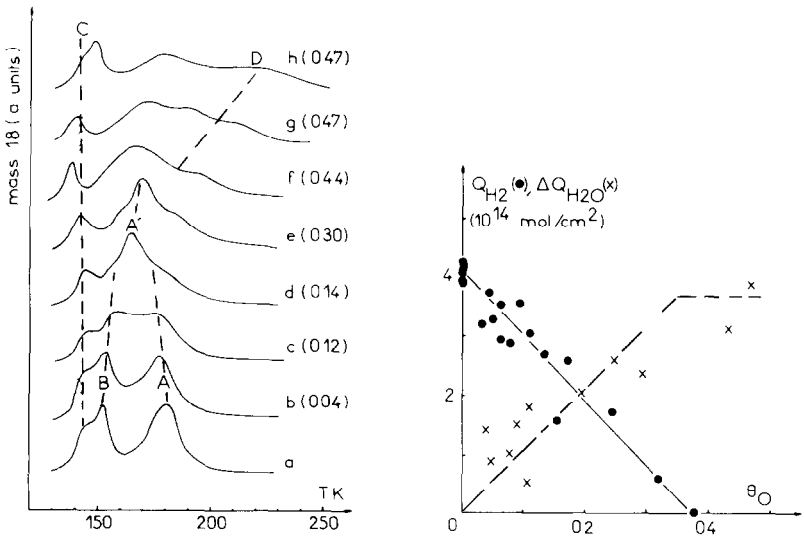

Fig 62 Left Desorption of water from oxygen-predosed Re(001) following exposure to 1 8 L of water Values of the oxygen precoverage (in monolayers) are indicated in brackets Right Variation of the amounts of hydrogen (●) and water (×) desorbed from Re(001) as a function of the initial oxygen precoverage The constant exposure of water is 1 8 L. Taken from Jupille et al [141]

ing effect of oxygen on otherwise active metals which form stable oxides has been noted by Barteau and Madix [75] for various surface oxidation reactions, and is discussed more extensively in section 6.2.2. The deactivating effect appears to correlate with the tendency of the metal to form a stable bulk oxide.

The interaction of water with surfaces of bulk metal oxides appears to be *fundamentally different* from the interaction of water with oxygen-doped surfaces of bulk metals. Therefore, the water–oxide surface chemistry is treated separately in section 7.1, but we note here that Blyholder and Sheets [242] find evidence for stabilization of molecular H_2O at 300 K on a highly oxidized Ni or V surface. Exposure of the clean films to 10 Torr of H_2O for 30 min at 300 K followed by evacuation to 10^{-6} Torr produces no H_2O adsorption as evidenced by the absence of infrared scissor modes. Exposure of films with preadsorbed BF_3 to H_2O vapor, however, causes a surface reaction which leaves the surfaces oxidized. The oxidized films retain undissociated H_2O, as shown by the presence of the scissors mode at 1630 cm^{-1}, which is not removed by extensive evacuation at 10^{-6} Torr. We suggest that this is an extreme case of a modified surface, and that bonding of the H_2O occurs via coordination with surface (or subsurface) cation sites pronounced by surface

reaction and oxidation. This experiment is noteworthy in that it clearly shows that adsorbed molecular H_2O can be retained on reactively-oxidized surfaces, although the exact composition [Ni, O, F(?), $\cdots$] of the adsorption sites, and the role of surface roughness in "trapping" H_2O, is not clear. It is of interest that H_2O exposure to an oxidized Ni(110) single crystal does not result in H_2O adsorbed at 300 K [162], as discussed in section 7.1.7, nor is a clean Ni surface found to adsorb H_2O at $T \gtrsim 250$ K [82,83,111,162]. Adsorption of H_2O on oxide surfaces is considered in section 7.1.

6.2.2. Electronegative additives: influence of oxygen on dissociation of H_2O

Although H_2O is adsorbed in molecular form on clean surfaces of metals such as Ag, Cu, Ni, Pt, and Pd, coadsorption of H_2O with fractional monolayers of oxygen predosed onto these surfaces leads to dissociative adsorption and OH_a formation. The first instance of this is reported by Fisher and Sexton in a study of H_2O_a and O_a coadsorbed on Pt(111) [80]. This is in contrast to the oxygen-dosed surfaces of both Ru(001) [241] and Re(001) [141] where dissociation of H_2O is *not* promoted. It also contrasts with fully oxidized surfaces of Ni, on which H_2O dissociation is not observed [162]. Dissociation on the oxygen-dosed surfaces generally appears to proceed via a hydrogen abstraction reaction,

$$H_2O_a + O_a \rightarrow 2\ OH_a.$$

The experimental basis for the identification of OH_a is discussed in section 3.2. In the following paragraphs, we first discuss the kinetics of H_2O dissociation as well as H_2O desorption from oxygen-dosed surfaces. The influence of oxygen on the structure of adsorbed H_2O, and the bonding structure of OH_a are then explored. Finally, we speculate on the electronic and chemical factors which govern the different reactivity of $H_2O_a + O_a$ on various surfaces.

Kinetics of formation of OH_a. In all cases where OH_a forms from reaction between H_2O_a and O_a, it appears that the reaction is substantially complete at $T \lesssim 200$ to 250 K. In most cases, H_2O adsorbs in molecular form at ~ 80 K, and dissociates to form OH_a upon heating. We now describe several studies of the kinetics of OH_a formation. For $H_2O + O_a$ on Pt(111), Creighton and White [150,243,244] use static secondary ion mass spectroscopy (SSIMS) to follow the reaction of adsorbed water and oxygen. In the temperature range 130–142 K, they find an activation energy of $E_a = 42.6 \pm 3.4$ kJ/mol for the bimolecular reaction to form OH_a [244]. They also report that laser excitation of the OH stretching mode of adsorbed H_2O produces *no* detectable increase in the reaction rate. Carley et al. [111] use XPS to follow the reaction between H_2O_a and O_a on Ni(210), and report the formation of OH_a at temperatures above 150 K. Au et al. [125] find (using XPS) that hydroxide formation on Zn(001) is induced by pre-exposure of the surface to oxygen, in the temperature range 80–200 K. There are also reports that H_2O dissociates to form OH_a

directly at low temperatures (90 to 110 K) on certain oxygen-dosed Ag and Pd surfaces. Ceyer [133] reports that OH_a appears at 90 K on oxygen-predosed Ag(311), on the basis of EELS and ESDIAD data. The EELS data of Nyberg and Tengstål [81] indicate that some H_2O molecules react with preadsorbed O_a on Pd(100) upon adsorption at 110 K to form OH_a. [In contrast, Stuve et al. [129] propose that this reaction occurs only above 175 K on the same surface.]

A system which has been extensively studied in several laboratories using a variety of experimental techniques (EELS, XPS, UPS, TDS, LEED and ESDIAD) is $H_2O_a + O_a$ on Ag(110). We emphasize here those experiments relating to the kinetics of formation of OH_a; desorption kinetics and structural aspects of this system are treated elsewhere in section 6.2.2. Stuve et al. [132] use EELS to study the adsorption of H_2O at 100 K onto 0.1 monolayer of atomic oxygen on Ag(110) (prepared by dosing and annealing at 300 K). A series of EEL spectra taken at 100 K following annealing at temperatures up to 300 K reveal changes in the OH stretching region which are interpreted to indicate activated OH_a formation for temperatures above 205 K. In this temperature range, a sharp feature at 3610 cm^{-1} due to the non-hydrogen-bonded OH stretch in molecular H_2O *decreases* in intensity as a new feature at ~ 3380 cm due to free OH_a *grows* in intensity. Above 250 K, the spectra are dominated by OH_a; desorption is complete above 300 K. Surprisingly, the authors find no evidence of a molecular H_2O scissors mode at ~ 1600 cm^{-1} at any temperature above 190 K, perhaps because of low sensitivity in that spectral region. Au and coworkers [164] base the interpretation of their XPS results for $H_2O_a + O_a$ on Ag(110) on the EELS data of Stuve et al. [132] and suggest that a small O 1s peak with a binding energy of 532 eV seen at ~ 200 K is due to OH_a. In apparent contrast to these findings, Bowker et al. [134] report TDS isotopic mixing data which indicate that $H_2O_a + O_a$ react on Ag(110) to form OH_a at temperatures as low as 160 K; Stuve et al. [132] interpret these results in terms of a solvation mechanism in which OH_a is a short-lived intermediate. More recent ESDIAD studies of Bange et al. [185] indicate that OH_a forms at temperatures as low as 80 K, and forms ordered arrays upon heating to ~ 200 K. Barteau and Madix [135] use UPS (He I and He II) to demonstrate that H_2O reacts stoichiometrically with O_a above 250 K to form a pure layer of adsorbed OH_a on Ag(110); the OH_a features are broad and weak.

In summary, the combined data for O_a/Ag(110) suggest that adsorbed water is predominantly molecular at 80–100 K, but that some dissociation to form OH_a occurs in this temperature range. Upon heating above 200 K, dissociation to OH_a is complete, and the OH_a species tend to form long-range ordered arrays with molecular axes inclined along [001] azimuths.

A surface on which molecular water appears to be stabilized by O_a prior to dissociation is Ni(111) [82]. In this case, ESDIAD provides evidence for a remarkable local ordering of the H_2O_a at temperatures below the formation of

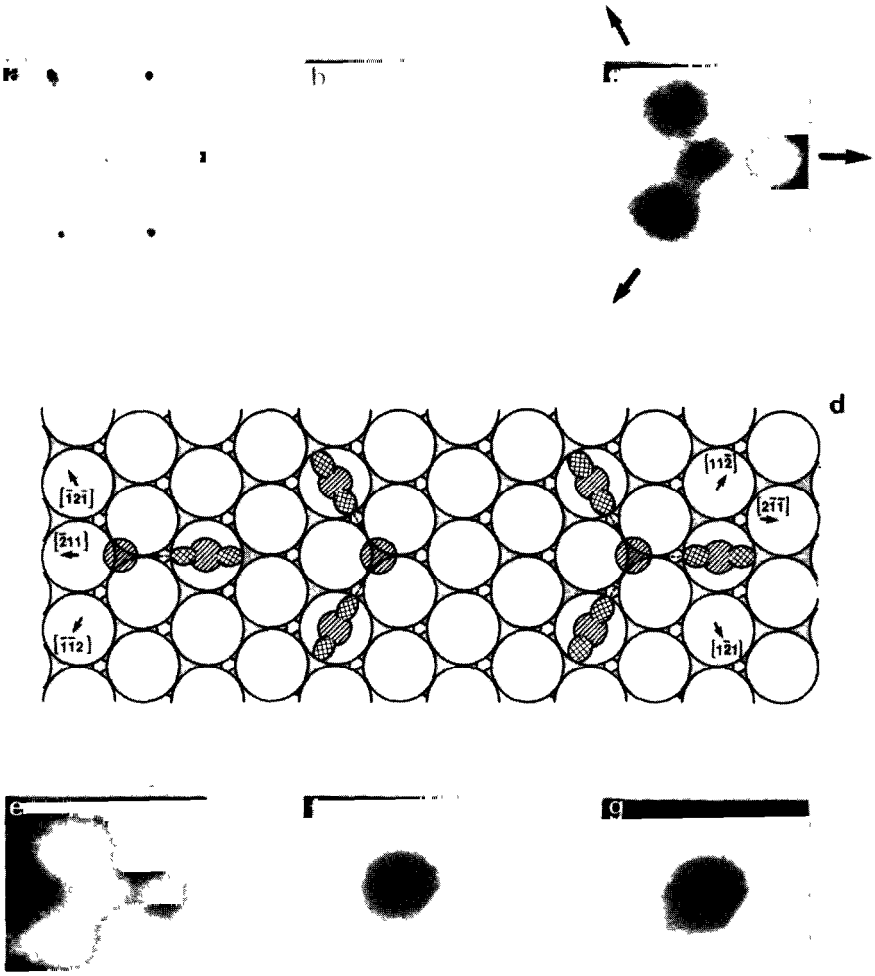

Fig 63. ESDIAD patterns and structural model for fractional monolayers of oxygen and water coadsorbed on Ni(111) Panel (a) also shows the LEED pattern of the clean metal surface Panel (b) shows the H^+ ESDIAD pattern of water on clean Ni(111), and panel (c) shows the H^+ ESDIAD pattern of water with oxygen coadsorbed. Panels (e–g) show the result of heating the surface, observed with ESDIAD The structural model in panel (d) is proposed for the three-fold pattern of (c) and (e). From Madey and Netzer [82].

OH_a. Fig. 63 contains LEED and ESDIAD patterns for the adsorption of H_2O on clean and oxygen-predosed Ni(111). Panel (a) contains a LEED pattern from the clean surface, and panel (b) is an H^+ ESDIAD pattern

characteristic of adsorbed H_2O on *clean* Ni(111) at 80 K, for fractional-monolayer coverages. The center of the pattern is dim, with most of the ion emission directed away from the surface normal. This is consistent with H^+ emission from hydrogen-bonded H_2O clusters on Ni(111) which have no preferred azimuthal OH bond orientation.

In contrast to adsorption on the clean surface, the adsorption of low doses of H_2O ($\theta_{H_2O} \lesssim 0.2$ monolayers) at 80 K onto the oxygen predosed and annealed Ni(111) surface produces a highly ordered and intense three-fold symmetric ESDIAD pattern [fig. 63, panel (c)] with intense ion emission along [112] azimuths. The O atoms on the annealed surface are adsorbed in equivalent three-fold hollow sites, and the three-fold ESDIAD pattern appears to be a consequence of different degenerate molecular configurations on the three-fold substrate. A model is shown in fig. 63d. If the O atoms are located in three-fold hollows above second-layer atoms, H_2O can be bonded in sites atop the Ni atoms, and can interact with oxygen, perhaps via a hydrogen bond. The surface O–O distance for O–H_2O is 2.87 Å, which falls within the range seen for the O–O distance in various forms of hydrogen bonded ice [27]. The H_2O molecules may "incline" toward the O atoms, so that only the non-hydrogen-bonded hydrogen atom is seen in ESDIAD; hence the three-fold pattern is observed due to three different configurations.

Upon heating the surface with the sharp three-fold ESDIAD pattern, the sequence of patterns shown in figs. 63e–63g is observed. At 120 K, a temperature well below the onset of desorption, the three outer lobes of the ESDIAD patterns nearly disappear (f) and only intense normal emission remains at 150 K (g). It is suggested [82] that hydrogen abstraction leads to rapid OH_a formation above ~ 120 K, and that the broad, normal H^+ beam (f, g) indicates that the Ni–O–H group is linear, with large amplitude bending modes, or slightly bent.

Note also that the model of fig. 63d for Ni(111) shows single O atoms hydrated by multiple H_2O molecules, consistent with both TDS and ESDIAD data. Evidence of O_a influencing the bonding of multiple H_2O molecules (i.e., hydration of O_a) is reported for many other systems also [132,134,170]. In the low-coverage limit, Bange et al. [118] report that 6 to 8 water molecules, on average, are bound to each adsorbed O atom on Cu(110).

Finally, we note that two studies [245,246] have recently used EELS to identify adsorbed hydroxyl, OH_a, as a stable intermediate in the reaction of adsorbed atomic oxygen and hydrogen to form water. Fisher and DiMaggio identify OH_a formed in this reaction on Rh(100) [245], and they report that its vibrational spectrum and thermal decomposition behavior are identical to OH_a formed by the reaction of adsorbed water with oxygen. This adsorbed hydroxyl can be formed only when the oxygen coverage exceeds 0.05 monolayers. At lower oxygen coverages, the adsorbed hydrogen and oxygen react directly to form water, with no observable OH_a intermediate [245]. The

"direct" reaction which takes place at $\theta_O \lesssim 0.05$ monolayers,

$$2\,H_a + O_a \rightarrow H_2O_g.$$

results in water desorption at 325 K [245]. The hydroxyl species formed at higher oxygen coverages react to form gas-phase water via disproportionation at about 275 K [245]. Assuming that the rate of water desorption in each reaction is limited only by its rate of formation on the surface, these data indicate that the disproportionation reaction occurs more readily (i.e. at lower temperatures) than the "direct" reaction. Fisher and DiMaggio [245] point out that the oxygen coverage at which hydroxyl formation begins is also the coverage at which oxygen island formation begins, about 0.05 monolayers. They suggest that hydroxyl formation may require coupled chains of hydroxyls. They further suggest that the reaction occurs preferentially at perimeters of oxygen islands. These two factors, taken together, could account for the fact that the amount of water formed reaches a sharp maximum at low oxygen coverages, in this and other systems.

Mitchell and White [246] identify OH_a formed in the water formation reaction on Pt(111). They report that reaction proceeds via sequential addition of hydrogen to oxygen (not disproportionation of an intermediate OH_a), and that the vibrational spectrum of the hydroxyl species formed by reaction of hydrogen and oxygen differs greatly from that of the hydroxyl formed by reaction of water with oxygen. These conclusions differ from those reached by Fisher and DiMaggio in their study of Rh(100) [245]. It may be that the water formation reaction is sensitive to electronic differences between different metals, and/or to differences in substrate geometry (types of available adsorption sites). Mitchell and White [246] also report that adsorbed water produced from reaction between hydrogen and oxygen has a vibrational spectrum much different than that of water adsorbed from the gas phase, which, they propose, is due to a lack of hydrogen bonding between water molecules formed in the reaction [246].

Kinetics of H_2O desorption from oxygen-dosed surfaces. The preceding paragraphs are concerned with the kinetics of formation of OH_a on oxygen-dosed surfaces determined using in situ surface sensitive methods. In this section we focus on the kinetics of desorption of H_2O from oxygen-dosed surfaces. We relate binding states seen in thermal desorption spectroscopy (TDS) to particular bonding modes of H_2O on these surfaces. The appearance of H_2O as a thermal desorption product does not necessarily imply that H_2O is present on the surface: recombination of OH_a also leads to desorption of molecular H_2O.

Thermal desorption studies of $H_2O + O_a$ on a variety of surfaces reveal rather similar results. For that class of metals on which H_2O adsorption is molecular (cf. section 3.1 and fig. 24) molecular H_2O desorbs completely below ~ 200 K in most cases. However, when H_2O is adsorbed on oxygen-dosed surfaces of metals such as Ag, Cu, Ni, or Pd, the TDS spectra exhibit a

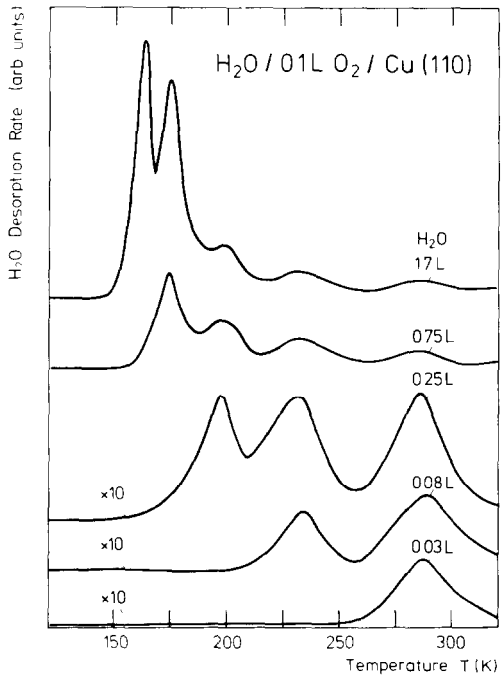

Fig 64 Thermal desorption spectra for different water coverages on Cu(110) after an oxygen exposure of 0.1 L. The two peaks at ~165 K and 175 K represent desorption from the multilayer state and the clean regions of the (110) surface, respectively Compared to the clean surface there are three additional oxygen-induced peaks at $T \geqslant 200$ K which are filled sequentially with increasing exposure Heating rate = 10 K/s Taken from Bange et al [118]

series of peaks for which the highest peak temperature ranges typically from ~ 240 to 360 K. Thus, the binding energies of H_2O on these O-dosed surfaces are dramatically increased over the clean surface values, and H_2O is retained to much higher temperatures. A surprising generalization, moreover, is that molecular H_2O is not retained under ultrahigh vacuum conditions at 300 K or above on any of the O-dosed surfaces studied to date (cf. table 12). Whenever a TDS H_2O peak is seen at ~ 250 K or above, it is due to recombination of adsorbed OH_a.

A good example of the influence of O_a on the surface chemistry of H_2O is given by the work of Bange et al. on Cu(110) [118]. The TDS data demonstrate that the adsorption behavior is very sensitive to the coverage of preadsorbed oxygen. Fig. 64 shows a typical series of TDS spectra for increasing H_2O exposures and a fixed oxygen predose of 0.1 L ($\theta_O \simeq 0.045$ monolayers) at 110 K. Five peaks are sequentially filled as the water coverage is increased. In comparison with the TDS peaks from the clean Cu(110) surface (cf. table 9, p.

260, and ref. [118]) it appears that the peaks at 175 and 165 K are due to desorption from oxygen-free patches of clean Cu(110) and from multilayer H_2O, respectively. The three high temperature features (200, 235 and 290 K) are clearly oxygen-induced. Comparison with the temperature dependence of the UPS spectra for this system [118] suggests that the two peaks at intermediate temperatures (200 and 235 K) correspond to oxygen-stabilized, tightly bound molecular water. The peak at 290 K correlates with the disappearance of OH_a from the surface which is believed to desorb via the disproportionation reaction:

$$2\ OH_a \rightarrow H_2O_g + O_a.$$

These above TDS spectra resemble closely the data of Stuve et al. [132] for H_2O on oxygen-dosed Ag(110), where a similar interpretation of the oxygen induced features has been given.

The dependence of the TDS data on the amount of predosed oxygen on Cu(110) is discussed in ref. [118]. The five desorption peaks described above are seen only at low oxygen exposures, with the peak at 175 K disappearing above 0.25 L. This exposure corresponds to an oxygen coverage of approximately 1/8 monolayer. It appears, therefore, that the adsorption of H_2O on the oxygen-free surface, which is characterized by the 175 K desorption peak, is blocked for higher oxygen coverages. There is also a shift of the two oxygen-induced molecular adsorption states to higher temperature with oxygen exposure; above 0.3 L they merge into a single broad feature at $T \simeq 225$ K.

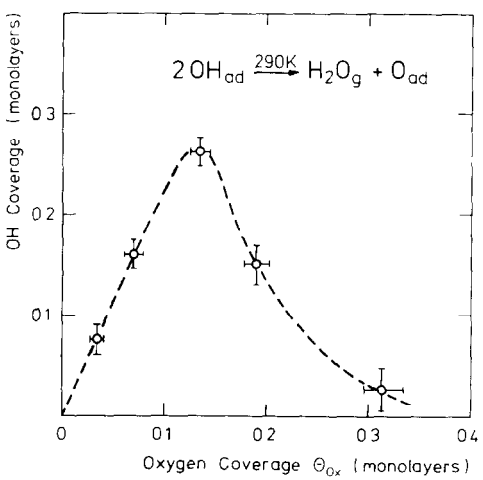

Fig. 65. Hydroxyl coverage as a function of initial oxygen coverage, θ_O, on Cu(110), determined from the integrated intensity of the thermal desorption peak at ~ 290 K (cf fig. 64) The maximum hydroxyl formation occurs for $\theta_O \simeq 1/8$ Taken from Bange et al [118].

The intensity of the peak at 290 K in fig 64 is identified with the concentration of OH_a, and its variation with oxygen coverage is shown in fig. 65. The maximum formation of hydroxyl species occurs at $\theta_O \simeq 1/8$. For higher oxygen coverages it decreases rapidly and at $\theta \approx 0.25$–0.30 it essentially disappears. The slope of the curve is 2 for $\theta_O \lesssim 0.1$, indicating that 2 OH_a species are formed by the reaction of one H_2O molecule with one oxygen atom, as expected from the hydrogen abstraction reaction. Data similar to fig. 65 are reported for Ag(110) [84,185], Ni(110) [113] and Pd(100) [129]. This is an important observation: only low coverages of oxygen are active for hydrogen abstraction; the oxygen-saturated surfaces are relatively unreactive. The maximum in the production of OH_a occurs for θ_O in the range of ~ 0.13 to 0.25. We return to this point later in this section.

Up to now, we have considered only one reaction pathway for the formation and desorption of H_2O from OH_a, viz., the reversible disproportionation reaction

$$2\ OH_a \leftrightarrows H_2O_g + O_a.$$

Other reaction routes can produce H_2O_g also, viz., dissociation and recombination, and whether a given reaction occurs depends upon the state of the reactants (H_a, O_a, OH_a):

$$OH_a \rightarrow O_a + H_a,$$

$$H_a + OH_a \rightarrow H_2O_g;$$

or

$$2\ H_a + O_a \rightarrow H_2O_g.$$

In fact, Norton [21] suggests that dissociation and recombination best describe the H_2O formation reaction (from $H_2 + O_2$) on most metals. He bases his arguments in part on the lack of conclusive experiments demonstrating the importance of OH groups in the overall kinetics of the H_2O formation reaction. Since the time of Norton's review (January 1980), there have been a number of experiments in which the existence of OH_a groups have been clearly shown (cf. the above discussion and table 12, p. 328). Many authors assume that H_2O_g is formed in TDS via the disproportionation reaction, but the best evidence for the importance of this reaction path involving OH_a is reported by Nyberg and Tengstål [81] and Stuve et al. [129] for Pd(100).

Fig. 66 contains a series of EEL spectra obtained after H_2O exposure to an oxygen precovered Pd(100) crystal [81]. Fig. 66a shows the vibrational spectrum of the Pd(100) surface containing 0.25 monolayers of O_a arranged in a $p(2 \times 2)$ lattice. After exposing this surface to 2 L of H_2O at a substrate temperature of 130 K, the spectrum shown in panel (b) is obtained. The loss at 197 meV (1589 cm^{-1}) is due to the H_2O scissoring mode and the broad loss centered at 396 meV (3195 cm^{-1}) is assigned to OH stretches of water and

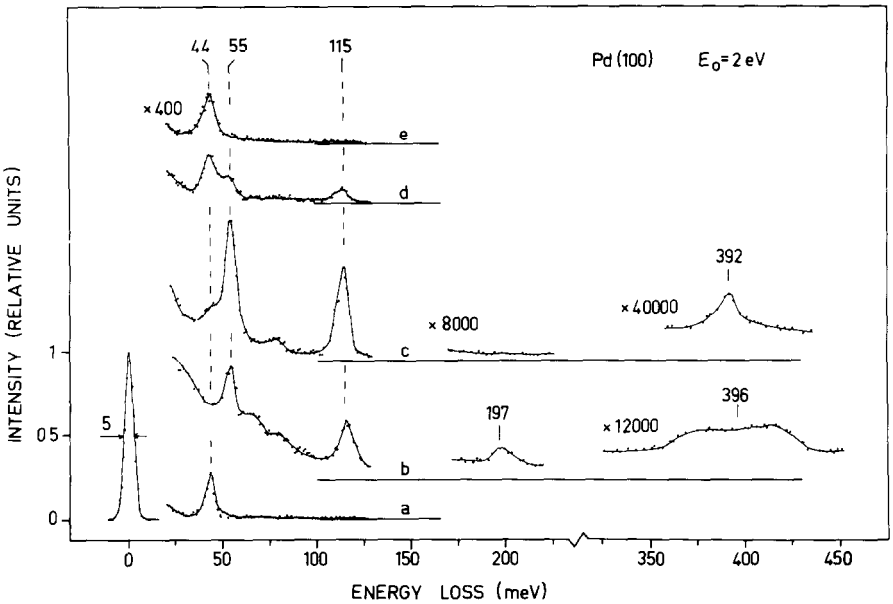

Fig. 66. (a) EEL spectra of p(2×2)O structure on Pd(100). (b) Same surface after exposure to 2 L water at 130 K (c) Same surface as in (b), after heating to 200 K (d) Heated to 210 K (e) Heated to 220 K. Taken from Nyberg and Tengstål [81]

hydroxyl. Fig. 66c shows the EEL spectrum obtained after heating the sample to 200 K; the water scissoring mode is absent and the hydroxyl modes have gained intensity, indicating that the remaining H_2O molecules have either desorbed or reacted to form OH_a. Upon further heating, the desorption of H_2O is observed at ~ 230 K [129].

After forming such an OH_a layer on Pd(100), both Nyberg and Tengstål [81] and Stuve et al. [129] perform isotope exchange experiments to demonstrate that the desorption of H_2O proceeds via disproportionation of OH_a. Fig. 67 illustrates the data of Stuve et al. [129] who expose the OH_a layer to a background of D_2 prior to their TDS measurement. This leads to formation of a layer of $OH_a + D_a$ on the Pd(100) surface. Curve a of fig. 67 shows the reaction peak for desorption of H_2O at 230 K followed by desorption of D_2. Curve b shows the desorption of the mixed isotope, HDO, and the tail of the D_2 desorption peak. Note that *no* HDO desorbs at 230 K. Moreover, coadsorbed atomic hydrogen and oxygen (not shown) produce H_2O desorption only in a peak at 330 K. (The H in the HDO in fig. 67b is adsorbed from residual gas in the vacuum chamber and is not due to H_2O or OH dissociation.)

The isotope exchange experiments prove that (1) no exchange between coadsorbed OH_a and D_a occurs at temperatures for which both are stable, and

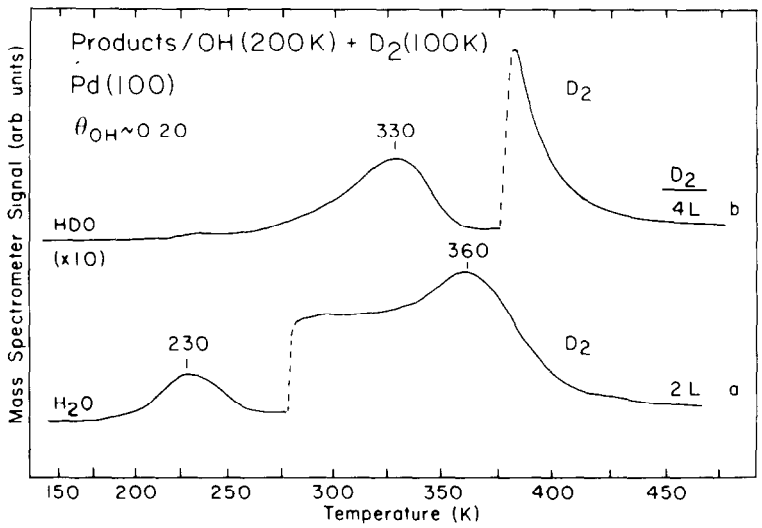

Fig 67. Thermal desorption spectra showing no evidence of H–D exchange between D atoms and hydroxyl groups on Pd(100). (a) H_2O and D_2 desorption following precoverage with 0 1 monolayers of atomic oxygen at 300 K and a 2 L exposure of D_2 at 200 K (b) HDO and D_2 desorption after the same conditions of coverage and exposure except that the D_2 exposure is 4 L Taken from Stuve et al [129]

(2) during the OH reaction, the hydrogen transfers directly from one OH group to another, so that dissociation and recombination can be ruled out. The temperature shift (230–330 K) between H_2O peaks is too great for a kinetic isotope effect; this appears to be evidence for a true disproportionation reaction.

To summarize, for $OH_a + D_a$ on Pd(100), the peak at ~ 230 K is due to the disproportionation reaction:

$$2\ OH_a \xrightarrow{230\ K} H_2O_g + O_a$$

The peak at ~ 330 K is due to a recombination reaction involving O_a, H_a and D_a:

$$H_a + D_a + O_a \xrightarrow{330\ K} HDO_g.$$

In addition, we note that evidence for the disproportionation of OH_a on Ag(110) [134] and Ni(110) [83] is based on the observation that recombination and desorption of H_a occur at temperatures *below* the desorption temperature of H_2O. This means that the reaction which produces water cannot possibly occur by reaction of adsorbed oxygen and adsorbed hydrogen, since no hydrogen remains on the surface at the time of water evolution.

Finally, we note Fisher and DiMaggio [245] observe very similar thermal desorption peaks of water on Rh(100). Water desorbs at 275 and 325 K following coadsorption of atomic hydrogen and oxygen. In that case also, disproportionation is believed to be the source of water formed at 275 K, whereas sequential addition of hydrogen to oxygen is the source of the H_2O which desorbs at 325 K [245].

In closing this discussion, we remind the reader that the kinetics of H_2O formation from the reaction between hydrogen and oxygen are reviewed extensively by Norton [21], and the details of this reaction are beyond the scope of this discussion. Our aim is to discuss the surface chemistry of $H_2O + O_a$ and the TDS processes which yield desorbed H_2O, rather than the full range of H_2O formation processes from $H_a + O_a$.

Structure of OH_a produced by $H_2O + O_a \rightarrow 2\ OH_a$ In discussing the structure of OH_a, we distinguish between long-range order (i.e., the presence or absence of extended periodic arrays of OH_a) and the local bonding geometry (i.e., the identification of the local bonding site, and the angle of the OH bond with respect to the plane of the surface).

Using low-energy electron diffraction (LEED), clear evidence for long-range ordered arrays of OH_a is seen on a number of different surfaces; cf. table 12. All of the cases in which LEED patterns have been identified correspond to LEED structures which, in a "perfect" adlayer, would result in an OH_a coverage of 0.5 monolayers: this is true for the (1×2) and (2×1) structures on the fcc(100) and fcc(110) surfaces, and the $c(2 \times 2)$ structure on the Ag(100). Yet, as indicated previously in this section, the TDS data often indicate total OH_a coverages somewhat lower than 0.5 monolayers on these surfaces (0.2 to 0.3 monolayers). Thus, it appears that the ordered OH_a species tend to form islands on the substrates, often in the presence of excess oxygen, and there is a net attractive interaction between neighboring OH_a species. Stuve et al. [129] even suggest that on Pd(100) the Pd–OH_a bond is bent or inclined, and that the bent configuration enhances attractive hydrogen bonding between neighboring OH_a species. Moreover, the fact that the OH_a groups form ordered structures at low temperatures (typically < 250 K) indicates that they are highly mobile species. To the authors' knowledge, there are not detailed LEED structure calculations for any OH_a layers so the adsorption sites are not identified.

Information about the local bonding geometry of OH_a on various surfaces is deduced from EELS [81,129,132], angle-resolved UPS [83], and ESDIAD [83,84,131]. In table 12, the results of these studies are summarized. The OH_a molecules are either bonded with the OH_a axis perpendicular to the macroscopic substrate surface, or with the OH_a axis tilted or inclined away from the perpendicular configuration. In all cases, the species are bound via the O atom, with the H atom pointing away from the surface. Inclined species are reported both on corrugated fcc surfaces [83,84,133] and stepped surfaces [131]

Table 12
Adsorption of H_2O on oxygen-predosed metal surfaces: characterization of OH_a

Metal	H_2O desorption peak temperatures (K) due to fractional monolayers of adsorbed H_2O [a]	Oxygen precoverage at which maximum OH concentration is formed in monolayers	Vibrational stretch of OH (cm^{-1})	Binding energy of OH UPS peaks – 1π and 3σ (eV)	Local bonding geometry [b]	Long-range order (LEED structure)	Refs.
Ag(110)	320, 240, 200, 170	0.25	3380	5.8, 8.7	Inclined along [001]	(1×2)	[84,132,135]
Ag(311)	310, 210, 175		3680		Inclined		[133]
Ag(100)					Perpendicular	c(2×2)	[131]
Ag(112)					Inclined		[131]
Cu(111)	>290						[122]
Cu(110)	290, 235, 200, 175	0.13		6.4, 9.3		(2×1)	[118]
				5.8, 9.8			[117]
Ni(111)	275–300, ~190, ~170				Perpendicular		[82,108]
Ni(110)	360, –, –	~0.15		5.7, 9.3	Inclined along [001]	(2×1)	[83,167]
Ni(210)	>290						[111]
Ni(100)	~240, 207, 183			6.0, 9.3			[115]
Pd(100)	~250, ~180	0.15±0.05	3250		Inclined	p(2×1)	[129]
	~220		3160		Inclined		[81]
Pt(111)	205, ~180		3480	7.8, 11.1	Inclined		[80,146]
	205, ~180						[150,253]

[a] Underlined number corresponds to temperature at which H_2O desorbs due to recombination of OH_a
[b] "perpendicular" and "inclined" refer to the angle of the OH_a bond relative to the plane of the macroscopic surface

as well as on planar Pt(111) and Pd(100) [81,129]; perpendicular species (with a broad distribution about the surface normal) are reported for smooth Ni(111) [82] and Ag(100) [131].

The EELS evidence for inclined OH_a is illustrated by the Pd(100) studies of Nyberg and Tengstål [81]. They find an intense OH_a bending mode (a hindered rotation) having a vibrational energy of 115 meV (928 cm^{-1}). Based on angle-resolved EELS measurements, they are able to determine that the mode is dipole active, so there is a large dynamic dipole moment normal to the surface. This implies that OH_a is adsorbed with its molecular axis tilted with respect to the surface normal. Similar conclusions are reached by Stuve et al. [129,132] for OH_a/Pd(100) and OH_a/Ag(110), and by Fisher and Sexton for OH_a on Pt(111) [80].

The ESDIAD evidence for inclined OH_a is illustrated by the work of Benndorf, Nöbl and Madey [83] for Ni(110). Angle-resolved UPS demonstrates the existence of azimuthally oriented OH_a, inclined with respect to the surface normal of Ni(110). Fig. 68 shows the ESDIAD H^+ emission pattern obtained from the coadsorption of $H_2O + O_a$ on Ni(110) at 300 K; this corresponds to OH_a in a (2×1) ordered structure. The clean LEED pattern (fig. 68a) provides the basis for identifying the azimuthal orientation of the ESDIAD patterns. The H^+ ESDIAD pattern (fig. 68b) shows two emission spots, each oriented 41° away from the surface normal, along [001] azimuths. A possible bonding model consistent with the inclined OH_a and the (2×1) OH_a/Ni(110) LEED pattern is shown in the lower part of fig. 68. In this model, the OH_a is bound to a three-fold site in the Ni(110) trough; the angle between the OH_a bond axis and the surface normal (α) is 35.3°, slightly smaller than the measured H^+ angle. This is expected due to the distortion of the ion trajectories by the surface image field [247]. Other models of inclined OH_a are discussed in ref. [83]. Evidence for inclined OH_a on Ag surfaces is presented in refs. [131] and [84].

It is interesting to speculate about the bonding structure of OH_a. The R–OH bond is *bent* in covalent molecules (R = H, CH_3, C_2H_5,...) but the M–OH bond is *linear* in complexes in which the bonding is highly ionic (M = Ca, Sr) [248,249]. On this basis, it is not surprising that many of the OH_a structures on metals are reported to be inclined (table 12). However, OH_a species are perpendicular on both Ag(100) and Ni(111) [82,131], and may be perpendicular to three-fold sites on Ni(110), so that no generalization based on substrate structure is obvious. It may be that singly-coordinated OH_a, bonded via the OH π orbital to a metal atop site, or to a single edge atom at a step site, is inclined due to a π–d hybridization. Alternatively, OH_a multiply-coordinated to two, three or four substrate atoms in high-symmetry bridges or hollow sites may find the π–d orbital overlap optimal in a standing up (perpendicular) configuration. This is an area where guidance from theorists would be most welcome!

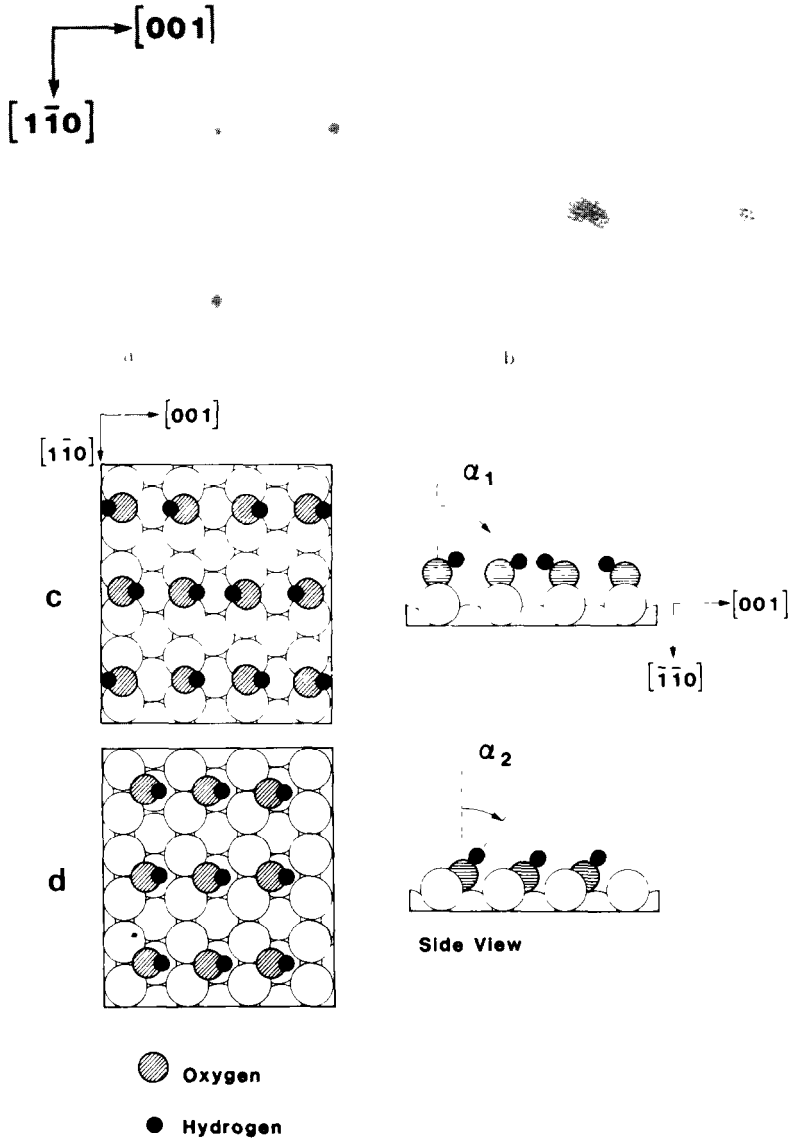

Fig. 68 Upper LEED and ESDIAD pattern for H_2O adsorption on oxygen-dosed Ni(110) (a) LEED pattern from clean Ni(110) (b) H^+ ESDIAD pattern of OH_a on Ni(110) Lower Models for the (2×1) LEED pattern and orientation of OH_a on Ni(110). (c) Short bridge adsorption site of OH_a involving two Ni atoms from a [110] Ni row, the hydrogen atoms are assumed to be pointing in [001] or [00$\bar{1}$] azimuthal directions (d) Three-fold adsorption site of OH_a involving two first-layer and one second-layer Ni, for this model, the two-spot ESDIAD pattern is assumed to be due to two different types of domains with (2×1) symmetry, the H atoms pointing either in the [001] or in [00$\bar{1}$] direction Taken from Benndorf et al [83]

Why is O_a active for H_2O dissociation? The hydrogen abstraction reaction ($H_2O + O_a \rightarrow 2\ OH_a$) appears to be very metal-specific. The presence of O_a on Re(001) *blocks* the dissociation of H_2O [141], and O_a on Ru(001) is inactive for H_2O dissociation [241]. In contrast, O_a on Ni, Pt, Ag, Cu, Pd surfaces (cf. table 12, p. 328) is extremely active for H_2O dissociation. Since the variation in the H_2O–metal binding energy varies little from metal to metal, the reason for this specificity may be related to the metal–oxygen interaction and the electronic structure of O_a. There appears to be no obvious correlation with ΔH_f(M–O), however (table 4, pp. 242–243): O_a activates H_2O dissociation on several metals with high and low values of ΔH_f(M–O), i.e., Zn (−348 kJ/mol), Ni (−244 kJ/mol) and Ag (−12 kJ/mol), whereas metals with intermediate values are inactive i.e., Re (−178 kJ/mol) and Ru (−153 kJ/mol). There is also no apparent correlation with the electronic structure of O_a on different metals as revealed by UPS or XPS.

The activity of O_a for hydrogen abstraction on Cu, Ag, Pd, Ni (table 12, p. 328, and fig. 65) is greatest for low coverages of O_a, below 0.1 to 0.25 monolayers; only in this regime is the conversion to OH_a quantitative. The question is: *why*? Is this a geometric site-blocking effect at high oxygen coverages, or is there a coverage-dependent change in the electronic properties of O_a? The latter does not seem to be the case, since the work function change as a function of oxygen coverage on most metals is linear over a wide coverage range. This implies little, if any, change in the total electronic charge of O_a, so that any changes in electronic properties of adsorbed oxygen must involve more subtle rearrangements in charge distribution and local fields. Thus, geometrical site-blocking may play a major role. It is curious that on several surfaces the maximum OH_a production corresponds to an oxygen coverage of ~ 0.15 monolayers. For significantly higher coverages of randomly adsorbed O_a, surface crowding would force an adsorbed H_2O molecule to interact with more than one O_a species in (perhaps) an unfavorable bonding configuration for reaction. Another factor which has not been addressed quantitatively concerns the role of islands of ordered O_a which form at higher oxygen coverages. The reaction to form OH_a surely occurs more readily at the edges of islands than in the high-coverage region where favorable bonding sites for H_2O_a and/or OH_a may not be available. This has been suggested also by Fisher and DiMaggio [245], and is supported by the recent work of Nyberg and Uvdal, which shows that hydroxyl formation *begins* at defects in a p(2 × 2) oxygen lattice on Pd(100) [81].

Carley et al. [111] point out that chemisorbed oxygen is more active for hydrogen abstraction from H_2O than is oxidic oxygen (the O^{2-} anion). They relate the activity of different oxygen species to the degree of coordinative unsaturation. As indicated above, the dependence of hydrogen abstraction activity on the coverage of chemisorbed oxygen shows that factors in addition to coordinative unsaturation of individual atoms are playing a role in this reaction.

Although the electronic structure of the active and inactive forms of O_a on various metal surfaces is not known, it is interesting to consider the *gas-phase* reaction:

$$O_g + H_2O_g \rightarrow 2\ OH_g.$$

This reaction is immeasurably slow at room temperature for ground-state atomic oxygen [$O(^3P)$], yet when the oxygen is electronically excited to the $O(^1D)$ state, 2.2 eV (212 kJ/mol) above the ground state, the rate constant for hydrogen abstraction is nearly the molecular collision frequency [250]. The electronic structure of "active" O_a may mimic the excited state of atomic O.

Anderson [63] considers the reactions of $H_2O + O_a$ on model Pt(111) and Fe(100) clusters using an atomic superposition and electron delocalization technique. The conclusion of his work pertinent to our discussion is that O_a lowers the activation barrier to H_2O dissociation in both cases.

6.2.3. Electropositive additives

Among the electropositive surface additives whose interaction with water have been studied to date, the alkali metals are the most common, but in addition there is recent work with boron-dosed rhodium [128] and a surprising study of HF in which hydronium ion (H_3O^+) is observed [116]. Perhaps the alkali metals receive the most attention because they are constituents of many electrochemical cells. Therefore, the interaction between H_2O and alkali-dosed metal surfaces is of interest in modelling and understanding processes at electrode interfaces. All of the published studies on the subject of H_2O coadsorbed with alkalis are recent ones: Bonzel's 1984 paper [251] on the subject of "Alkali-Promoted Gas Adsorption and Surface Reactions on Metals" does not list any references to H_2O!

A tabulation of the available references to the H_2O + adsorbed alkali interactions is given in table 13, along with an indication of some of the major conclusions regarding the adsorption and reactivity of H_2O. In each case, H_2O does not dissociate on the clean substrate (Ag, Cu, Ru, Pt), but the surface chemistry is changed markedly by alkali coadsorption. In the following paragraphs, we focus on the probability of dissociation of H_2O, the kinetics of desorption and reaction, the thermal stability of OH_a, evidence for "tilting" of H_2O by interaction with adsorbed alkalis, and possible hydration of the adsorbed alkali species.

A wide range of reaction probabilities are reported for H_2O plus adsorbed alkalis, ranging from *no* dissociation under any conditions to dissociation even at 80 K. Sass and coworkers [123,231,253] report that H_2O apparently does not dissociate in the presence of adsorbed Li and Cs on Ag(110) under any conditions of coverage and temperature (fractional monolayers of alkali; H_2O adsorbed at $\sim$ 130 K and heated to desorb). A coverage- and temperature-dependence for the H_2O dissociation reaction is reported by Doering, Semancik

Table 13
Coadsorption of H_2O + alkali metals on metal substrates

Adsorbate/ substrate	H_2O dissociation?	Maximum temperature for stability of OH_a (K)	Evidence for tilting of H_2O molecular (C_2) axis?	Refs
Li/Ag(110)	No		–	[231]
Li/Cu(110)	Yes		–	[231]
Li/Ru(0001)	Yes – depends on θ_{Li} and T		Yes – ESDIAD	[252]
Na/Ru(0001)	Yes – for $\theta_{Na} > 0.25$ (90 K) $\theta_{Na} > 0.1$ (200 K)	550	Yes – ESDIAD	[154]
K/Pt(111)	Yes – for $\theta_K > 0.06$	570	–	[213–215]
K/Ru(0001)	Yes	580	–	[211]
Cs/Ag(110)	No		Yes – work function	[123]

and Madey [154,252] for H_2O on Na- and Li-dosed Ru(001). For $\theta_{Na} \lesssim 0.25$ monolayers, H_2O is reported *not* to dissociate following adsorption at 90 K; even upon heating to > 200 K, no dissociation occurs for $\theta_{Na} < 0.1$ [154]. Higher coverages of Na are effective in dissociating H_2O, however, and a hydroxyl layer containing both long-range order and preferred local bond orientation exists. It appears that "ionic" Na (the low-coverage form) is ineffective for dissociation, whereas "metallic" Na (the high-coverage form) is reactive [154]. Semancik et al. [252] report that Li-dosed Ru(001) is much more reactive toward H_2O than is the Na-dosed surface: for $\theta_{Li} \gtrsim 0.05$ monolayers, H_2O dissociation is seen at 80 K, and activated dissociation is observed at all lower Li coverages upon heating (in marked contrast to Li/Ag(110) [231]). The system K/Pt(111) is also reactive for H_2O dissociation at 80 K [213,215], but recent measurements have shown that a critical K coverage of ~ 0.06 monolayers is needed to initiate dissociation. In this work, illustrated in fig. 69, OH_a species are identified using XPS and UPS [213–215]. Reaction of H_2O with K on Ru(001) to form KOH is seen by Thiel et al. [211] using EELS; these measurements extend over a very wide range of coverage ($0.1 < \theta_K < 10$ monolayers). Note that the critical coverages required for low-temperature H_2O dissociation on Li/Ru(001) and K/Pt(111) (i.e., $\theta \gtrsim 0.05$ monolayers of alkali) are quantitatively different from Na/Ru(001), where $\theta_{Na} \approx$

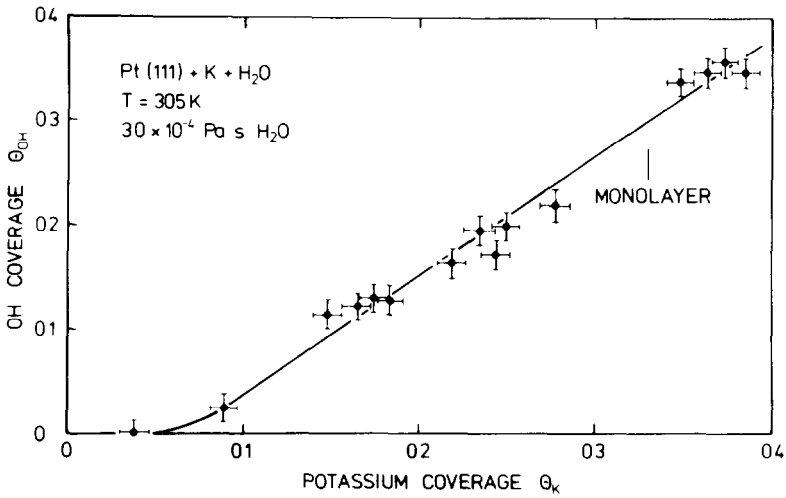

Fig 69 Variation of OH coverage versus K coverage on Pt(111) These data result from reaction between water and adsorbed K at 305 K. Note that there is a "critical coverage" of K (~ 0 06 monolayers) necessary to initiate formation of OH Taken from Kiskinova et al [215]

0.25 monolayers is required. Although the ionicity of the alkali may be the critical factor in these measurements, the possible role of steps, defects, etc. in trapping small amounts of alkali cannot be discounted.

It is difficult to characterize the systematics of dissociative adsorption on alkali-dosed metals. It is not clear why Li should be active for dissociation on Ru(001) and Cu(110) but not on Ag(110), nor is it apparent why Li and K are active on Ru(001) even at low θ, whereas higher coverages of Na are required. Any argument based solely on ionic radii, or ionic versus metallic character of the alkali will find an exception, even in the (rather small) data set of table 13, p. 333. When one examines the charge densities for alkalis on jellium calculated by Nørskov, Holloway and Lang [232], there is no apparent reason based on electronic structure why the different alkali/substrate combinations behave so differently. Some subtle (but not yet identified) geometric and/or electronic factors must be involved.

Another interesting effect relating to H_2O adsorption and dissociation is the observation by Thiel et al. [211] and Kiskinova et al. [215] that multilayers of K on Ru and Pt are *not* reactive to H_2O at room temperature. Despite the fact that there is a strong thermodynamic driving force to KOH formation [ΔH_f(KOH) = −424.7 kJ/mol], the residence time of an adsorbed H_2O molecule at 300 K is probably not sufficiently long for dissociation to occur [222].

The existence of OH_a on Na- and K-dosed Ru(001) and Pt(111) has been established convincingly using XPS, UPS, EELS and ESDIAD [211,213,215,

252]. Unlike the OH_a species formed by reaction of H_2O with O_a (table 12, p. 328), however, the alkali-stabilized OH_a species are remarkably stable: whereas the OH disproportionation reaction is rapid at 205 K on Pt(111), the K-stabilized OH_a remains on the surface up to ~ 570 K [213,215]! Similarly, Na- and K-stabilized OH_a on Ru(001) remain on the surface until 550–580 K. Thiel et al. [211] asign vibrational modes at ~ 1340 cm^{-1} and ~ 3600 cm^{-1} on Ru(001) to the K^+–OH^- stretch and the O–H stretch, respectively, of a KOH complex. Kiskinova et al. [215] also believe that the stability of OH_a on Pt(111) is due at least partly to a direct K^+–OH^- interaction.

Wagner and Moylan have recently shown that HF dissociates to yield hydrated hydronium ions, H_3O^+, on Pt(111) [116]. The hydronium ion is identified by a distinctive loss feature in EELS at 1150 cm^{-1}, and forms during coadsorption at 100 K, even at very low coverages of HF [116]. This is the first identification of hydronium ion in a UHV experiment, and provides a good basis for expecting that the results of UHV single crystal experiments will have direct bearing on the surface chemistry of electrodes in solution.

In a study with somewhat different emphasis, Kiss and Solymosi report that contamination of a Rh foil with the electropositive element boron can induce dissociation of water and can also strengthen the chemisorption bond of molecular water [128]. In agreement with the data presented in section 4, they find that no dissociation occurs on the clean Rh foil or on clean Rh(111) [128]. Using TDS, they observe new desorption states of molecular H_2O at 320 and 370 K, as well as significant desorption of H_2, when they allow boron to segregate from the bulk to the surface of the Rh sample. Using EELS to identify the electronic transitions of the adsorbates, they find that a B–O bond forms at about 270 K and is stable up to 650 K; they attribute this to formation of a boron oxide [128].

The remainder of this discussion focuses on the structure and chemistry of the molecular H_2O species which interact with adsorbed alkali ions (and with any reaction products). In all cases where ESDIAD or work function measurements are applied to the interaction of H_2O with an alkali on a metal surface, there is evidence for direct H_2O–alkali interactions which lead to a "tilting" of the H_2O molecular axis [123,154,252,253]. This is manifest in changes (both in magnitude and in sign) in the dipole moment per adsorbed H_2O molecule, as well as in marked changes in the H_2O ESDIAD patterns. The tilting of the molecular axis apparently originates in the electrostatic interactions [232] between the H_2O dipole and the adsorbed alkali ion. This interaction also results in the "breaking up" of the hydrogen-bonded H_2O clusters which exist on the clean surface, in favor of surface hydration of adsorbed alkali ions (cf. section 6.1 and figs. 54 and 55).

There are many cases where adsorbed alkali ions or adsorbed electronegative ions (O, Br) are solvated by adsorbed H_2O (i.e., surrounded by clusters of H_2O), but in most cases the alkali or electronegative ion remains bonded to

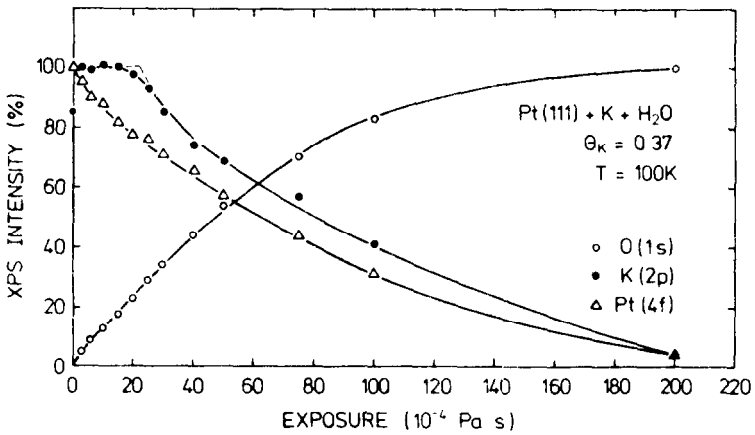

Fig. 70 Evidence for the hydration of K on Pt(111) variation of integrated intensities of the K 2p, O 1s and Pt 4f core level XPS peaks as functions of H_2O exposure at 100 K The initial K coverage on the Pt(111) surface is 0 33 monolayers Taken from Bonzel et al [213]

the surface, with H_2O clustered around [120,123,132,135,136,154,231]. In several cases, however, there is evidence that Li^+ or K^+ may be fully solvated by multiple H_2O molecules, and be "lifted off" the surface. Thiel et al. [211] report TDS spectra for H_2O + K/Ru(001) in which molecular water desorbs at ~ 305 K (a surprisingly high temperature), and which they identify as due to H_2O from hydrated potassium. Fig. 70 shows the data of Bonzel et al. [213] which they believe demonstrates the hydration of K on Pt(111). The figure show integrated XPS intensities as a K-covered Pt(111) surface ($\theta_K = 0.33$ monolayers) is dosed with increasing coverages of H_2O. As expected, the Pt 4f peaks are attenuated by the H_2O layer as the O 1s features grow in intensity. The surprising observation is that the intensity of the K 2p feature is unchanged for the initial H_2O doses. The authors propose that the adsorbed K species are solvated by the adsorbed H_2O molecules, and that the solvation sphere of each K is sufficiently "open" that the attenuation of K 2p emission is negligible. They also believe that OH^- species in the adlayer are solvated.

Connell and Dumesic [254] have obtained intriguing results using Auger electron spectroscopy, which indicate that the mobility of potassium on iron and alumina surfaces at 670 K is enhanced in the presence of water vapor. They attribute this to formation of hydrated or hydroxylated potassium species which essentially "float" on the surface [254]. It would be most interesting to identify the species associated with this particularly high mobility!

In conclusion, although many new insights into H_2O surface chemistry have arisen from studies of coadsorbed H_2O + additive atoms, many challenges to our scientific understanding remain.

7. Adsorption on nonmetallic surfaces

7.1. Well-characterized oxides

7.1.1. Introduction

The adsorption of water on oxidic surfaces is characterized by several features which are different from those on the clean metal surfaces. First, well-ordered ionic single-crystal samples are often unreactive for H_2O dissociation. This is surprising since work on powders of common oxides such as Al_2O_3 [23,24] and zeolites [256] indicates that H_2O is usually very efficient in hydroxylating the surface. It may be that the dissociation of H_2O on the powders is dominated by reaction at the defect sites and facet edges in the powders, and such sites are only present in small concentrations on the single crystals.

A second noteworthy feature is that H_2O does not generally form hydrogen-bonded clusters at low coverage. Apparently the tendency to cluster, which is so strong on clean metal surfaces, can be overridden by the oxide substrate–H_2O interaction, which ties the H_2O to specific cation sites. Examples of oxides for which this is true include $Na_{0.7}WO_3(001)$ [257], Ti_2O_3 [258], and $SrTiO_3$ [259]. As suggested by Aitken et al. [257], this has the intriguing implication that "the double layer at a metal oxide/electrolyte interface is more highly structured than with conventional metal electrodes".

The third distinctive feature of H_2O adsorption is the formation of relatively strong chemisorption bonds on *some* (not all) ionic surfaces, so that molecular adsorbed H_2O can be stable even up to room temperature. This has been suggested to occur, for instance, on ZnO [260] and Ti_2O_3 [258]. This is in contrast with the clean metals, where chemisorbed states desorb well below room temperature in most cases (section 4.2).

The influence of defect lattice sites and "nonlattice" oxygen atoms at oxide surfaces appears to be quite important. Surfaces of oxide single crystals which have been ion-bombarded to produce defects can cause dissociation of H_2O to the hydroxide, whereas the more "perfect" surfaces of the same compounds do not. This is true, for instance, for $TiO_2(110)$ (e.g. [261–264] and NiO(100) (e.g. [83,265]). Also, there appears to be a fundamental difference between the surface of a *bulk oxide* and the surface of a bulk sample (metal or oxide) which has "*nonlattice oxygen*", i.e., chemisorbed oxygen atoms. Like defects, chemisorbed oxygen makes many surfaces more reactive toward water decomposition and hydroxylation. Carley, Rassias and Roberts have suggested that the reason for differences in reactivity with oxygen treatment lies in the differences in the degree of coordinative unsaturation between the various types of oxygen [111]; this is discussed in section 6.2.2.

In the following sections, these general observations are discussed in more detail. Comparisons between data from single crystals and powdered or

polycrystalline samples are made. With respect to hydrogen-bonded systems (such as water) adsorbed on powdered or polycrystalline oxides, the reader is directed to useful reviews by Knözinger [23] and Hair [24].

7.1.2. Titanium oxide

Much of the research on water–titanium oxide surface chemistry has been motivated by the relatively high efficiency of titanium oxides in photocatalytic decomposition of water, which is potentially important as a solar energy conversion process. The initial demonstrations of the photocatalytic properties of these materials in aqueous media, presented in the mid-1970's, have inspired work on well-characterized single crystals of the oxides. The latter body of work is reviewed by Henrich [261].

The main purpose of the single-crystal experiments has been to identify the factors which cause H_2O to dissociate. As more experiments have been performed, there has been a steady evolution of increasingly refined models for the mechanism of H_2O dissociation. Early work by Somorjai and co-workers indicates that Ti^{3+} ions are particularly important in H_2O dissociation on TiO_2 [263]. The desire to clarify the role of Ti^{3+} has subsequently led researchers to compare the reactivities of oxide surfaces which have different types of Ti ions exposed. This has also spurred experiments which compare the adsorptive properties of well-annealed or cleaved, low-defect-density surfaces with ion-bombarded, high-defect-density surfaces of the titanium oxides.

The materials and surfaces which have been studied are summarized in table 14, together with conclusions regarding whether or not H_2O adsorbs at room temperature, what the adsorbed species are, and what type(s) of Ti ions are exposed at the ideal surface. In many cases, table 14 illustrates that the adsorption behavior of water on these oxides is strongly influenced by the degree of perfection of the surface, i.e., the defect density.

Henrich and coworkers have surveyed types of titanium oxide surfaces using UPS; they find that water chemisorbs molecularly at room temperature on nearly perfect surfaces of TiO_2 and Ti_2O_3. The observation of molecular water on $Ti_2O_3(102)$ at 300 K leads them to suggest that Ti 3d electrons alone are not sufficient to induce dissociation (cf. table 14) [261]. At the same time, Cox, Egdell and Naylor suggest that an oxygen vacancy adjacent to a Ti^{3+} site is the only site where H_2O can adsorb on $SrTiO_3(100)$, based upon EELS, XPS and UPS data. They find that the low-defect-density surface is entirely inert toward H_2O adsorption at room temperature, but ion bombardment and generation of Ti^{3+} in an oxygen-deficient lattice creates a surface at which molecular water *can* adsorb [259,267]. The original work of Lo et al. would be consistent with H_2O dissociation at a highly irregular surface, since they observe this to occur on $TiO_2(100)$ surfaces which are ion bombarded or which are covered with evaporated titanium [263]. Furthermore, work with TiO_2

Table 14
Adsorption of H_2O on the titanium oxides

Sample	Adsorption at room temperature?	Adsorbed species ($\theta \lesssim 1$)	Surface Ti ions	Refs
TiO_2(100)				
(a) Smooth (annealed) 1×3	Yes	H_2O (UPS)		[263]
(b) Rough (sputtered or with Ti film)	Yes	OH (UPS, ESD)	Ti^{3+} $3d^1$	[262,263]
TiO_2(110)				
(a) Smooth (cleaved)	Slight	? (UPS)	Ti^{4+} $3d^0$	[261]
(b) Rough (bombarded and annealed)	Yes	OH, followed by H_2O (UPS)	Ti^{4+}, Ti^{3+}, Ti^0	[261,264]
Ti_2O_3(102)				
(a) Smooth (cleaved)	Yes	H_2O (UPS)	Ti^{3+} $3d^1$	[258,266]
(b) Rough (ion-bombarded)	Yes	OH (UPS)		[258,266]
$SrTiO_3$(100)				
(a) Smooth (well-annealed)	No	–		[259,261,267, 268]
(b) Rough (ion-bombarded)	Yes	H_2O (UPS)	Ti^{3+} $3d^1$	[259,261,264, 267,268]
$SrTiO_3$(111)	Yes	OH (UPS, TDS)		[269,270]

powders in photocatalytic reactors appears to consistently point toward the importance of Ti^{3+} ions in the H_2O decomposition reaction [16,95,271,272]. In the present authors' judgment, H_2O probably interacts strongly with the surface when both Ti^{3+} *and* defect sites (oxygen vacancies) are present, and may even require that these two sites be adjacent [16,259,267], although the relative importance of these two factors remains open to investigation.

Interestingly, hydroxylation of TiO_2 powders has been discussed by Hair [24], who points out that dehydroxylated, annealed samples are quite inert to H_2O unless a bit of oxygen is present also in the gas phase. The inertness of TiO_2 powders under these conditions compares favorably with the inertness of smooth TiO_2 single crystals summarized in table 14.

7.1.3. Zinc oxide

The adsorption of H_2O on zinc oxide (ZnO) powders has been studied via infrared, thermogravimetric, volumetric, and conductivity measurements. The results are summarized concisely by Hirschwald [273]. It is generally agreed that H_2O dissociates in the first layer, exhibiting narrow IR bands at 3670 and 3620 cm^{-1} (the O–H stretch). These hydroxyl groups can be stable up to ~ 900 K [273]. At higher coverage, IR data indicate that molecular water

adsorbs through hydrogen-bonding to existent hydroxyl groups. This is supported by the fact that adsorption isotherms show a discontinuity after the first OH layer is filled, and the isosteric heat of adsorption of water in the multilayer is 67 to 42 kJ/mol, consistent with hydrogen-bonded molecular H_2O. There has been some speculation regarding the influence of atomic defects and different types of crystal facets on the measured properties of H_2O adsorbed on ZnO powders [273], and a study of H_2O on ZnO single crystals addresses this exact issue [260].

Zwicker and Jacobi [260] examine H_2O adsorption on three simple types of ZnO surfaces: the zinc-rich (001) face, the oxygen-rich $(00\bar{1})$ face, and the polar (100) face which has both Zn and O atoms exposed. After dosing the sample to H_2O and heating, these authors observe only molecular water evolving in the gas phase, which exhibits rich desorption spectra, as shown in fig. 71. Water interacts most strongly with the Zn sites available on the (001)

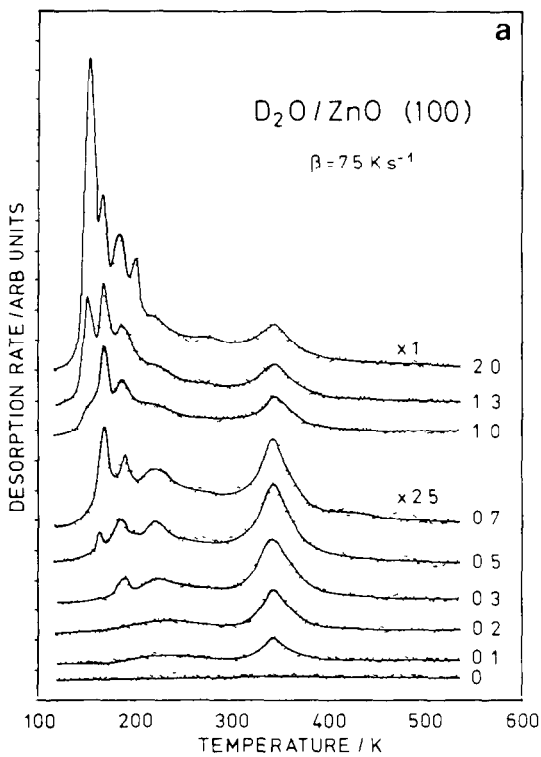

Fig. 71. (a) Thermal desorption spectra of D_2O on ZnO(100). The parameter which varies is the D_2O exposure in langmuirs. The heating rate is constant at 7.5 K/s. Taken from Zwicker and Jacobi [260]. Continued on next pages

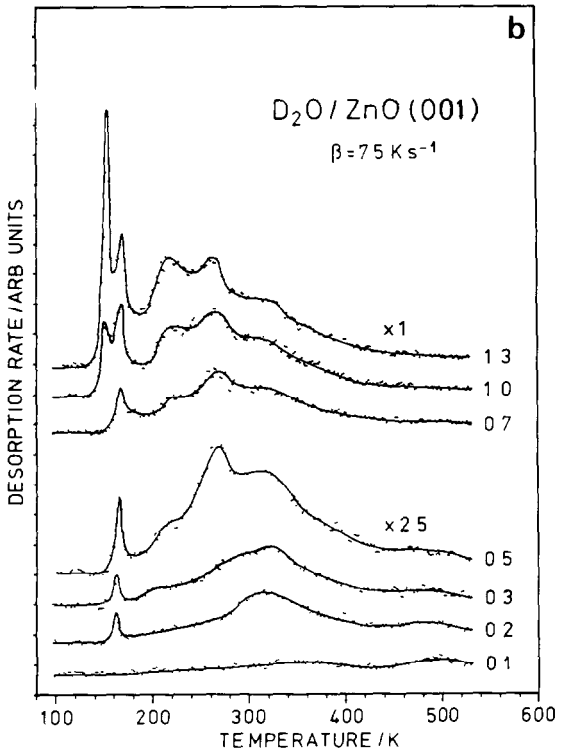

Fig. 71 (b) Thermal desorption spectra of D_2O on ZnO (001)

and (100) faces, with a characteristic desorption state at 320 to 340 K. Water interacts more weakly with the oxygen sites on the (00$\bar{1}$) and (100) faces, with a desorption state which peaks at 190 K. Adsorption occurs preferentially, therefore, at the surface cation sites, where the adsorbed species is stable even at approximately room temperature. Zwicker and Jacobi have identified the adsorbed species in all cases as molecular H_2O, based largely upon UPS spectra [260]. However, due to interference with Zn 3d states, only one orbital of the chemisorbed species could be clearly observed, as shown in fig. 72; this alone does not unambiguously exclude hydroxyl formation. As with the titanium oxides, the UPS measurements could be complemented by data from other techniques to resolve the issue of whether or not H_2O dissociates on these surfaces.

Another study of H_2O on ZnO is reported by Au, Roberts and Zhu, who expose single-crystal metallic Zn to oxygen at 77 K, then to water at the same temperature, and warm the surface [125]. With no measurement of the oxygen

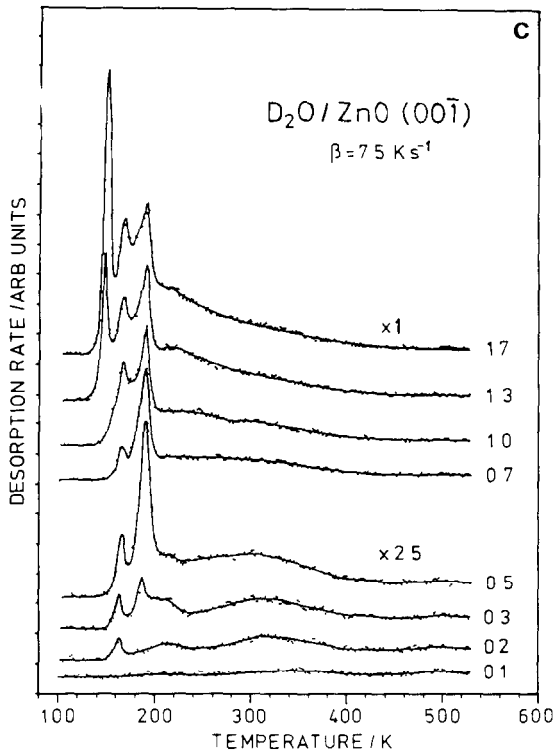

Fig. 71. (c) Thermal desorption spectra of D_2O on ZnO (00$\bar{1}$)

coverage or the oxide lattice structure under these conditions, and with no annealing of the oxygen after adsorption, it is difficult to assess what sort of surface this represents. It may be that many defect sites are present. In any case, XPS data show the presence of hydroxyl species which are stable up to ~ 500 K, and which decompose to yield gaseous hydrogen. On the other hand, Zwicker and Jacobi [260] observe only gaseous D_2O while heating their D_2O-dosed samples, which seems to indicate a basic difference between the results of these two studies.

We suggest that the question of whether H_2O dissociates at ZnO surfaces, and under what conditions, is not yet resolved. In particular, the possible influence of defect sites has not yet been addressed systematically. Work with ZnO crystals which have been deliberately roughened, e.g., by ion bombardment, could provide useful insight to this problem in much the same way that work with ion-etched titanium oxide single crystals has confirmed the important role of defect sites in H_2O adsorption and dissociation on those materials (see section 7.1.2).

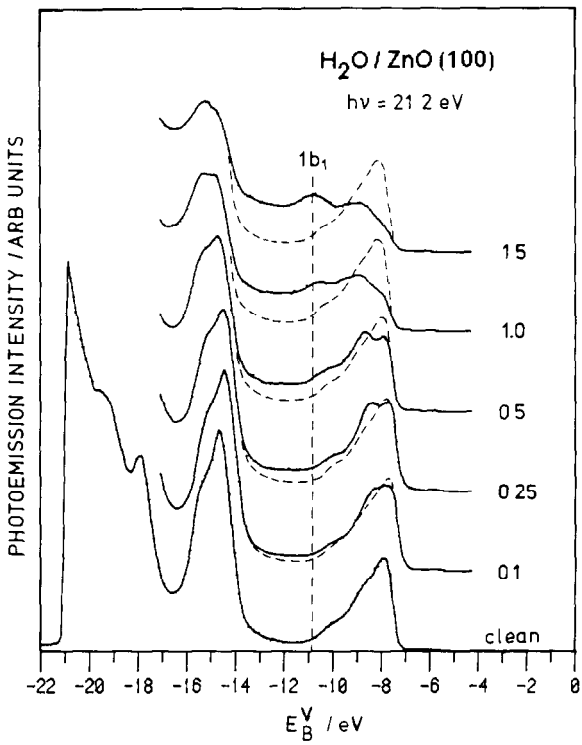

Fig. 72. Photoemission spectra of H_2O on ZnO(100) for several H_2O exposures, in langmuirs The binding energy E_B is related to the vacuum level. For the H_2O-covered surfaces the spectrum of the clean surface is repeated in broken lines Emission associated with the $1b_1$ orbital of H_2O is labelled Taken from Zwicker and Jacobi [260]

7.1.4. Tungsten oxide

There is only one study reported of H_2O adsorption on a well-characterized tungsten oxide, to our knowledge. Using EELS and UPS, Aitken and co-workers [257], are able to identify non-hydrogen-bonded, molecular H_2O at coverages up to (presumably) one monolayer at 150 K (up to 4 L exposure) on tungsten bronze, $Na_{0.7}WO_3(001)$. Using the frequency of the substrate–oxygen stretch at 600 cm^{-1} as a fingerprint, they identify the tungsten cations as the preferred adsorption sites. Their vibrational spectra are reproduced in fig. 73. At higher coverage, the O–H stretching vibration gives evidence of hydrogen bonding as the multilayer formed. The adsorbed water is not stable at room temperature. The UPS data are reported to confirm the assignment of molecular adsorption by exhibiting the three characteristic peaks of H_2O (section 3.2).

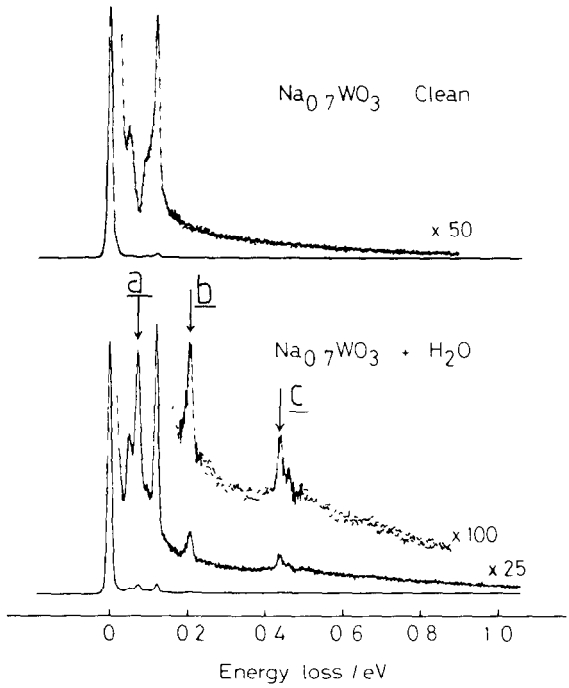

Fig 73 Electron-energy-loss spectra of $Na_{0.7}WO_3$ recorded at 150 K before (upper) and after (lower) exposure to 1 L H_2O The three adsorbate-induced loss features are indicated by arrows in the lower spectrum These features are assigned as ν(OH) at 3590 cm^{-1}, δ(HOH) at 1740 cm^{-1}, and the metal–oxygen stretch at 600 cm^{-1} Taken from Aitken et al. [257]

7.1.5. Lead oxide

Carley, Rassias and Roberts [111] have used XPS to study the interaction of water with lead and oxidized lead surfaces. Some of their data are shown in fig. 74. On clean lead or annealed lead oxide (PbO) surfaces, the XPS gives evidence for molecular water only, with an O 1s binding energy of 533.9 eV. This water desorbs in vacuum above 150 K. On a lead surface where oxygen has been deposited at low temperature *without* annealing, however, there is evidence for hydroxyl formation, with the O 1s peak at 531.0 eV. The hydroxyl groups are stable to ~ 200 K.

We note that the conditions necessary for obtaining the adsorbed hydroxide most probably produce a very imperfect oxide surface, which these authors discuss in terms of coordinatively unsaturated oxygen ([111]; section 6.2.2). As for the titanium oxides and NiO, the presence of defects (or coordinatively unsaturated oxygen) at the oxide surface seems important in influencing H_2O decomposition on PbO.

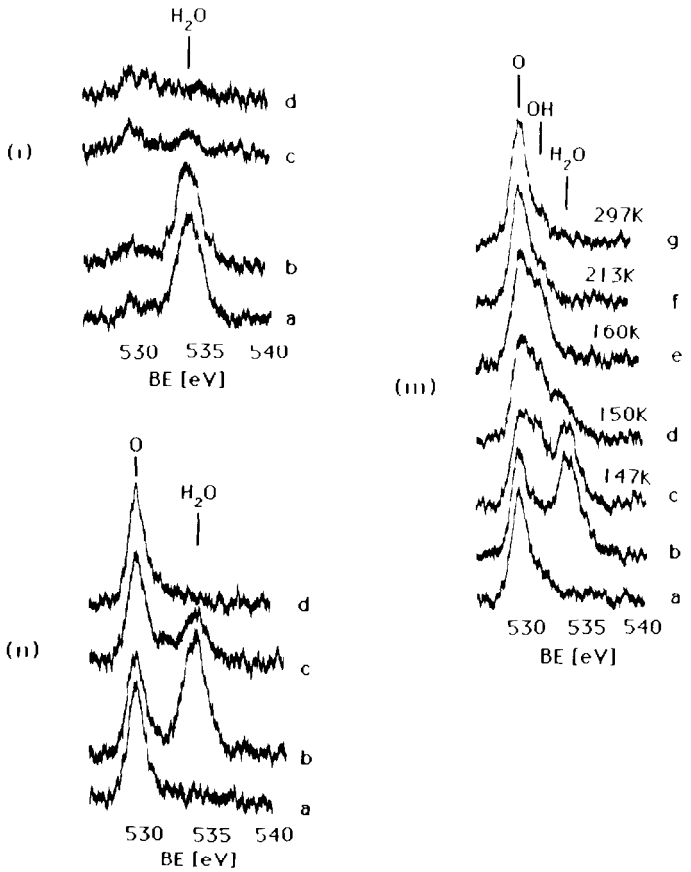

Fig 74. XPS spectra of the O 1s level for water and oxygen on a lead surface (i) Spectra from a clean lead surface exposed to 15 L H_2O at 77 K (curve a), then warmed to 140 K (curve b), 148 K (curve c), and 151 K (curve d) (ii) Spectra from a lead surface exposed to 300 L oxygen at 297 K (curve a), followed by 15 L H_2O at 77 K (curve b), then warmed to 143 K (curve c) and 160 K (curve d). (iii) Spectra from a lead surface exposed to 150 L oxygen at 77 K (curve a) followed by 15 L water vapor at 77 K (curve b), then warmed slowly to room temperature (curves c–g) The data are interpreted to mean that clean or oxidized lead does not dissociate H_2O, rather, H_2O condenses at 77 K and desorbs intact as temperature is raised [cf sequence (i) and (ii)] The XPS feature at 531.0 eV in sequence (iii) is taken as evidence that hydroxyl groups can form under similar conditions on a lead surface which contains chemisorbed oxygen Taken from Carley et al [111]

7.1.6. Aluminum oxide

Aluminum oxide (Al_2O_3) has attracted particular interest due to its widespread use as a catalyst and catalyst support. Infrared data concerning OH and H_2O on alumina powders is reviewed by Knözinger [23] and Hair

[24]. On these surfaces, exposure of dehydroxylated alumina to water vapor leads partly to rehydroxylation (for sample temperatures above 320 K) and partly to coordination of water molecules to exposed aluminum ions [23]. Hydroxyl groups are stable up to ~ 1000 K [24]. The hydroxyl groups appear to be of several types, based upon different O–H stretching frequencies from 3700 to 3800 cm^{-1} and based upon the independent behaviors of these features when samples are heated or isotopically exchanged [23,24]. Water can adsorb in multilayer states by hydrogen bonding to the first-layer OH or H_2O groups, under favorable conditions of temperature and pressure. As with the zinc oxides, however, there has been speculation regarding the role of defect sites, different kinds of crystallite faces, and potential difference in chemical composition between the bulk and surfaces of these powders [24]. This type of speculation, with respect to H_2O adsorption and reaction, is only addressed in three studies of Al_2O_3 single crystals to date. In a study of H_2O on $Al_2O_3(001)$, Almy et al. report UPS data which support hydroxyl formation at room temperature [274]. Chen and coworkers find that H_2O dissociates to form adsorbed hydroxyl groups even at 150 K on an oxidized Al(111) substrate [275], with a distinctive O–H stretching frequency at 3720 cm^{-1}. This is in good agreement with the frequency range cited above for OH groups on Al_2O_3 powders [23]. On oxidized Al(100), Paul and Hoffman also find evidence for dissociation of H_2O following ice condensation at 80 K and annealing to 300 K [217]. In summary, the three studies of H_2O adsorption on aluminum oxide single crystals which have been reported to date agree that dissociation occurs readily at room temperature [217,274,275], and one report concludes that dissociation takes place even at 150 K [275]. It is apparent that dissociation of H_2O occurs very easily on aluminum oxide surfaces.

7.1.7. Nickel oxide

The only published studies of H_2O or OH at nickel oxide surfaces are relatively recent and deal with single-crystal surfaces, either of bulk oxides or oxidized metals. Three of these studies indicate that a low-defect-density surface of the bulk oxide or of bulk-oxide-like material is inert toward H_2O adsorption or hydroxylation at room temperature [83,265,276]. A fourth indicates that hydroxyl groups form most readily, and are most stable, on a nickel surface which is oxidized at low temperature, 77 K, with no annealing [111]. A fifth reports that hydroxylation occurs on a NiO(111) surface at room temperature [174]. The first four papers mentioned appear to be rather consistent in pointing toward the importance of lattice defects and/or "non-lattice oxygen" for hydroxylating NiO.

Perhaps the two most incisive studies are those by McKay and Henrich [265] and Benndorf et al. [83]. McKay and Henrich have found that H_2O does not interact with cleaved, low-defect-density NiO(100) at room temperature, but dissociative adsorption *does* take place if "nonlattice oxygen" is present

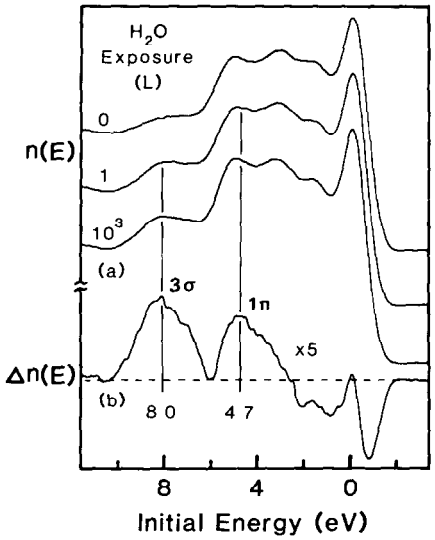

Fig. 75. (a) Photoemission spectra of ion-bombarded NiO(100) pre-exposed to 10 LO_2 as a function of H_2O exposure (b) Difference spectrum between 10^3 L and 0 L exposure of H_2O. The two adsorbate-induced features, especially visible in the $\Delta n(E)$ spectrum, are assigned as the 3σ and 1π orbitals of OH_a. $h\nu = 40.8$ eV Taken from McKay and Henrich [265]

[265]. The latter species can be deliberately produced by oxygen exposure to the ion-bombarded surface. These authors base their conclusions on UPS and XPS data, and postulate that the nonlattice oxygen acts as a promoter to dissociation, which *also* requires surface defect sites, perhaps adjacent to Ni cations [265]. In short, the nonlattice oxygen facilitates the abstraction of hydrogen from H_2O, and the defect site next to the cation accommodates the resultant hydroxyl fragment. A set of UPS spectra which clearly demonstrate OH formation on the ion-bombarded, oxygen-dosed NiO(100) surface is shown in fig. 75. It is possible that such a model could also explain the great sensitivity to oxygen which TiO_2 powders exhibit in water decomposition (section 7.1.2; [24]). It may be that the oxygen is necessary to act as a promoter for the defect sites which are probably plentiful in these samples, which can then form adsorbed hydroxyl groups by reaction with water. In the second work, Benndorf and coworkers show that, at room temperature, both metallic Ni(110) *and* the heavily oxidized metal surface are completely inert to H_2O adsorption [83]. A series of thermal desorption spectra which illustrates this effect is shown in fig. 76. The desorbing H_2O here represents adsorbed hydroxyl groups which recombine [83]. It is clear that some H_2O adsorbs and decomposes when the coverage of oxygen is in a critical intermediate range, but for the more heavily oxidized sample, the surface is inactive.

These two papers illustrate rather clearly that these particular NiO surfaces do not hydroxylate at room temperature. A third report of a similar effect is given by Norton et al. [276], who grow oxide layers at 300 K and above on single-crystal surfaces. They find that a thick oxide is "converted" (examination of the data indicates that this probably means "hydroxylated") far more slowly than a thin NiO film, which is about three layers deep. Again, these results could be interpreted in terms of a higher reactivity at the surface of a thin, high-defect film than at the surface of a more bulk-like oxide.

These results may be compared to those of Andersson and Davenport [174], who prepare NiO(111) epitaxially on clean Ni(100) by exposure to oxygen at room temperature, then saturate the NiO with OH groups by exposure to water. The OH groups are stable up to 500 K; the epitaxial oxide is about 6 Å (2 layers) deep. Based upon the results of Norton et al. [276], the ease with which hydroxylation occurs is a function of the oxide film thickness; the relatively thin film of Andersson and Davenport may hydroxylate more easily than a thicker film would. The hydroxyl groups are characterized by a sharp ν(OH) at 3710 cm^{-1}, and exhibit nondipolar scattering in the EELS. The EEL spectrum of the hydroxide is shown in fig. 77.

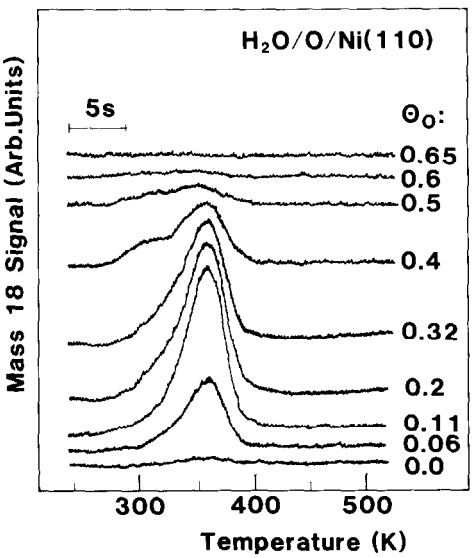

Fig. 76. Thermal desorption spectra for H_2O on clean and oxygen covered Ni(110) The oxygen coverage is determined with AES The calibration is achieved by assuming an oxygen coverage of $\theta_O = 0.5$ for the oxygen (2×1) LEED pattern The H_2O exposure is constant in each curve Taken from Benndorf et al [83]

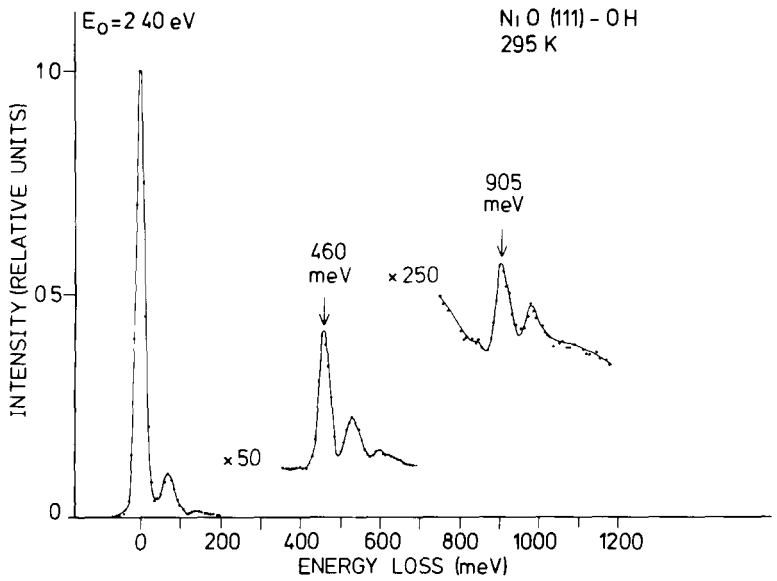

Fig 77 Electron energy loss spectrum of the NiO(111)–OH surface. The fundamental and overtone of the O–H stretch are seen at 460 meV (3710 cm^{-1}) and 905 meV (7300 cm^{-1}), respectively. Satellite features are assigned to excitation of the NiO(111) surface phonon, which also produces the intense loss at 65 meV (524 cm^{-1}). Taken from Andersson and Davenport [174].

7.1.8. Iron oxide

Adsorption of water on iron oxide surfaces is important in the oxidative corrosion and passivation of steels [12,13]. Doped iron oxides are also promising materials for electrochemical solar energy conversion cells which split H_2O (e.g. [14,15,17,277]). The electronic properties of Fe_2O_3 which make it useful in this application are summarized by Somorjai [278]. Experimental work by Dwyer and coworkers shows that oxidation of Fe(100) and Fe(110) does not proceed as efficiently with water as with oxygen, because hydroxyl groups form and serve to passivate the Fe surfaces toward oxidation by water [104,152,153]. The same observation is made by Roberts and Wood for polycrystalline Fe [209], who propose that passivation is due to formation of FeO–OH groups. On both clean and oxidized iron, Dwyer and coworkers find that water readily decomposes to form adsorbed hydroxyl groups at about 225 K [104]. Similarly, Kurtz and Henrich use UPS to show that H_2O adsorbs dissociatively on an α-Fe_2O_3 (hematite) surface at room temperature, with dissociation occurring more readily (at lower exposure) on a surface with high defect density than on an annealed surface [279]. Calculations by Debnath and Anderson support the idea that water can dissociate at oxidized iron surfaces

[86]. Hendewerk et al. [255] report that the *basal* plane of α-Fe_2O_3 is extremely inert toward water, however; water adsorbs as ice on this surface at low temperature and desorbs in the range 175 to 220 K. Only sputtered surfaces containing Fe^{2+} species can dissociatively chemisorb water, producing OH_a [255]. There is a large body of work on hematite powders, reviewed by Knözinger [23], which shows that H_2O forms a layer of hydroxyl groups on hematite surfaces, then forms hydrogen-bonded layers atop the hydroxyl groups. These results are in agreement with the single-crystal data described above.

7.1 9. Tin oxide

Studies of tin oxide (SnO_2) have been motivated by the use of this material both in gas sensing and catalytic applications. Yamazoe et al. [280] have studied water adsorption (at 13 Torr) on polycrystalline SnO_2 powders using TDS, and report desorption peaks near 375 and 675 K. Based on infrared spectroscopic work by Thornton and Harrison [281], these TDS features are attributed to the desorption of molecular water, and the recombination of hydroxyl groups, respectively. Adsorption isotherm measurements [282] also indicate that the amount of water which adsorbs per unit area on tin oxide powders depends strongly on the thermal history of the material.

The interaction of water with single-crystal tin oxide has recently been studied by Semancik and coworkers [283–286]. Their work on SnO_2(110) involves adsorption onto disordered surfaces (produced by ion bombardment) as well as on ordered (annealed) surfaces which exhibit (4×1) and (1×1) LEED periodicities; these ordered surfaces are shown by AES and XPS to be oxygen deficient [283,284]. Water adsorption at 90 K is predominantly molecular, but the presence of some dissociated water is not ruled out. Water doses in the range of 1 L at low temperature also produce TDS and UPS results that are different for the (4×1) and (1×1) structures at the SnO_2(110) surface [283], but multilayers do grow on both surfaces as the H_2O exposure is increased.

Water adsorption at 300 K has also been studied on nearly stoichiometric (110) surfaces produced by in-situ "oxidation" (heating the SnO_2 crystal at 700 K in 0.1 Torr O_2). Such surfaces show practically no H_2O chemisorption at room temperature even at doses as large as 10^8 L. Adsorption does occur at 300 K on defective (oxygen deficient) surfaces, however, and ultraviolet photoemission spectra indicate that water interacts with defect electronic states in the band gap [285]. Conductivity changes produced by H_2O adsorption on SnO_2(110) have also been measured using a UHV four-point probe, and the results are correlated to water-induced band bending effects [286]. Based on UPS results, the adsorption occurring at 300 K is thought to be dissociative, but a conclusive determination of the exact nature of the adsorbed form(s) has not been made. (Interpretation of the UPS features is

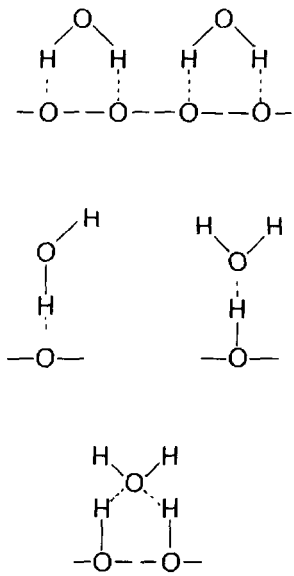

Fig 78 Various configurations possible for water molecules hydrogen-bonded to oxygen atoms and hydroxyl groups on silica surfaces Taken from Knozinger [23].

particularly difficult because such small amounts of water adsorb, i.e. the adsorbate-induced features are very small and weak.)

7.1.10. Silicon oxide

The review by Knözinger [23] deals largely with water adsorption at silica surfaces, which are normally hydroxylated. That is to say, normal atmospheric exposure results in a surface covered with Si–OH groups. Further adsorption of molecular water appears to occur via hydrogen bonding to the OH groups. Configurations such as those in fig. 78 have been proposed [23].

In agreement with these observations, vibrational spectroscopies show that water dissociates to OH_a and H_a upon adsorption at 300 K on oxidized Si single crystals, much as it does on the clean Si surface [287,288]. (See section 7.3.1).

7.2. Ionic and polar solids (non-oxidic)

In this section we briefly discuss the work which deals with water adsorption on surfaces of ionic, non-oxidic solids. Although there has been no ultrahigh-vacuum, single-crystal work to date, there is a longstanding interest in water adsorption on ionic solids due to the meteorological importance of cloud seeding. It is interesting that one of the founders of modern-day surface

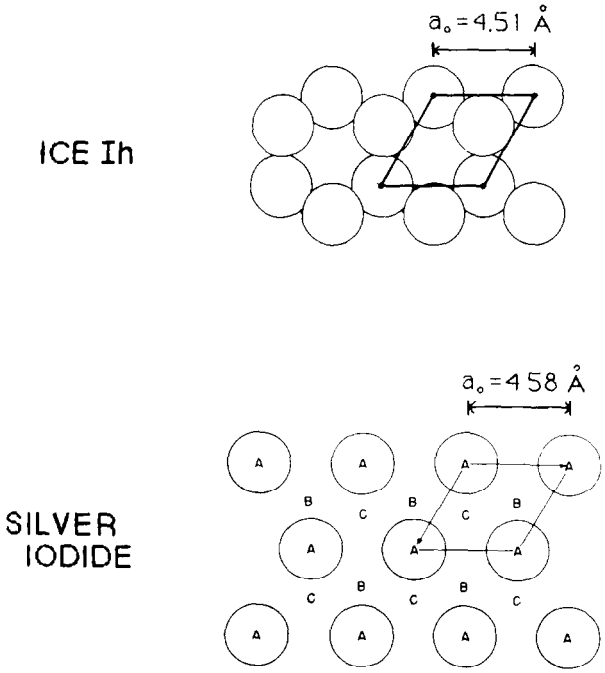

Fig 79 Comparison of the crystal structures and lattice parameters of ice Ih and a AgI surface, showing the (001) basal planes Taken from Manson [4]

science, Irving Langmuir, also played a role in the science of cloud seeding [289]. In 1946, he was the first person to observe precipitation induced artificially by dropping dry ice into supercooled clouds [4,289] and so modern weather modification began. Subsequently, Vonnegut reported that silver iodide was an efficient nucleant; AgI is still the best material known for this purpose [4], at least partly because it has common low-index planes which provide a close crystallographic match with crystalline ice [4], as illustrated in fig. 79 for the (001) plane. The lattice constant (a_0) of silver iodide is 4.58 Å, whereas the corresponding O–O separation in ice Ih is very close, 4.51 Å.

Since then, investigators have studied the relative importance of the nucleant's lattice symmetry and structural match with ice, the chemical composition of the nuclei, and the presence of defect sites at the nuclei surfaces. All three of these factors appear to be very important (e.g. [4,5,137,290]) and thorough reviews of the experimental studies are given by Mason [4] and by Pruppacher and Klett [5].

Meteorological studies of nucleation efficiency usually involve measurement of the threshold nucleation temperature in a supersaturated cloud of H_2O using aerosol samples of materials such as AgI, PbI_2, NiO, CuO, or HgTe

[4,5]. A high nucleation temperature is equated with high nucleation efficiency. It is rare that all three factors which affect nucleation efficiency can be controlled independently in these studies. Thus, although the substrate lattice structure is clearly an important factor, there is no experimental correlation between the lattice mismatch and the ice-nucleating efficiency, presumably because the other two factors (chemical composition and defect distribution) are also important. The importance of good lattice match between the substrate and ice is indicated by the fact that ice grows epitaxially on most "good" nucleants (e.g. [4]). Furthermore, Evans shows that the phase of ice

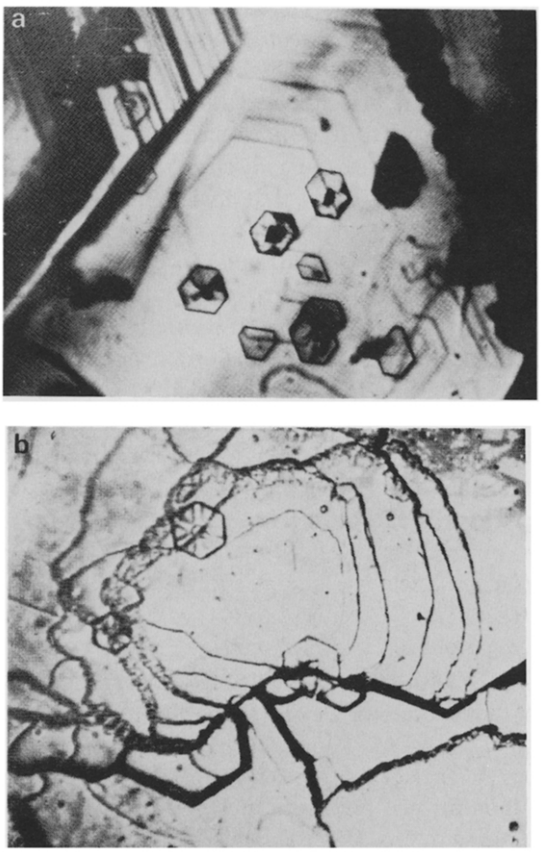

Fig 80 Illustration of ice crystals growing at nucleation crystal steps, from Mason [4] (a) Ice crystals growing on a single crystal of cadmium iodide. They form preferentially at the edges of growth steps which emanate in a spiral terrace from the cadmium-iodide surface. (b) Oriented ice crystals originating at the edges of steps deeper than 0.1 μm on the basal plane of lead iodide. No ice crystals appear on the shallow growth steps

prepared by nucleation is determined by which phase has a lattice constant closest to that of the nucleating material [290].

The importance of structural defects are demonstrated by many direct observations of an epitaxial ice layer which grows outward from microscopic steps, cracks, and cavities (refs. [4,5], and references therein.) Under these circumstances, ice grows via heterogeneous surface nucleation at the defects, as illustrated by the micrographs of fig. 80. This implies that H_2O is more strongly adsorbed, or (perhaps) more easily dissociated to OH, at structural defects. Surrounding H_2O molecules are then fixed loosely in place by hydrogen bonding. This is strikingly similar to phenomena we have described for metal and oxide surfaces (see sections 4, 5 and 7.1), where defect sites and atomically rough surfaces are generally more reactive in H_2O adsorption.

Finally, the importance of chemical composition is shown by comparisons of the ice-nucleation efficiencies of hydrophobic and hydrophilic materials. These studies show that it is better to use a material which is hydrophobic, i.e. one in which the water–substrate bond is not very strong [5]. At first glance, this seems to contradict the foregoing discussion of step activity. However, it can be understood on the grounds that hydrophilic substances form strong chemisorption bonds throughout the water layer and thereby lock the entire first layer of H_2O molecules into a particular orientation. This orientation may not be one which is favorable for hydrogen bonding to a second layer, so that formation of ice-like clusters can be prevented [5]. In other words, it is postulated that the balance between the strength of the surface bond and the strength of the hydrogen bond, first introduced in section 2.3, tips too far in the direction of the surface bond. As discussed in section 7.1, observations on oxide surfaces (under UHV conditions) actually confirm that adsorbed water can be strongly bound to specific cation sites in some cases, and hydrogen-bonded clusters can be precluded.

7.3 Semiconductors

7.3.1. Silicon

The oxidation of Si with water, so-called "wet oxidation", is a commercially useful process in semiconductor device preparation [291]:

$$2\ H_2O_g + Si \rightarrow SiO_2 + 2\ H_{2,g}.$$

The SiO_2 layers thus formed are more inert, and can be grown more rapidly, than layers prepared with $O_{2,g}$ [292]. Ghidini and Smith have characterized the conditions of H_2O pressure and substrate temperature which are necessary for oxide growth [293]. Results are comparable for both Si(111) and Si(100) surfaces, and are shown in fig. 81. They find evidence for a surface species which is present under select conditions during wet oxidation, but which is not present during oxidation with $O_{2,g}$ [293]. They postulate that this represents a

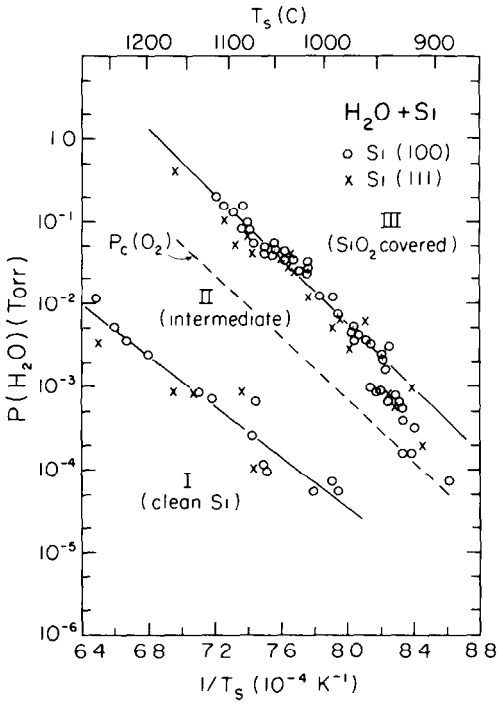

Fig. 81. The critical conditions for the growth of SiO_2 via the reaction of H_2O with Si(111) and Si(100). P_{H_2O} is the water vapor pressure, T_s is the substrate temperature. The solid lines represent boundaries of Si surface conditions obtained during oxidation with H_2O, whereas other results obtained for the $O_2 + Si$ reaction are indicated by the dashed line Region I represents conditions under which clean Si is maintained by formation and rapid desorption of SiO (etching), region III represents conditions under which SiO_2 grows; and region II represents an intermediate case. The intermediate phase is only obtained by oxidation with water, not with oxygen Identification of the surface composition is based upon measurements of surface emissivity using optical pyrometry. Taken from Ghidini and Smith [293]

mixture of adsorbed OH and H groups. Presumably, this surface layer is responsible for the unique properties of SiO_2 prepared by wet oxidation [292]. The commercial applications of the wet oxidation process have thus provided a strong impetus for basic research on the surface chemistry of water on Si, and a large amount of work has been done using Si single crystals.

Si exhibits a rich variety of surface reconstructions, which are pertinent to this discussion. The reader can find descriptions of these surfaces and their possible structures in reviews by Duke [294], Eastman [295], Kahn [296], Lieske [297] and Robinson [298]. The Si(100) face exhibits a (2×1) reconstruction which is thought to consist of paired Si dimers. The Si(111) face

exhibits (2 × 1) periodicity when prepared by cleavage in vacuum, but converts to a complex (7 × 7) reconstruction upon annealing.

The thermodynamic feasibility of water dissociation on Si can be estimated using the simple approach developed in section 3.1 for metals. The Si–O bond strength in crystalline SiO_2 is −453 kJ/mol [94], and the Si–H bond strength of chemisorbed hydrogen, reported by Schulze and Henzler, is −240 to −336 kJ/mol [299]. This approach leads to a value for ΔH_d (defined in fig. 23, p. 241) of −700 to −892 kJ/mol, much more negative than the typical chemisorption bond strength of molecular water, ΔH_m, −50 kJ/mol. Dissociation is *very* strongly favored over associative adsorption on Si surfaces, on the basis of these simple arguments.

Nonetheless, there is one central controversy which currently dominates the literature concerning the reaction of H_2O with Si surfaces: is adsorbed H_2O dissociated at room temperature or is it not? We review the evidence on both sides of the argument here in detail, which we feel is warranted by the high degree of controversy and confusion which currently prevails. This controversy has its beginnings in 1971, when Meyer first studied adsorption of water on Si(111) and Si(100) at room temperature, using ellipsometry [300]. He concluded that complete dissociation to O_a and H_a occurs under these conditions, a hypothesis which has not been supported by subsequent research. In 1975, Fujiwara and Nishijima used ELS to study the electronic transitions at 0–25 eV for H_2O on Si(111) at 300 K [301]. They interpreted their spectra to mean that water does not dissociate under these conditions. The next work was reported by Fujiwara in 1981 [302] who used ultraviolet photoemission spectroscopy and observed the three valence-band features which are shown in fig. 82 [302], for the same systems which Meyer had studied. Because these could not be explained simply as a superposition of features from atomic oxygen and atomic hydrogen, Fujiwara rejected Meyer's model, as had Fujiwara and Nishijima before him, and instead proposed that the three valence-band features correspond to the $1b_1$, $3a_1$, and $1b_2$ orbitals of the H_2O molecule. He did not, however, consider the possibility that the UPS spectrum may represent a superposition of features due to adsorbed OH, O and H

Fujiwara's interpretation subsequently came under heavy attack, mainly because vibrational spectroscopies (both IR and EELS) yield little or no evidence for molecularly adsorbed H_2O on these surfaces at room temperature [171,175–179,287,303–305]. Ciraci and Wagner predict that H_2O should be unstable with respect to dissociation on Si surfaces, based on semi-empirical calculations, and suggest a possible reinterpretation of Fujiwara's data [306], which is depicted in fig. 83. They point out that one of the three observed valence features could be due to Si–H, whereas the two more tightly bound states could represent the 1π and 3σ orbitals of Si–OH [306]. (See section 3.2.)

It is not even clear whether Fujiwara's UPS data are experimentally reproducible. In a 1983 paper, Schmeisser, Himpsel and Hollinger [307]

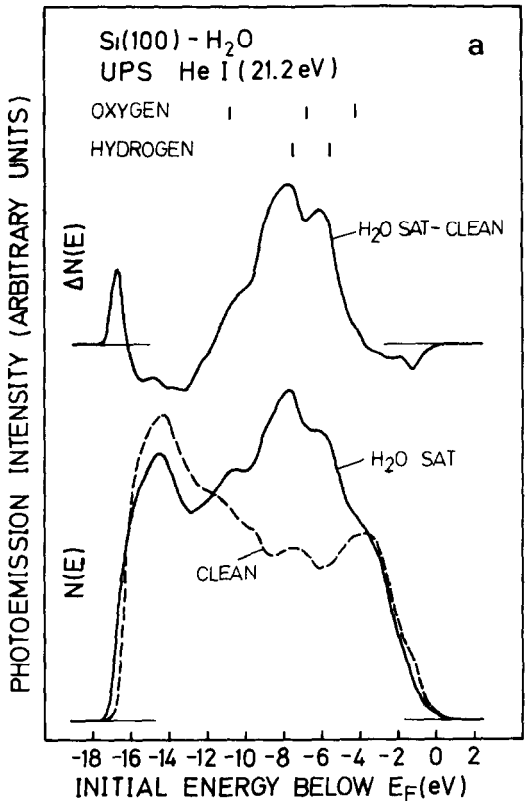

Fig. 82. (a) He I UPS spectra for clean and H_2O-saturated Si(100) surfaces and difference spectrum (H_2O-saturated minus clean surface). For comparison, energy positions of the characteristic UPS peaks for atomic hydrogen and atomic oxygen chemisorbed on the Si(100) surfaces are also indicated by vertical bars. (b) He I UPS spectra for clean and H_2O-saturated Si(111) surfaces and difference spectrum (H_2O-saturated minus clean surface) Taken from Fujiwara [301]

describe differences between positions and relative intensities of features in their spectra [for water adsorbed on Si(100) at 300 K] and Fujiwara's; in a 1984 publication, it is reported that spectra similar to Fujiwara's can be obtained on the (100) face only under conditions where surface contamination is most likely present [308]. Although Schmeisser and coworkers reach the same conclusion as Fujiwara regarding the nature of water adsorbed on Si(100) at room temperature, the data used to support this conclusion are quite different. In a 1985 paper, Schmeisser and coworkers report that the spectra of Fujiwara can be reproduced by room temperature adsorption of H_2O on the Si(111)-(7 × 7) surface [309,310]; however, they adopt the interpretation of Ciraci and Wagner [306] for this spectrum, i.e., they attribute it to Si–OH,

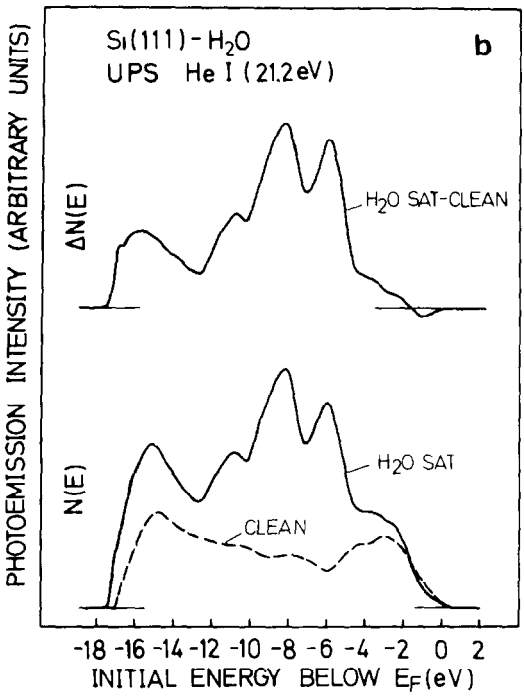

Fig 82 Continued

Si–H, and possibly Si–O species [179,303,309,310].

Since Fujiwara's report, Schmeisser and his colleagues have used UPS extensively to study H_2O on Si surfaces [303,307–310]. Their interpretation of the UPS data can be described as follows.

(1) Adsorption at room temperature on the reconstructed Si(111)-(7 × 7) and the Si(110) surfaces results in dissociation to OH_a and H_a, and also possibly O_a [179,303,309,310]. This conclusion is based upon spectra such as that shown in curve B of fig. 84 [179], which exhibit valence-band features at ~ 7 eV (with a distinct shoulder at lower binding energy) and at 11 to 11.9 eV. This interpretation agrees with results from the vibrational spectroscopies, except for the hypothesis that atomic oxygen is present already at room temperature.

(2) Adsorption at room temperature on the reconstructed Si(100)-(2 × 1) face yields molecularly adsorbed H_2O, based upon spectra such as those shown in fig. 85 [303,307–310]. Here the valence-band features at 6.2, 7.2, and 11.5 eV are assigned to the $1b_1$, $3a_1$, and $1b_2$ orbitals, of H_2O_a, respectively, the features at 6.2 and 7.2 eV are not completely resolved. This is in disagreement with data from the vibrational spectroscopies.

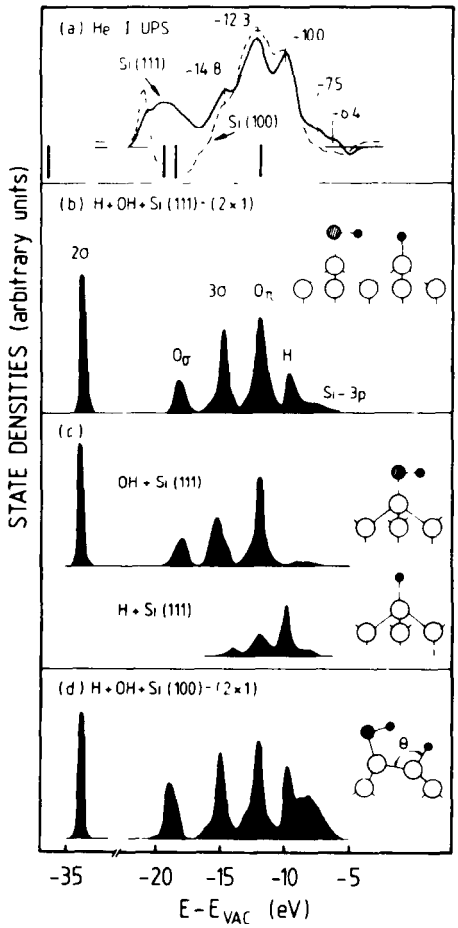

Fig. 83 (a) He I UPS difference curves of the Si(111) and Si(100) surfaces exposed to H_2O at room temperature, reproduced from refs. [301,302]. Bars at the bottom of the panel indicate the calculated states of molecularly adsorbed H_2O (b) Local density of states (LDOS) calculated for a model structure where OH and H are attached to closely lying silicons to form a (2×1) structure on the ideal (111) surface of the 12-layer slab (c) LDOS of OH, and H overlayers, each adsorbed on different surfaces of the 12-layer Si(111) slab. (d) LDOS of OH, and H on closely lying surface silicons of the 36-layer (100) slab reconstructed to form an asymmetric dimer $\theta = 109°$ Insets describe the atomic configurations for each geometry Empty, shaded, and small black circles denote Si, O, and H atoms, respectively Taken from Ciraci and Wagner [306]

(3) Adsorption of H_2O at 100 K on any low-index Si plane, i.e. (100)-(2×1), (111)-(7×7), and (110), followed by heating to room temperature yields undissociated H_2O_a [179,308–310]. The UPS spectrum obtained under these conditions is shown in fig. 84, curve B, for Si(111)-(7×7) [307]. Based upon

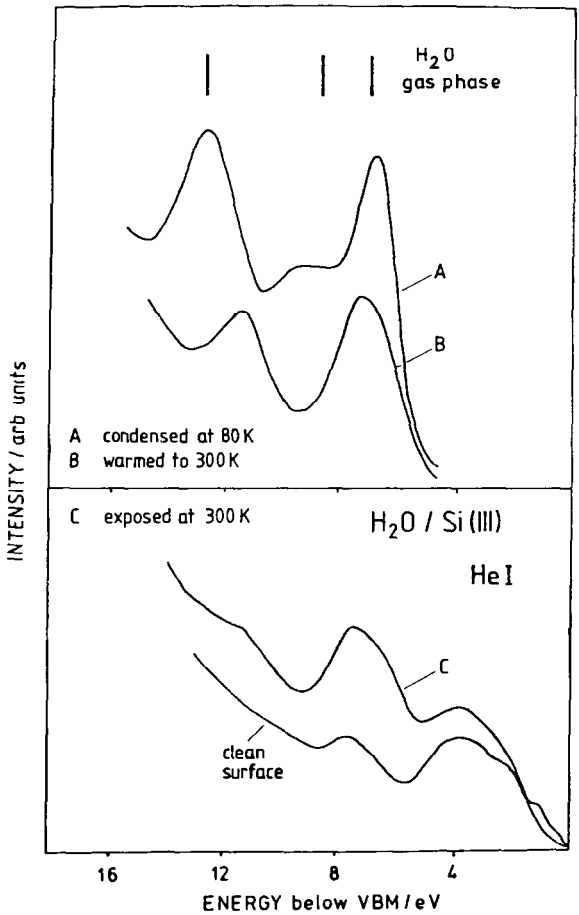

Fig 84. Photoelectron spectra of water on Si(111)-(7×7) adsorbed at 80 K (curve A), annealed to 300 K (curve B), and exposed at 300 K (curve C) Spectrum of clean surface is shown also The abscissa shows the energy below the valence band maximum (VBM) Taken from Schmeisser and Demuth [179]

this observation, Ranke, Schmeisser and Xing [309,310] propose that H_2O induces the non-(100) faces to reconstruct into (100)-facets, although this has not yet been studied with LEED or any structure-sensitive technique. The water is adsorbed molecularly at low temperature [179,308–310]. These conclusions about H_2O adsorption are also in disagreement with data from the vibrational spectroscopies.

The first vibrational work in this area is that published by Ibach, Wagner and Bruchmann in 1982 [175]. These authors use the technique of EELS, and their spectra are shown in fig. 86. They were followed shortly by Kobayashi,

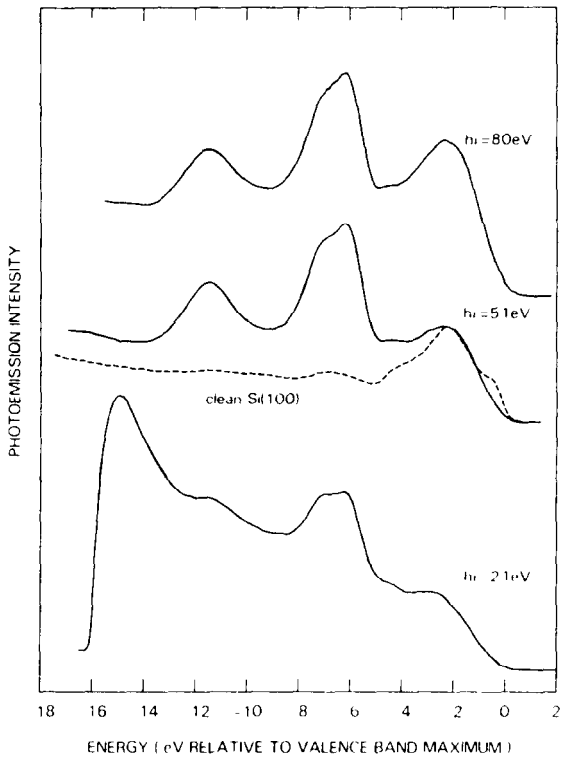

Fig. 85. Angle-integrated photoelectron spectra for saturation coverage of H_2O on Si(100)-(2×1) taken at room temperature with different photon energies The Fermi level is 0.4 eV above the valence-band maximum. The three features at 6.2, 7 2, and 11.5 eV below the valence-band maximum are assigned as the $1b_1$, $3a_1$, and $1b_2$ valence orbitals, respectively, of *molecular* H_2O. Taken from Schmeisser et al [307]

Kubota, Onchi and Nishijima in 1983 [305]. Since then, many reports have appeared, including those by Chabal and Christman using infrared [177,178,304]; Lapeyre and colleagues using EELS [171,176,288]; and Nishijima et al. who also use EELS [287]. The spectra have been consistently interpreted to support dissociative adsorption of water, i.e. formation of OH_a and H_a, on Si(100)-(2 × 1), Si(111)-(7 × 7), and Si(111)-(2 × 1) surfaces at temperatures between 80 and 400 K [171,175–178,287,304,305].

There are three main exceptions to this statement. The first is the Si(111)-(2 × 1) cleavage surface, where Schaefer et al. find evidence for a few percent of molecular water at room temperature [288]. The second is presented by Si(111)-(7 × 7) surfaces, where vibrational spectroscopies detect no dissociation at 80–100 K, but dissociation appears to take place upon heating an adsorbed layer to room temperature [175,178]. This is in contrast to both the

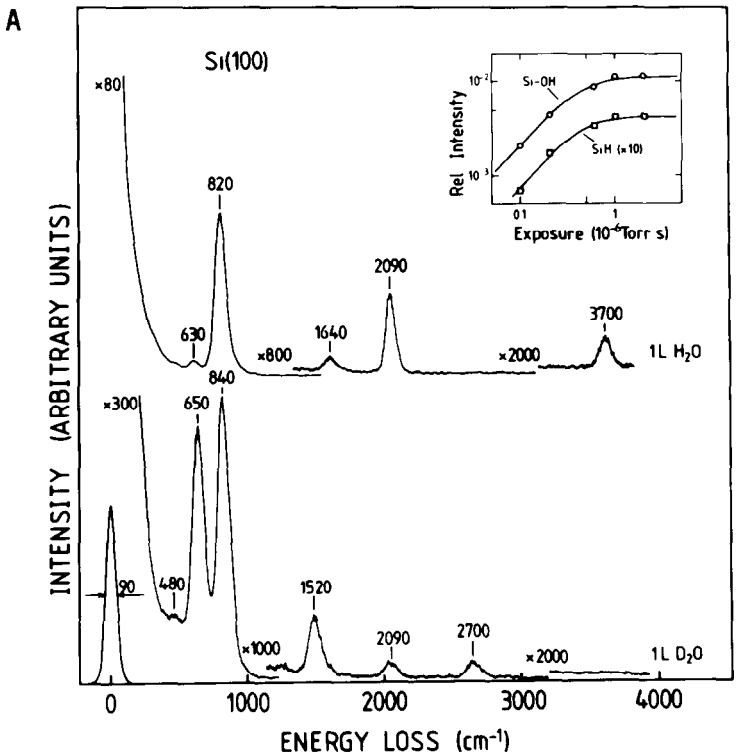
A
Si(100)
×80
820
630
×800
1640
2090
×2000
3700
1L H2O
×300
650
840
90
480
1520
×1000
2090
2700
×2000
1L D2O
INTENSITY (ARBITRARY UNITS)
0
1000
2000
3000
4000
ENERGY LOSS (cm-1)
Rel Intensity
Si-OH
SiH (×10)
Exposure (10-6 Torr s)

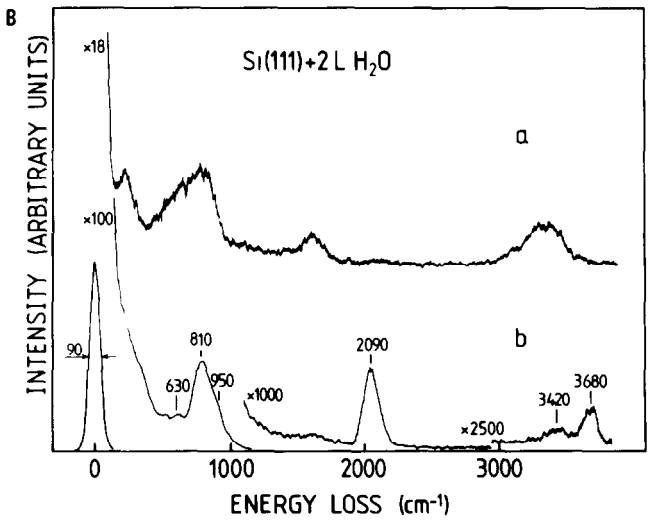
B
Si(111)+2 L H2O
×18
a
×100
90
810
630
950
×1000
2090
b
×2500
3420
3680
INTENSITY (ARBITRARY UNITS)
0
1000
2000
3000
ENERGY LOSS (cm-1)

(100)-(2 × 1) and (111)-(2 × 1) surfaces, where adsorption is dissociative already at 80–100 K and Si–OH and Si–H groups are detected in vibrational spectra [171,175,178]. This is illustrated by the infrared data of Chabal and Christman in fig. 87 [178]. The third exception is trivial: molecular water can be condensed atop the adsorbed surface layer at temperatures less than ~ 160 K [171,175,178], similar to the condensation of ice on metal surfaces described in section 4.

In addition to the vibrational spectroscopies, Rosenberg et al. [311] have studied photon-stimulated desorption of H^+. They conclude that water dissociates to H_a and OH_a following exposure to Si(111)-(7 × 7) surfaces at room temperature [311]. This supports the results from vibrational spectroscopies described above.

The main evidence for the *presence of OH_a and H_a* from vibrational data, such as that shown in figs. 86 [175] and 87 [178], can be summarized as follows:

(1) The Si–H stretch is observed at 2090–2100 cm^{-1}. Weaker transitions at 630 and 480 cm^{-1} are assigned to Si–H bending modes. As shown in fig. 88, vibrational spectroscopy can also distinguish between the monohydride and dihydride on the basis of the presence or absence of the H–Si–H scissoring mode at 915 cm^{-1} [288].

(2) A narrow peak at 3680–3700 cm^{-1} is assigned to the O–H stretch of Si–OH (2700 cm^{-1} for Si–OD).

(3) A lower-frequency mode at 810–830 cm^{-1} is due to the Si–OH stretch and/or Si–OH bend. This splits into two features at 650 and 840 cm^{-1} upon deuteration. This feature has been successfully modelled, using variable interaction force constants to couple the Si–OH stretching and Si–OH bending modes, by Black, Bopp and Wolfsberg [312].

These three features have been observed on Si(100)-(2 × 1) and Si(111)-(2 × 1)surfaces at temperatures between 80 and 400 K, and on Si(111)-(7 × 7) at room temperature [171,175–178,287,304,305].

It is important to note that there is no fundamental vibrational transition of molecular H_2O at 1900–2100 cm^{-1}. The presence of a sharp and strong

◂ Fig 86 (A) Electron energy loss spectra of 1 L H_2O and D_2O, respectively, on a Si(100) surface at 300 K The loss at 1640 cm^{-1} in the upper spectrum is interpreted as a double loss of 820 cm^{-1} and not due to molecular water The 2090 cm^{-1} loss on the D_2O exposed surface is produced through some H–D exchange or H_2O contamination The electron impact energy is 14 eV. The inset shows the intensities of the Si–H and Si–OH losses as a function of coverage (B) (a) EEL spectra of 2 L H_2O condensed on a Si(111)-(7×7) surface held at 100 K (b) the same surface after annealing briefly to 300 K. In all cases, for H_2O, the features at 3680–3700, 2090 and 810–820 cm^{-1} are assigned to the O–H stretch, Si–H stretch, and Si–OH stretch combined with the Si–OH bend, respectively, of adsorbed hydroxyl and hydrogen resulting from water dissociation The features in curve (a) of the lower frame are attributed to condensed ice Taken from Ibach et al. [175].

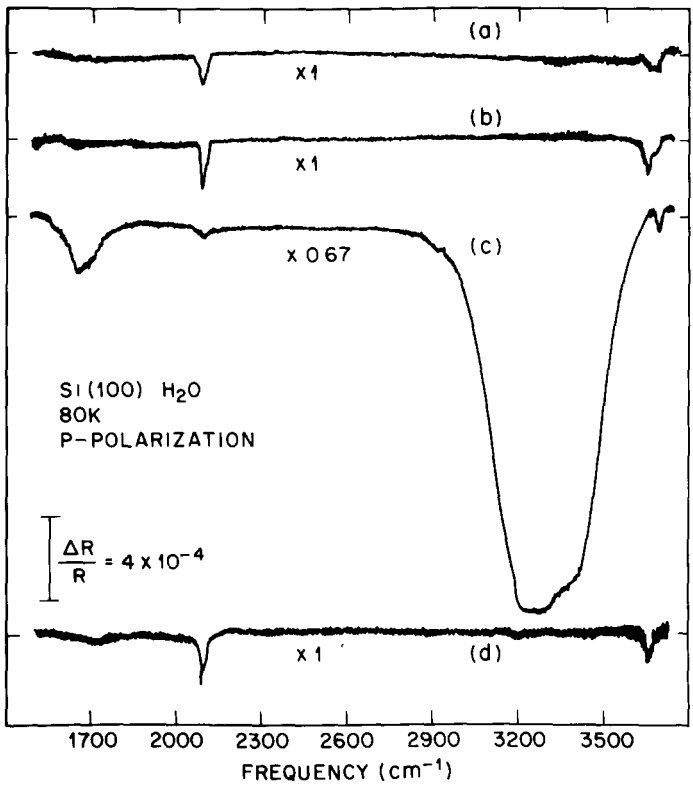

Fig. 87 Water-induced reflection-absorption infrared spectra, after water exposure to clean Si(100)-(2×1) at 80 K. The relative change in reflectance, $\Delta R/R$, is plotted as a function of infrared frequency in cm^{-1}. (a) 0.5 L with $T_s = 80$ K, (b) 0.5 L with $T_s = 80$ K and after annealing to 285 K for 1 min with no additional water exposure, (c) 10 L with $T_s = 80$ K, (d) 10 L with $T_s = 80$ K and after annealing to 280 K for 1 min. The broad, intense feature at ~ 3300 cm^{-1} in (c) is assigned to ν(OH) of condensed ice. In the three other spectra, the sharp feature at 3680 cm^{-1} is assigned to the O–H stretch of adsorbed hydroxyl, and the feature at 2100 cm^{-1} is assigned to the Si–H stretch of the monohydride Taken from Chabal and Christman [178]

feature in this frequency range, in a vibrational spectrum such as that shown in fig. 86 or 87, together with the appropriate downward frequency shift upon deuteration, is very strong evidence that Si–H groups are present on a Si surface. The other two vibrational features mentioned above are quite distinctive for OH_a groups, and are similar to vibrational transitions observed for surface metal hydroxides. The vibrational spectroscopies therefore point strongly toward the conclusion that at least some water dissociates to form OH_a and H_a on low-index Si surfaces between 80 and 400 K. The concomitant absence of the H–O–H scissors mode at 1600–1640 cm^{-1}, together with the absence of the broad O–H stretch at 3200–3400 cm^{-1} (which usually

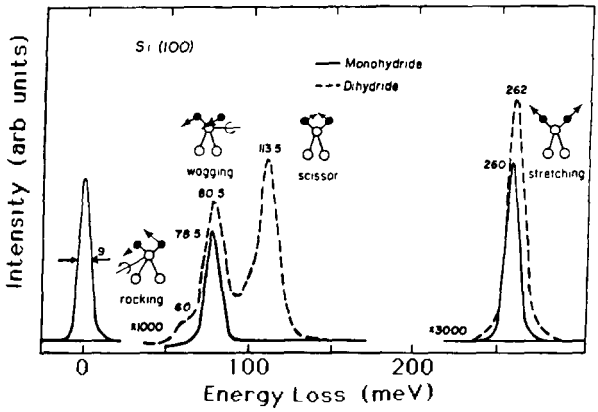

Fig 88. Electron energy loss spectra of monohydride Si(100)-2×1 H (solid line) and dihydride Si(100)-1×1. 2H (dashed line) Taken from Schaefer et al [288]

signifies hydrogen-bonded molecular water), is taken as evidence that *molecular water is absent*. However, absolute sensitivity is difficult to judge in these situations and it is therefore difficult to set an upper limit on the amount of molecular water which might be present.

EELS and IR data indicate that dissociation of water occurs when Si samples are exposed to water *at low temperature and heated to 300 K*, as well as when adsorption occurs *at 300 K* [171,175,178,179]. As far as vibrational spectra are concerned, these two methods of sample preparation yield identical end results: the surface is covered with OH and H groups. On the other hand, Schmeisser et al., have used photoemission data as a basis to argue that the former treatment yields a unique form of molecular water on the (111)-(7 × 7) and (110) surfaces, together with varying amounts of dissociation products, whereas the latter treatment results only in dissociation of water on these surfaces. In other words, they argue that these two methods of sample preparation yield much *different* end results [179,303,307–310]. As proof, they cite the differences between photoemission spectra obtained under these two conditions. An example is shown in fig. 84 for the Si(111)-(7 × 7) surface [179]. In their model, curve B represents only chemisorbed H_2O, whereas curve C represents a mixture of adsorbed H, OH, and O. Schmeisser et al. [307,308] also argue that molecular water adsorbs without dissociation, under all circumstances, on the (100)-(2 × 1) face. Vibrational data do not support the existence of molecular chemisorbed water on Si(100)-(2 × 1) between 80 and 400 K, and so are directly at odds with this conclusion as well. Table 15 summarizes the various conclusions which have been drawn from the UPS, IR and EELS studies.

Table 15
Summary of conclusions drawn from EELS, IR, and UPS studies of H_2O adsorption on Si surfaces (references are given in the text)

	$T = 80$–150 K	$T = 300$ K
Si(100)-(2×1)	Dissociation [a]	Dissociation [a]
	No dissociation [b]	No dissociation [b]
Si(110)	No dissociation [b]	Dissociation [a]
		Results depend on adsorption conditions [b]
Si(111)-(2×1)	Dissociation [a]	Mainly dissociation [a]
Si(111)-(7×7)	No dissociation [a]	Dissociation [a]
	No dissociation [b]	Results depend on adsorption conditions [b]

[a] Conclusions are drawn from EELS and IR data
[b] Conclusions are drawn from UPS data

In order to rationalize the discrepancy between photoemission and vibrational spectroscopies, Schmeisser questions the ability of vibrational spectroscopies, particularly EELS, to detect molecular water on Si surfaces, postulating that UPS has superior sensitivity in this particular case [179,308]. He suggests that nondipolar scattering for molecularly adsorbed water versus dipolar scattering for its dissociation products could lead to a large sensitivity enhancement for the dissociation products relative to molecular water [179,308] Schmeisser et al. also raise another possibility: perhaps the EELS studies are done on surfaces with much higher step densities than those used for the UPS studies, with dissociation taking place preferentially at steps rather than at terraces [307,308]. Finally, Schmeisser and Demuth suggest that the electron beam used in EELS may itself induce dissociation in the system under study [179]. Based upon data to be reviewed in the following paragraphs, however, none of these possibilities appears to be a valid reason for discarding the conclusions of the EELS and IR studies. On the other hand, Chabal and Christman [178] suggest that the three-feature UPS spectrum observed by Schmeisser could be reinterpreted to support OH_a and monohydric H_a, a possibility which seems difficult to exclude This interpretation would be similar to that proposed by Ciraci and Wagner (see fig. 83) [306]. However, Ranke and Schmeisser argue that the UPS feature which would be observed 6 eV below the Fermi edge due to H_a is too weak to account for any of the features which they observe upon water adsorption [309].

Two studies clarify the scattering mechanisms for the transitions observed with EELS after water exposure to Si surfaces [176,287]. Stucki et al. observe unusually intense first and second overtones in the O–H stretching vibration on Si(100)-(2 × 1) at 300 K [176]. They attribute this enhancement to the temporary formation of a negative OH ion which occurs when the incident electron is briefly trapped in a shape resonance in the 4σ orbital [176], similar

to the scattering mechanism for OH_a on NiO reported by Andersson and Davenport [174]. The observation of overtones allows them to calculate the O–H bond dissociation energy as 4.6 ± 0.7 eV (442 ± 67 kJ/mol) [176]. In the second study, Nishijima et al. report the way in which the vibrational loss intensities vary with emission angle and primary electron energy, on Si(111)-(7 × 7) at 300 K [287]. They find that the O–H stretch and Si–O–H bending vibrations can be partly excited by resonance scattering, mainly in the primary energy region ~ 2–7 eV [287]. Finally, the idea that dipole scattering can also, at least partly, account for the O–H stretching vibration in vibrational spectroscopies is shown by the work of Chabal and Christman [178] and Chabal [177,304]. These authors consistently observe the O–H fundamental in infrared spectra, where shape resonances are clearly excluded and only dipolar scattering can occur. Their studies deal primarily with Si(100)-(2 × 1), and the O–H stretch is clearly visible at 3660 cm^{-1}, as illustrated in fig. 87. In summary, the data indicate that both dipolar and resonance scattering mechanisms operate in the EELS transitions of Si–OH.

Chabal has also studied the role which steps play during water decomposition on Si surfaces [304]. Using polarized infrared radiation, he is able to separate vibrations of adsorbates on terraces from those at steps, using vicinal Si(100)-(2 × 1) planes at 300 K [304]. His spectra are shown in fig. 89 [304]. These spectra show the Si–H stretching vibration following water exposure. The s-polarized radiation is uniquely sensitive to hydrogen adsorbed at the steps: the p-polarized radiation is sensitive to the Si–H stretch on the (100) terraces. Very little hydrogen is adsorbed at the steps, compared with the terraces. Chabal concludes that dissociation takes place preferentially on the terrace dimers; the steps are relatively inactive [304].

Finally, it must be noted that no electron beam is used in infrared spectroscopy, and Chabal and Christman further take great pains to exclude stray electrons from their system [178]. Yet their infrared data clearly indicate that dissociation occurs on Si(100)-(2 × 1), as shown by fig. 87. This result excludes electron beam-induced dissociation as a possible explanation for all of the dissociation observed on Si(100)-(2 × 1) surfaces with EELS.

Aside from the issue of whether dissociation occurs at 80–400 K, several aspects of H_2O chemistry on Si surfaces are generally agreed upon. Adsorption of water on Si(100)-(2 × 1) and Si(111)-(7 × 7) surfaces does not affect the surface periodicity, i.e. does not remove the reconstruction [175,288]. Water adsorption at room temperature does lift the reconstruction of the Si(111)-(2 × 1) cleavage surface, however [171,288]. The initial adsorption probability of water on Si(111)-(7 × 7) at 300 K is at least two orders of magnitude lower than on Si(100)-(2 × 1), where it is about unity [175,313]. The adsorption probability on the cleaved Si(111)-(2 × 1) surface represents an intermediate case, with an adsorption probability roughly one order of magnitude lower than on Si(100)-(2 × 1) [288]. The saturation coverage of water on Si(100)-(2 ×

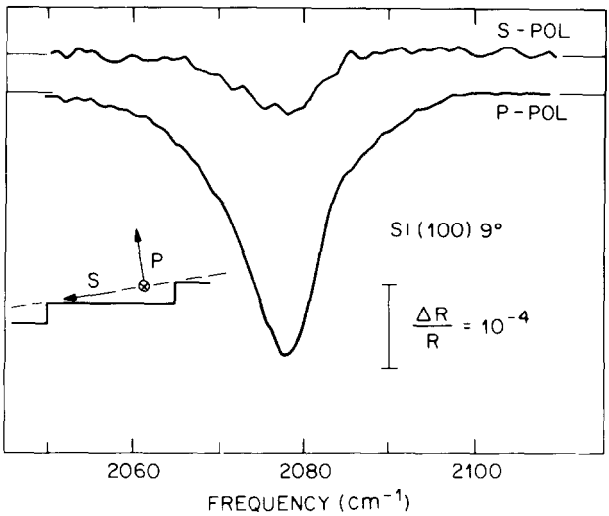

Fig 89 Water induced reflection-absorption infrared spectrum of stepped Si(100) obtained after 2 L H_2O exposure at room temperature The ordinate is the change in reflectance, ΔR, divided by the reflectance prior to absorption, R The abscissa is the frequency in cm^{-1} The experiment is configured such that s-polarized radiation almost exclusively senses vibrations of hydrogen atoms at the steps, whereas p-polarization preferentially senses vibrations of hydrogen atoms on the terraces The mode at 2078–2080 cm^{-1} is the Si–H stretch of the monohydride These data indicate that there is much less hydrogen at the steps than at the terraces Taken from Chabal [304]

1) at room temperature is 0.5 monolayers, compared with about 0.25 monolayers on the (111) plane, as illustrated in fig. 90 [175,300,314]. Saturation coverages on the other low-index planes are intermediate between these two cases [314]. The (100)-(2 × 1) surface does seem to be uniquely reactive, to the extent that "reactivity" is defined as a relatively high sticking coefficient and high saturation coverage [308,309]; conversely, the (111)-(7 × 7) surface exhibits minimum reactivity. All of these findings, taken together, suggest that the paired Si atoms which form under the (2 × 1) reconstruction are responsible for the unique adsorption properties of the (100) surface.

The saturation water coverage, $\theta = 0.5$, on Si(100)-(2 × 1) is consistent with a model such as that shown in fig. 91, where dissociation to OH_a and H_a is assumed. Half of the surface Si sites are occupied by OH groups and half by single H atoms [175,315]; every Si–Si dimer of the reconstructed (2 × 1) surface accepts the fragments from dissociation of one water molecule. Such a model is consistent with the fact that vibrational data support monohydride, but not dihydride, formation on this surface as a result of water exposure [175,177,178,288].

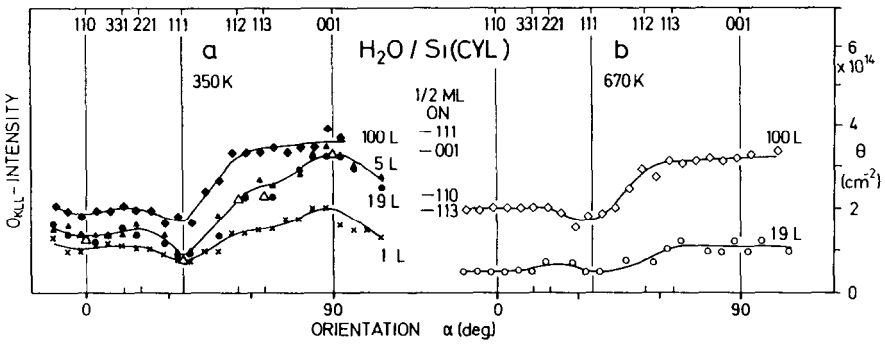

Fig. 90. Orientation dependence of the oxygen KLL Auger peak intensity after exposure of a cylindrical Si crystal to the indicated amounts of water (a) Exposure at 350 K. (b) Exposure at 670 K The intensity corresponding to $\theta = 0.5$ oxygen atoms per surface unit cell for the main orientations is indicated. Taken from Ranke and Xing [314]

It is not possible to conclude from the infrared measurements how the OH bond is geometrically oriented with respect to the axis of the Si–Si dimer bonds on the surface. Recent ESDIAD data for OH adsorbed on planar and stepped Si(100)-(2 × 1) surfaces indicate, however, that the OH bond is perpendicular to the dimer axis [316]. Fig. 92 illustrates ESDIAD perspective and contour plots for H_2O adsorbed on a planar Si(100) surface at 300 and 140 K. The only ionic desorption product is H^+, and the H^+ yield from OH is substantially higher than that from adsorbed H. There is an emission minimum in the center of the patterns, in the direction of the surface normal, so that the OH groups must be tilted or "inclined" with respect to the surface normal. The low-temperature pattern contains four peaks along [011] azimuths, which arise from two domains of Si(100) dimers, rotated by 90° from one another. The pattern also exhibits a reversible temperature dependence between 140 K and 300 K, indicating that the OH species are not rigidly fixed to the surface, but undergo large amplitude low-frequency bending vibrations [181,316].

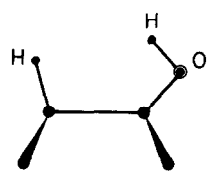

Fig. 91 Suggested arrangements monohydride with OH nearest neighbor. Note that the angles shown are associated with the effective dynamic dipole moment measured with infrared spectroscopy rather than the geometric bond. Taken from Chabal [177]

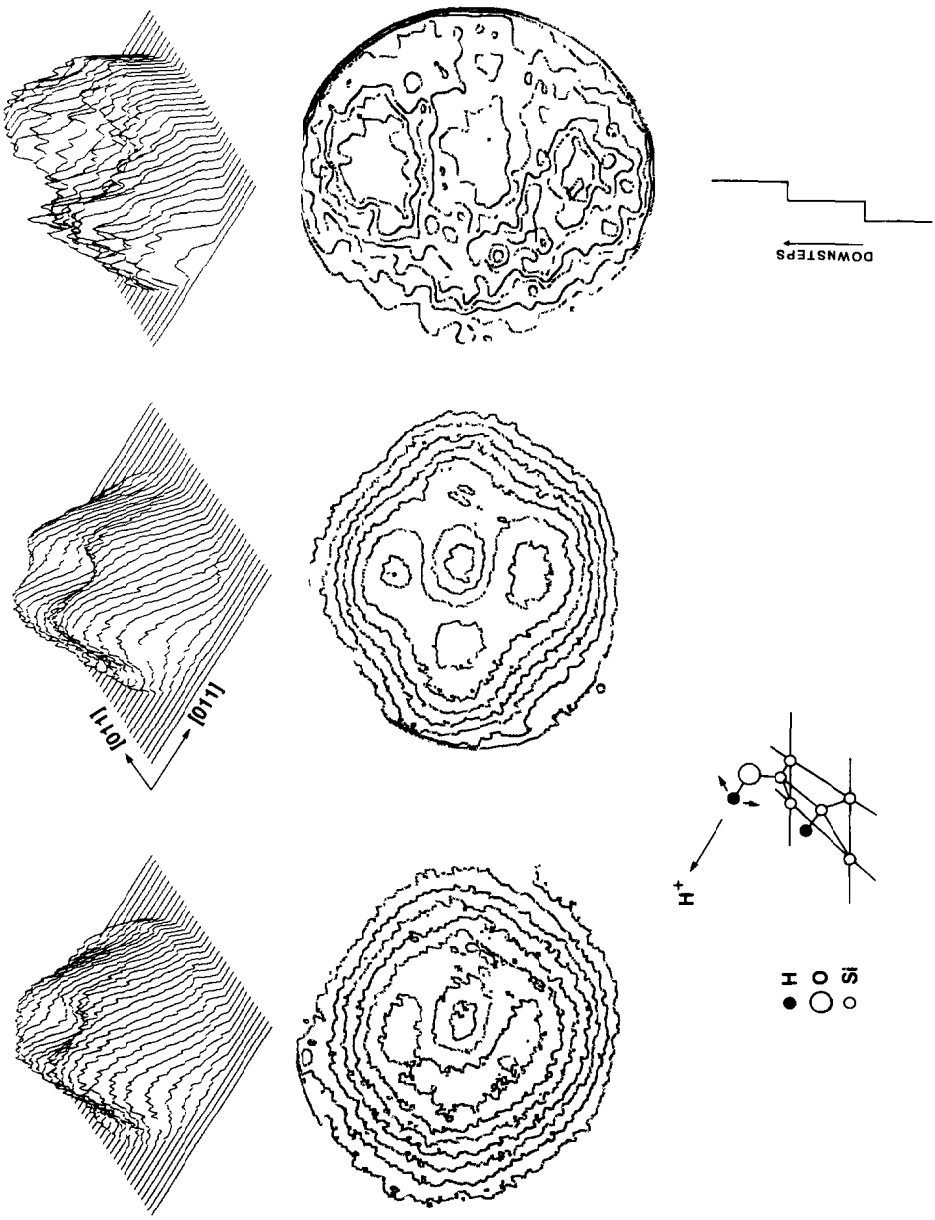

Fig. 92 H^+ ESDIAD and schematic models illustrating the bonding of OH to planar and stepped Si(100)-(2×1) surfaces (From Larsson et al [316] and Madey [181]) Column (a) Planar Si(100), H^+ ESDIAD (perspective and contour plots) for $T = 300$ K Column (b). Planar Si(100); H^+ ESDIAD for $T = 140$ K Column (c) Stepped Si(100), H^+ ESDIAD for $T = 140$ K The H^+ emission maxima are along azimuths perpendicular to the step direction, i e , perpendicular to the Si–Si dimer axis

The data of figs. 92a and 92b are ambiguous concerning the relationship between the orientation of the OH bond axis and the Si–Si dimer axis. To remove this ambiguity, experiments have been performed on a Si surface cut such that only *one* (2×1) domain is present, and dimers having the Si–Si axis parallel to the steps are predominant [316]. The ESDIAD data for OH on the stepped surface are shown in fig. 92c. The H^+ emission maxima are along azimuths perpendicular to the steps, i.e., perpendicular to the Si–Si dimer axes. Thus the OH species are believed to be stabilized by an interaction between the oxygen lone-pair electrons and the Si dangling bonds, leading to a greater population of OH bonds directed perpendicular to the dimer axis.

Based upon data from vibrational spectroscopies, dissociation of H_2O_a to O_a and 2 H_a occurs by 500 K on all Si surfaces [175,178,287].

In summary, the interaction of water with silicon single-crystal surfaces is technologically important and has been the subject of exhaustive studies over the past ten years. There is consensus that the Si(100)-(2×1) surface exhibits a uniquely high sticking coefficient for water (~ 1), and high saturation coverage, presumably because of the way the water molecule interacts with the Si–Si dimers which are present in the (2×1) reconstruction. Whether this interaction leads to dissociation at room temperature is presently the subject of some controversy, with vibrational spectroscopic data clearly in favor of dissociation to OH_a and H_a, and photoemission data interpreted to favor molecularly adsorbed H_2O. There is strong evidence that steps are *less active* toward water dissociation than are the Si(100) terraces, presumably because the special dimeric sites exist at the Si terraces. This is in contrast to metal and oxide surfaces, where steps are thought to be exceptionally reactive. There has been important work to elucidate the scattering mechanism in EELS for this system, as well as a spectroscopic determination of the O–H bond dissociation energy from overtone frequencies. Vibrational data indicate that dissociation occurs on the Si(111)-(7×7) surface at room temperature, but the barrier to dissociation is higher than on the (100) face.

7.3.2. Germanium

There is quite an extensive body of literature, published up to 1975, concerning water adsorption on Ge surfaces. This literature has been reviewed both by Meyer and Sparnaay [317], and Williams and McGovern [318]. In these earlier studies – most notably by Green and Maxwell [319], Meyer [300], Sparnaay [320], Ertl and Giovanelli [321], Henzler and coworkers [322–324] – there is general agreement that adsorption of water is dissociative. Henzler and Töpler show that adsorption requires two empty adjacent sites on Ge(111), which is very much reminiscent of the picture developed in section 7.3.1 for Si surfaces [322]. Furthermore, Henzler and Töpler show that adsorption of *each* H_2O molecule induces structural changes within the Ge substrate over an area as large as 50–80 Ge atoms [322]. More recently, there have been three

publications concerning water adsorption at Ge surfaces. Chabal and Christman use infrared spectroscopy to study the reconstructed Ge(100)-(2 × 1) surface at room temperature [178]. They report that molecular adsorption occurs at 90 K, followed by dissociation upon heating to 300 K [178]. Exposure at room temperature, however, does not lead to the appearance of a Ge–H stretching vibration in infrared, either because adsorption does not occur under these conditions (low sticking coefficient) or because adsorption occurs without dissociation. Either case contrasts with the Si(100)-(2 × 1) surface, where dissociative adsorption occurs with high probability (see section 7.3.1).

Schmeisser et al. report that water dissociates on both the Ge(100) and Ge(111) surfaces, and adsorbs in the former case with low probability [303]. They base these conclusions on UPS and EELS experiments. This result could explain why Chabal and Christman did not observe the Ge–H stretching mode develop in the infrared experiment described above.

Finally, Broughton et al. have studied H_2O adsorption on a Ge–Si (100)-(2 × 1) alloy [325]. They find that adsorption does not remove the (2 × 1) reconstruction, which is similar to the results presented in section 7.3.1 for water adsorption on Si(100)-(1 × 2). Water dissociates to OH_a and H_a at room temperature, giving an O–H stretch in the EEL spectrum at 3710 cm^{-1} and an OH bend at 790 cm^{-1}. The frequency of the first overtone of the O–H stretch indicates that the O–H bond dissociation energy of Ge–OH is 4.7 ± 1.0 eV, identical to that of Si–OH [176]. The surface is predominantly covered with Ge due to preferential surface segregation; about three times more Ge atoms than Si atoms are present. With this in mind, their conclusions are comparable to those obtained by Chabal and Christman [178] and Schaefer et al. [303] with pure Ge(100)-(2 × 1) surfaces.

7.3.3 Gallium arsenide

Gallium arsenide is currently emerging as a device material which is more desirable than Si in some applications. Its oxidation by O_2 and H_2O is therefore a subject of research. A process of particular interest (first proposed by Cho and Tracy in 1976 [326]), consists of a chemical etch followed by a rinse in de-ionized water. This is a commonly used method of preparing GaAs substrates for molecular beam epitaxy. Massies and Contour have used XPS to study the nature of the oxide which forms in a stagnant aqueous environment, and the mechanism by which an oxide is removed under running water. Their XPS data show that the oxide which forms in the former case is Ga-rich, which they take as evidence that a mixture of separate Ga and As oxides form, rather than a stoichiometric mixed oxide such as $GaAsO_4$ [327]. They postulate that arsenious acid (H_3AsO_3) and gallium hydroxide are the main species which develop under water, with H_3AsO_3 having a higher solubility than GaOH. Under running water, H_3AsO_3 dissolves freely and the solubility

of gallium hydroxide is enhanced by the continuous removal of Ga^{3+} ions from solution. Consequently, both the Ga and As are removed at about equal rates. In contrast, under static conditions, the concentration of Ga^{3+} ions in solution builds up, thereby blocking the dissolution of gallium hydroxide. Meanwhile H_3AsO_3 continues to dissolve, thereby producing arsenic-depleted layers. Massies and Contour have thus clarified the mechanism of a simple, nonthermal preparation of an oxide-free GaAs substrate which relies upon the reactions of GaAs with water [327]. The gallium hydroxide which they postulate in their model may be the same as that reported by Webb and Lichtensteiger, described below [328].

There are only three studies of water adsorption on GaAs surfaces in a vacuum environment, to our knowledge [328–330]. In the first, Büchel and Lüth [329] report UPS data which they interpret to mean that water adsorbs without dissociation at 300 K on GaAs(110), forming two phases: a chemisorbed phase and a physisorbed phase. Their work encompasses the exposure range below 10^6 L. Webb and Lichtensteiger [328], however, report that dissociation results in Ga–OH species at room temperature on polycrystalline GaAs. They base this conclusion on data from XPS, UPS, and SIMS. Their work encompasses the exposure range from 10^9 to 10^{12} L. In summary, these two reports are in disagreement about whether H_2O dissociates at 300 K on GaAs. These differences may be due to the two different exposure ranges studied, and/or due to the morphological differences between GaAs(110) and polycrystalline GaAs.

In the third study, Mokwa et al. [330] use TDS and LEED to study H_2O adsorption on GaAs(110). These authors find a main first-order desorption peak at 350 K, with a desorption energy of 67 kJ/mol, measured by variation of heating rate. They interpret this as due to molecular H_2O bound to As atoms via oxygen lone-pair orbitals [330]. The nature of a high-temperature shoulder is unknown; one possibility is that this is recombination of dissociation fragments. These data are obtained following exposures of up to 10^4 L. The sticking coefficient is 10^{-4} or less at 250 K. The LEED data are interpreted to mean that molecular H_2O removes the relaxation of the clean GaAs(110) surface [330]. These data and their interpretations are in good agreement with those of Büchel and Lüth [329].

8. Areas for future research

In this section, we briefly mention those areas which, in our opinion, present exciting opportunities for future work.

One obvious area is the study of interactions between water and coadsorbed species. This is certainly important from the perspective of electrochemistry, where the influence of the solvent (usually water) on species which undergo

reactions at the electrode surface remains largely uninvestigated. Some work has been done concerning hydration of surface halides and alkali metals, as we discuss in section 5, and the surprising discovery of hydronium ion in a UHV experiment bodes well for the ability of these simple model experiments to mimic the real chemistry which takes place at electrode surfaces [116]. However, many types of interactions other than hydration of an ionic species may also take place. For instance, it is well-known from surface science studies that formic acid adsorbs on Pt surfaces as a bidentate formate species. However, electrochemical oxidation of this molecule at a Pt electrode occurs in the presence of water, and it is conceivable that the aqueous solvent perturbs the adsorption bond of the formic acid by competing for hydrogen bonds to the formate's oxygen atoms.

Interactions between water and other molecules adsorbed on surfaces are also interesting from the point of view of catalysis, where the influence of water in heterogeneous reactions is generally not understood. Recent work has shown that water has a marked aggressiveness in displacement of cyclohexane, which would not have been predicted on the basis of chemisorption bond strengths alone [331]. Displacement of other molecules, such as lubricants, by coadsorbed water may have direct practical applications in terms of understanding adhesion and stability of these molecules at surfaces.

Another topic which begs to be addressed is this: What comparison, if any, can be made between a water layer which is formed by the processes of dynamic adsorption–desorption equilibrium and a water layer which is "frozen" in UHV? For instance, is there any chance that the small, highly-structured water clusters which we describe in such minute detail in section 4 would actually be present on a single-crystal electrode surface in solution at room temperature, or on a catalyst surface in the presence of water vapor at typically high temperatures? One approach to answering these questions is illustrated by the work of Spohr and Heinzinger, who have performed a molecular dynamics simulation of an interface between bulk water and a Pt(100) surface. These authors find that the water–platinum interaction leads to unusual structure in the first water layer [332]. An experimental approach to these questions may be provided in the future by reactive molecular beam scattering, which has not yet been applied to this area. (The water formation reaction from hydrogen and oxygen *has* been studied with molecular beam techniques, however [21].)

A related topic is that of order–disorder transitions in chemisorbed water layers, which have not yet been observed experimentally. These could be quite different from most surface phase transitions observed to date, since the interactions between water molecules are rather strong relative to other adsorbate–adsorbate interactions.

A very fundamental area which needs to be investigated in more detail is the *mechanism* of water dissociation. Can activation barriers to water dissocia-

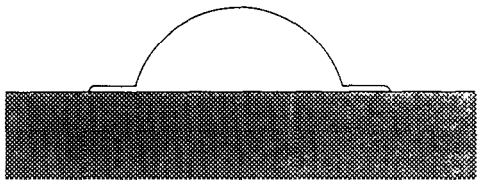

Fig 93 Schematic cross-section of a drop of liquid spreading on a solid support (not drawn to scale) Taken from ref. [334], based on deGennes [333]

tion be measured and understood? Can we isolate a precursor to dissociation? What residence times are necessary for water dissociation under conditions of dynamic adsorption–desorption equilibria? In particular, why do the critical coverages of coadsorbed species which we note in section 6 play such an important and consistent role in water dissociation? For instance, no water dissociates when the coverage of alkali metals falls below a certain critical value. On the other hand, in the presence of coadsorbed oxygen, the extent of water dissociation passes through a distinct maximum as oxygen coverage increases; this has been observed now on several metals. This idea of "critical coverages" implies that long-range interactions between alkali metal ions or between oxygen atoms are very important in water dissociation, or (alternatively) that long-range cooperation between water molecules leads to dissociation, and such cooperation is either enhanced or destroyed by the structure of coadsorbed layers. In either case, these effects will not be successfully understood on the basis of electronic structure models until rather large calculations are undertaken which include *many* adsorbed atoms/molecules.

The importance of water–surface interactions in wetting phenomena has been reviewed by deGennes [333]. A drop of water spreading on a solid surface exhibits the shape shown in fig. 93. The "precursor film", a thin lip of liquid, spreads outward from the base of the drop. This lip influences the mechanism and rate of macroscopic wetting of the solid. The lip is attributed (at least in part) to the short-range forces between water molecules and solid surfaces which we have been discussing throughout this article. The wetting process is important in technological applications such as adhesion and corrosion protection. An understanding of the molecular forces involved in the wetting may be within reach, based on the data which we have summarized in this article.

In conclusion, we feel that the area of water–surface chemistry remains filled with intriguing, unsolved problems, both on fundamental and applied levels. It is our hope that this review provides a summary of current knowledge which is useful to scientists who are working in the area or planning to do so, as well as to those who are simply curious about this fascinating scientific frontier.

Acknowledgements

We are pleased to acknowledge the considerable efforts and organizational skills of our coworkers, S. Beauvais, R. Carnazzo, T. Raife, K. Voga and T. Young, in the preparation of this manuscript. Without their patience and hard work, it could not have been published. We also thank the following persons for generously sharing information and ideas with us: H.P. Bonzel, S.T. Ceyer, Y. Chabal, A.E. DePristo, D.L. Doering, C.B. Duke, G.B. Fisher, R.S. Hansen, F.M. Hoffmann, A.L. Johnson, D.C. Johnson, R.L. Kurtz, U. Landman, C.F. Melius, J. Müller, J. Paul, K. Ruedenberg, J.K. Sass, D. Schmeisser, S. Semancik, W. Stevens, R.H. Stulen, E. Stuve, F.T. Wagner and J.T. Yates, Jr. Special thanks are due to W. Stevens and S. Semancik for drafting short portions of sections 2 and 7, respectively, and to C.B. Duke for his encouragement and constructive criticism throughout the preparation of the manuscript.

Ames Laboratory is operated for the US Department of Energy by Iowa State University under Contract No. W-7405-ENG-82. One of us (P.A.T.) gratefully acknowledges important support from an Alfred P. Sloan Research Fellowship during the preparation of this manuscript. This has also been supported in part by the Office of Basic Energy Sciences, US Department of Energy.

All figures taken from other work are reproduced with permission from at least one author.

Appendix A. Symbols, acronyms and abbreviations used in the text

ε:	Exposure
θ_x:	Coverage of species x on the surface under discussion. A coverage $\theta = 1$, one monolayer, is defined as one adsorbate particle per substrate surface atom
ν:	Vibrational frequency
ϕ.	Surface work function
L:	Langmuir, a unit of exposure: 1 L $\equiv 10^{-6}$ Torr s $\equiv 1.33 \times 10^{-4}$ N cm^{-2}
S:	Adsorption probability, also known as sticking coefficient
BFP:	Bernard–Fowler–Pauling (rules)
EEL(S):	Electron energy loss (spectroscopy)
ESDIAD:	Electron-stimulated desorption, ion-angular distribution
LEED:	Low-energy electron diffraction
TDS:	Thermal desorption spectroscopy
UHV:	Ultrahigh vacuum
UPS:	Ultraviolet photoemission spectroscopy
XPS:	X-ray photoemission spectroscopy

References

[1] As quoted by G Bailey, Nashville Banner (June 22, 1985)

[2] L da Vinci, Codex Hammer (also known as Codex Leicester, or Of the Nature, Weight and Movement of Water), as described in Leonardo da Vinci, The Marvelous Works of Nature and Man by M Kemp (Dent, London, 1981)

[3] L. Pauling, J. Am Chem. Soc. 57 (1935) 2680

[4] B J. Mason, Clouds, Rain and Rainmaking, 2nd ed. (Cambridge University Press, Cambridge, 1975),
B J Mason, The Physics of Clouds, 2nd ed (Clarendon, Oxford, 1971),
J E. Manson, Ice Nucleation and the Structure of Nuclei Crystal Faces, in Artificial Stimulation of Rain, Eds H Weickmann and W Smith (Pergamon, London, 1957) pp 360–368.

[5] H.R Pruppacher and J.D Klett, Microphysics of Clouds and Precipitation (Reidel, Dordrecht, 1978) pp 257–268

[6] P.A Shumskii, Principles of Structural Glaciology (Dover, New York, 1964)

[7] K Hutter, Theoretical Glaciology (Reidel, Dordrecht, 1983)

[8] L R Faulkner, J Chem. Ed. 60 (1983) 262

[9] J O 'M Bockris and A K N Reddy, Modern Electrochemistry, Vols 1 and 2 (Plenum/The Rosetta Edition, New York, 1970)

[10] E Gileadi, E Kirowa-Eisner and J Penciner, Interfacial Electrochemistry (Addison-Wesley, Reading, MA, 1975)

[11] B E Conway and H. Angerstein-Kozlowska, Acc Chem Res 14 (1981) 49

[12] K Bartón, Protection Against Atmospheric Corrosion Theories and Methods (Wiley, London, 1976)

[13] G Butler and H C.K Ison, Corrosion and Its Prevention in Waters (Reinhold, New York, 1966)

[14] S Sato and J.M White, Chem Phys. Letters 72 (1980) 83

[15] C Leygraf, M Hendewerk and G A Somorjai, J Catalysis 78 (1982) 341

[16] T Kawai and T Sakata, Chem Phys Letters 72 (1980) 87

[17] J.E. Turner, M. Hendewerk and G A Somorjai, Chem Phys Letters 105 (1984) 581

[18] J.A. Don and J.J.F Scholten, Faraday Disc Chem. Soc 71 (1981) 145

[19] J R. Butler, Separation Sci Technol 15 (1980) 371

[20] M Van Thiel, E D Becker and G C Pimentel, J. Chem Phys 27 (1957) 486

[21] P R Norton, The Hydrogen–Oxygen Reaction on Metal Surfaces, in The Chemical Physics of Solid Surfaces and Heterogeneous Catalysis, Vol 4, Eds D A King and D P Woodruff (Elsevier, Amsterdam, 1982) ch 2, pp 27–72

[22] A C. Zettlemoyer, F J. Micale and K Klier, Adsorption of Water on Well-Characterized Solid Surfaces, in· Water A Comprehensive Treatise, Vol. 5, Ed F Franks (Plenum, New York, 1975) ch 5

[23] H Knozinger, Hydrogen Bonds in Systems of Adsorbed Molecules, in The Hydrogen Bond, Vol 3, Eds P Schuster, G. Zundel and C Sandorfy (North-Holland, Amsterdam, 1976) ch 27, pp. 1263–1364.

[24] M L Hair, Infrared Spectroscopy in Surface Chemistry (Dekker, New York, 1967)

[25] L H. Little, Infrared Spectra of Adsorbed Species (Academic Press, New York, 1966) pp 228–295.

[26] A.V Kiselev and V I Lygin, Infrared Spectra of Surface Compounds (Wiley, New York, 1975)

[27] D. Eisenberg and W Kauzmann, The Structure and Properties of Water (Oxford University Press, New York, 1969)

[28] F A. Cotton, Chemical Application of Group Theory, 2nd ed (Wiley–Interscience, New York, 1971)

[29] V H. Smith, Jr , Phys Scripta 15 (1977) 147
[30] W Stevens, National Bureau of Standards, Gaithersburg, MD, private communication
[31] R C. Weast, Ed , Handbook of Chemistry and Physics, 53rd ed (Chemical Rubber Co , Cleveland, OH, 1972)
[32] D W. Turner, C Baker, A.D Baker and C R Brundle, Molecular Photoelectron Spectroscopy (Wiley–Interscience, London, 1970).
[33] M Dupuis, IBM Corporation, Kingston, NY, private communication
[34] W L. Jorgensen and L Salem, The Organic Chemist's Book of Orbitals (Academic Press, New York, 1973)
[35] I N Levine, Quantum Chemistry, 3rd ed (Allyn and Bacon, Boston, MA, 1983) pp 424–442
[36] B.J Rosenberg and I Shavitt, J Chem Phys 63 (1975) 2162
[37] A W Potts and W C Price, Proc. Roy Soc (London) A326 (1972) 181.
[38] S F. Boys, in Quantum Theory of Atoms, Molecules and the Solid State, Ed P O Lowdin (Academic Press, New York, 1966) p. 253,
C Edmiston and K Ruedenberg, in Quantum Theory of Atoms, Molecules and the Solid State, Ed P O. Lowdin (Academic Press, New York, 1966) p 263
[39] L Pauling, The Nature of the Chemical Bond (Cornell Univ Press, Ithaca, NY, 1948)
[40] W. von Niessen, Theoret Chim. Acta 29 (1973) 29
[41] A Novak, Struct Bonding (Berlin) 18 (1974) 177.
[42] C N.R. Rao, Theory of Hydrogen Bonding in Water, in: Water A Comprehensive Treatise, Vol 1, Ed. F Franks (Plenum, New York, 1972) ch 3, pp 93–114
[43] F Franks, The Properties of Ice, in Water A Comprehensive Treatise, Vol 1, Ed F Franks (Plenum, New York, 1972) ch. 4, pp 115–149
[44] E Whalley, The Hydrogen Bond in Ice, in The Hydrogen Bond, Vol 3 Dynamics, Thermodynamics and Special Systems, Eds P Schuster, G Zundel and C Sandorfy (North-Holland, Amsterdam, 1976) ch. 29
[45] G H F Diercksen, Theoret Chim Acta 21 (1971) 335
[46] F H. Stillinger, Science 209 (1980) 451
[47] J D Bernal and R.H Fowler, J. Chem Phys 1 (1933) 515.
[48] L Pauling, General Chemistry (Freeman, San Francisco, CA, 1970).
[49] A H Hardin and K B Harvey, Spectrochim. Acta A29 (1973) 1139
[50] M J Campbell, J Liesegang, J D Riley R.C G. Leckey, J G Jenkin and R T Poole, J. Electron Spectrosc Related Phenomena 15 (1979) 83
[51] I Abbati, L Braicovich and B DeMichelis, Solid State Commun 29 (1979) 511
[52] T Shibaguchi, H Onuki and R Onaka, J Phys. Soc Japan 42 (1977) 152
[53] R Stockbauer, E Bertel and T E Madey, unpublished results
[54] K Nakamoto, Infrared and Raman Spectra of Inorganic and Coordination Compounds (Wiley–Interscience, New York, 1970) p 226, and references therein
[55] J R Ferraro, Low-Frequency Vibrations of Inorganic and Coordination Compounds (Plenum, New York, 1971) pp 65–72
[56] S Andersson, C Nyberg and C G Tengstål, Chem Phys Letters 104 (1984) 305
[57] D Schmeisser, F J Himpsel, G Hollinger, B Reihl and K Jacobi, Phys Rev. B27 (1983) 3279.
[58] T E. Madey and J T Yates, Jr , Chem. Phys Letters 51 (1977) 77
[59] P A Thiel, R A DePaola and F.M. Hoffmann, J. Chem Phys 80 (1984) 5326
[60] P.A Thiel, F M Hoffmann and W H Weinberg, J Chem. Phys. 75 (1981) 5556.
[61] H Itoh, G Ertl and A B Kunz, Z Naturforsch 36A (1981) 347.
[62] B C Khanra, Chem. Phys Letters 84 (1981) 107
[63] A B. Anderson, Surface Sci 105 (1981) 159
[64] J Paul and A Rosén, Intern J Quantum Chem 23 (1983) 1231

[65] S. Holloway and K.H. Benneman, Surface Sci. 101 (1980) 327
[66] M.W Ribarsky, W.D. Luedtke and U. Landman, Phys. Rev B32 (1985) 1430
[67] C W. Bauschlicher, Jr , J. Chem Phys 83 (1985) 3129.
[68] S K. Saha and N.C. Debnath, Chem. Phys. Letters 121 (1985) 490
[69] J E. Muller and J. Harris, Phys Rev. Letters 53 (1984) 2493.
[70] M. Trenary, H.F. Schaefer III and P.A. Kollman, J. Chem. Phys 68 (1978) 4047.
[71] W McLean, J A Schultz, L.G. Pedersen and R.C. Jarnagin, Surface Sci. 83 (1979) 354.
[72] M A Leban and A.T. Hubbard, J. Electroanal Chem. 74 (1976) 253
[73] M R.A Blomberg, U.B Brandemark and P E.M Siegbahn, Chem. Phys Letters 126 (1986) 317.
[74] P.C Stair, J Am. Chem Soc 104 (1982) 4044.
[75] M. Barteau and R.J. Madix, in The Chemical Physics of Solid Surfaces and Heterogeneous Catalysis, Vol 4, Eds D A. King and D P. Woodruff (Elsevier, Amsterdam, 1982) p 95
[76] K G. Lloyd, B.A. Banse and J C. Hemminger, Phys Rev. B33 (1986) 2858.
[77] R H Hauge, J W Kauffman and J.L Margrave, J Am Chem Soc 102 (1980) 6005.
[78] H Kistenmacher, H. Popkie and E. Clementi, J. Chem. Phys. 61 (1974) 799.
[79] D Doering and T E. Madey, Surface Sci 123 (1982) 305.
[80] G.B. Fisher and B A. Sexton, Phys. Rev. Letters 44 (1980) 683.
[81] C Nyberg and C.G. Tengstål, J. Chem. Phys. 80 (1984) 3463;
C. Nyberg and P. Uvdal, J Chem. Phys. 84 (1986) 4631
[82] T E. Madey and F.P Netzer, Surface Sci 117 (1982) 549;
F.P Netzer and T.E. Madey, Phys Rev. Letters 47 (1981) 928.
[83] C. Benndorf, C. Nobl and T E. Madey, Surface Sci 138 (1984) 292
[84] K. Bange, T.E. Madey and J.K Sass, Surface Sci 152/153 (1985) 550
[85] I.N Levine, Physical Chemistry, 2nd ed. (McGraw-Hill, New York, 1983)
[86] N C. Debnath and A.B. Anderson, Surface Sci 128 (1983) 61
[87] A.B. Anderson and N C. Debnath, J. Am Chem. Soc 105 (1983) 18
[88] S Katsumata and D.R Lloyd, Chem Phys Letters 45 (1977) 519.
[89] J.A. Connor, M. Considine, I.H. Hillier and D Briggs, J. Electron Spectrosc Related Phenomena 12 (1977) 143.
[90] J W. Davenport and P.J Estrup, Hydrogen on Metals, in The Chemical Physics of Solid Surfaces and Heterogeneous Catalysis, Vol. 3A, Eds. D A. King and D.P Woodruff (Elsevier, Amsterdam, to be published).
[91] C.R Brundle and J.A. Broughton, The Initial Interaction of Oxygen with Well-Defined Transition Metal Surfaces, in· The Chemical Physics of Solid Surfaces and Heterogeneous Catalysis, Vol. 3A, Eds D.A. King and D.P Woodruff (Elsevier, Amsterdam, to be published)
[92] K Toyoshima and G.A Somorjai, Catalysis Rev Sci Eng 19 (1979) 105
[93] J B. Benzinger, Appl. Surface Sci 6 (1980) 105.
[94] D.D Wagman, W H. Evans, V B Parker, R H Schumm, I Halow, S.M. Bailey, K.L Churney and R.L. Nuttall, J Phys Chem Ref. Data 11, Suppl. 2 (1982)
[95] J G. Mavroides, J A Kafalas and D R. Kolesar, Appl Phys. Letters 28 (1976) 241.
[96] M.A. Pick, Phys. Rev. B24 (1981) 24
[97] D.W. Goodman, T E Madey, M Ono and J.T. Yates, Jr., J. Catalysis 50 (1977) 279.
[98] J.T Yates, Jr., P.A. Thiel and W H. Weinberg, Surface Sci 84 (1979) 427
[99] D E Ibbotson, T.S. Wittrig and W.H Weinberg, J Chem. Phys 72 (1980) 4885
[100] R Stockbauer, D M. Hanson, S.A Flodström and T E Madey, Phys. Rev B26 (1982) 1885, J Vacuum Sci. Technol 20 (1982) 562.
[101] E Bertel, D E Ramaker, R.L. Kurtz, R Stockbauer and T.E. Madey, Phys Rev. B31 (1985) 6840.
[102] J Fuggle, L.M Watson, D.J Fabian and S. Affrossman, Surface Sci 49 (1975) 61.

[103] A M. Baró and W Erley, J. Vacuum Sci. Technol. 20 (1982) 580
[104] D J. Dwyer, S R Kelemen and A. Kaldor, J. Chem Phys 76 (1982) 1832
[105] J M Heras and E V. Albano, Appl Surface Sci. 7 (1981) 332
[106] J M Heras, H Papp and W Spiess, Surface Sci 117 (1982) 590.
[107] R B Moyes and M W. Roberts, J. Catalysis 49 (1977) 216
[108] R H. Stulen and P.A. Thiel, Surface Sci 157 (1985) 99
[109] R. Suhrmann, J M Heras, L V deHeras and G Wedler, Ber Bunsenges Phys Chem 68 (1964) 990
[110] M.W Roberts, Proc Indian Nat. Sci. Acad 51 (1985) 165
[111] A.F. Carley, S. Rassias and M W. Roberts, Surface Sci 135 (1983) 35
[112] L. Ollé, M Salmerón and A M Baró, J Vacuum Sci. Technol A3 (1985) 1866
[113] C Nóbl, C Benndorf and T E Madey, Surface Sci 157 (1985) 29
[114] J.L Falconer and R.J Madix, J Catalysis 51 (1978) 47
[115] D.E. Peebles and J M White, Surface Sci 144 (1984) 512
[116] F T Wagner and T.E Moylan, Surface Sci 182 (1987) 125
[117] A Spitzer and H. Lüth, Surface Sci. 120 (1982) 376
[118] K. Bange, D E Grider, T E Madey and J K Sass, Surface Sci. 137 (1984) 38
[119] A Spitzer, A Ritz and H Luth, Surface Sci 152/153 (1985) 543.
[120] K. Bange, R Dohl, D E Grider and J K Sass, Vacuum 33 (1983) 757
[121] J K Sass, N.V Richardson, H. Neff and D K Roe, Chem. Phys Letters 73 (1980) 209
[122] C T Au, J Breza and M W. Roberts, Chem. Phys. Letters 66 (1979) 340
[123] E M. Stuve, K. Bange and J K. Sass, in Proc NATO ASI Institute on Interfacial Electrochemistry, Oporto, 1984, Ed. A Fide Silva, in press.
[124] P Sen and C N.R Rao, Surface Sci. 172 (1986) 269
[125] C T Au, M W. Roberts and A R Zhu, Surface Sci 115 (1982) L117.
[126] S J Atkinson, C R. Brundle and M W Roberts, Faraday Disc. Chem Soc 58 (1974) 62
[127] J.J Zinck and W H Weinberg, J. Vacuum Sci Technol 17 (1980) 188,
R.I. Hedge and J M White, Surface Sci 157 (1985) 17
[128] J Kiss and F Solymosi, Surface Sci 177 (1986) 191
[129] E Stuve, S N Jorgensen and R J Madix, Surface Sci 146 (1984) 179
[130] R H Stulen, in Desorption Induced by Electronic Transitions DIET II, Eds. W Brenig and D Menzel (Springer, Berlin, 1985) p 130
[131] M. Klaua and T E Madey, Surface Sci 136 (1984) L42
[132] E.M. Stuve, R.J. Madix and B A Sexton, Surface Sci. 111 (1981) 11
[133] S.T. Ceyer, to be published.
[134] M. Bowker, M A Barteau and R J Madix, Surface Sci. 92 (1980) 528
[135] M A. Barteau and R J Madix, Surface Sci 140 (1984) 108
[136] K Bange, T.E. Madey and J K Sass, Surface Sci 162 (1985) 252
[137] X Ding, E Garfunkel, G Dong, S Yang, X Hou and X Wang, J Vacuum Sci Technol A4 (1986) 1468.
[138] F M. Propst and T C. Piper J Vacuum Sci Technol 4 (1967) 53
[139] J. Jupille, P Pareja and J Fusy, Surface Sci 139 (1984) 505,
J. Fusy, G Antoine, J Jupille and A Cassuto, J Chim. Phys 78 (1981) 795
[140] P D Schulze, S L Schaffer, R L Hance and D L Utley, J Vacuum Sci Technol A1 (1983) 97
[141] J Jupille, J. Fusy and P Pareja, Surface Sci 143 (1984) L433
[142] M Alnot, B Weber, J.J Ehrhardt and A Cassuto, Appl Surface Sci 2 (1979) 578
[143] T S Wittrig, D E. Ibbotson and W H Weinberg, Surface Sci. 102 (1981) 506
[144] H. Ibach and S Lehwald, Surface Sci. 91 (1980) 187
[145] G.B. Fisher, Monolayer and Multilayer Adsorption of Water on the Pt(111) Surface, General Motors Research Publication No. GMR-4007/PCP-171 (1982)

[146] G.B. Fisher and J.L Gland, Surface Sci 94 (1980) 446
[147] B A Sexton, Surface Sci. 94 (1980) 435
[148] E Langenbach, A Spitzer and H Lüth, Surface Sci 147 (1984) 179
[149] W J Tornquist and G L Griffin, J Vacuum Sci Technol A4 (1986) 1437
[150] J R Creighton and J M White, Chem. Phys Letters 92 (1982) 435.
[151] N D Shinn, unpublished results
[152] G W. Simmons and D J Dwyer, Surface Sci. 48 (1975) 373
[153] D J. Dwyer, G W Simmons and R P Wei, Surface Sci 64 (1977) 617.
[154] D L Doering, S. Semancik and T E. Madey, Surface Sci. 133 (1983) 49
[155] P. Danielson, Res. Develop. 28 (1986) 101
[156] W.R. Wheeler, Phys. Today (August 1972) 52.
[157] L.D Talley and M C Lin, AIP Conf Proc 61 (1980) 297.
[158] G S Selwyn and M C. Lin, Langmuir 1 (1985) 212
[159] D.E Tevault, L D Talley and M C Lin, J. Chem. Phys. 72 (1980) 3314, Chem Phys Letters 66 (1979) 584
[160] J T Keiser, M A Hoffbauer and M C Lin, J Phys Chem 89 (1985) 2635
[161] A Rosen, S Ljungstrom, T Wahnström and B. Kasemo, J Electron Spectrosc Related Phenomena 39 (1986) 15.
[162] C. Benndorf and T E. Madey, Surface Sci. in press
[163] Y K. Peng and P T. Dawson, Can. J. Chem 55 (1977) 1658
[164] C T Au, S. Singh-Boparai, M W Roberts and R Joyner, J Chem Soc. Faraday Trans I, 79 (1983) 1779
[165] J M. Heras and L. Viscido, Appl. Surface Sci. 4 (1980) 238
[166] J M. Heras, L Viscido and V Amorebieta, Ber Bunsenges Phys. Chem. 82 (1978) 1035
[167] C. Benndorf, C. Nöbl, M Rüsenberg and F Thieme, Surface Sci. 111 (1981) 87
[168] H.H. Rotermund and K. Jacobi, Solid State Commun. 44 (1982) 493
[169] C. Nobl and C. Benndorf, unpublished results
[170] K. Kretzschmar, J.K. Sass, A M. Bradshaw and S. Holloway, Surface Sci. 115 (1982) 183
[171] J.A. Schaefer, J. Anderson and G.J. Lapeyre, J Vacuum Sci. Technol A3 (1985) 1443.
[172] F.J Szalkowski, J Chem. Phys. 77 (1982) 5224
[173] J.E Crowell, J.G. Chen, D.M. Hercules and J T. Yates, Jr , J. Chem. Phys. 86 (1987) 5804
[174] S. Andersson and J.W Davenport, Solid State Commun. 28 (1978) 677
[175] H. Ibach, H. Wagner and D Bruchmann, Solid State Commun 42 (1982) 457
[176] F Stucki, J Anderson, G.J Lapeyre and H H Farrell, Surface Sci 143 (1984) 84
[177] Y J Chabal, Phys. Rev B29 (1984) 3677
[178] Y J. Chabal and S.B Christman, Phys. Rev. B29 (1984) 6974.
[179] D. Schmeisser and J E Demuth, Phys. Rev. B33 (1986) 4233.
[180] T E. Madey, F P. Netzer, J.E Houston, D.M Hansen and R Stockbauer, in: Desorption Induced by Electronic Transitions, Springer Series in Chemical Physics, Vol 24, Eds N H Tolk, M.M Traum, J.C Tully and T.E Madey (Springer, Heidelberg, 1983) p 120
[181] T E Madey, Science 234 (1986) 316.
[182] R L Kurtz, N. Usuki, R. Stockbauer and T E Madey, J Electron Spectrosc Related Phenomena 35 (1985) 307
[183] K Jacobi and H.H. Rotermund, Surface Sci 133 (1983) 401.
[184] R. Gomer, Field Emission and Field Ionization (Harvard Univ Press, 1961) pp 134–135
[185] K. Bange, T E. Madey, J.K. Sass and E Stuve, Surface Sci 183 (1987) 334
[186] J R. Arthur and A.Y Cho, Surface Sci. 36 (1973) 641
[187] E. Bauer, F Bonczek, H. Poppa and G Todd, Surface Sci 53 (1975) 87.
[188] P J. Schmitz, J A. Polta, S -L. Chang and P.A Thiel, Surface Sci 186 (1987) 219.
[189] L.E. Firment and G A Somorjai, J Chem. Phys 63 (1975) 1037, Surface Sci. 84 (1979) 275
[190] K Christmann, R J Behm. G Ertl, M A Van Hove and W H Weinberg, J Chem. Phys. 70 (1979) 4168

[191] R Imbihl, R J Behm, K Christmann, G Ertl and T Matsushima, Surface Sci 117 (1982) 257
[192] E D Williams and D L Doering, J Vacuum Sci Technol A1 (1983) 1188
[193] M Polak and T E. Madey, to be published.
[194] C. Benndorf and J Weichart, unpublished data
[195] K Morokuma, J Chem Phys 55 (1971) 1236
[196] H Umeyama and K Morokuma, J Am Chem Soc 99 (1977) 1316
[197] F.T. Wagner and T.E Molan, Surface Sci , in press,
D Doering, unpublished data
[198] B.A. Sexton, J. Vacuum Sci. Technol 16 (1979) 1033.
[199] I Pockrand, Surface Sci 122 (1982) L569
[200] C G. Blatchford, M Kerker and D -S Wang, Chem Phys Letters 100 (1983) 230
[201] J E Demuth, H Ibach and S Lehwald, Phys. Rev Letters 40 (1978) 1044
[202] F M Hoffmann and T H Upton, J Phys Chem 88 (1984) 6209
[203] J R Scherer, The Vibrational Spectroscopy of Water, in Advances in Infrared and Raman Spectroscopy, Vol 5, Eds R J H Clark and R E Hester (Heyden, London, 1978) ch 3, pp 149–216
[204] M L Koszykowski, J S Binkley and C F Melius, unpublished results
[205] P F Meier, R H. Hauge and J L Margrave, J Am Chem Soc 100 (1978) 2108
[206] R.H Hauge, P F Meier and J L. Margrave, Ber Bunsenges. Phys Chem 82 (1978) 102
[207] H.R. Oswald, Helv Chim Acta 48 (1965) 600
[208] R.E Ballard, Photoelectron Spectroscopy and Molecular Orbital Theory (Wiley, New York, 1978)
[209] M.W. Roberts and R.P Wood, J Electron Spectrosc Related Phenomena 11 (1977) 431
[210] J Paul, Surface Sci 160 (1985) 599
[211] P A Thiel, J Hrbek, R.A DePaola and F M Hoffman, Chem Phys Letters 108 (1984) 25
[212] H P. Bonzel, G. Pirug and A Winkler, Surface Sci 175 (1986) 287
[213] H.P. Bonzel, G. Pirug and A Winkler, Chem Phys Letters 116 (1985) 133.
[214] G Pirug, A Winkler, M. Kiskinova and H P Bonzel, Surface Science Symposium, Obertraum, Austria, January 1985.
[215] M Kiskinova, G. Pirug and H P Bonzel, Surface Sci 150 (1985) 319
[216] J.A Schultz, M H Mintz, T R. Schuler and J W Rabelais, Surface Sci 146 (1984) 438.
[217] J Paul and F M Hoffmann, J. Phys Chem 21 (1986) 5321
[218] F P Netzer and T E Madey, Surface Sci 127 (1983) L102
[219] S B Nornes and R G. Meisenheimer, Surface Sci 88 (1979) 191
[220] G Strasser, G Rosina, E Bertel and F P Netzer, Surface Sci. 152/153 (1985) 765
[221] R. Kumar, M H. Mintz and J W Rabelais, Surface Sci. 147 (1984) 37
[222] J H deBoer, The Dynamic Character of Adsorption, 2nd ed. (Oxford, 1968) p 30
[223] D D Eley and P R. Wilkinson, Proc Roy Soc (London) A254 (1960) 327.
[224] W H Krueger and S R Pollack, Surface Sci 30 (1972) 263
[225] W H Krueger and S R Pollack, Surface Sci 30 (1972) 280
[226] M.Q Ding and E M. Williams, Surface Sci 160 (1985) 189
[227] D R Baer and M.T. Thomas, Appl Surface Sci 26 (1986) 150
[228] R.B. Comizzoli, R P Frankenthal, P C Milner and J.D Sinclair, Science 234 (1986) 340.
[229] F.P Fehlner, Low Temperature Oxidation The Role of Vitreous Oxides (Wiley, New York, 1986)
[230] R.J Madix, in The Chemical Physics of Solid Surfaces and Heterogeneous Catalysis, Vol 4, Eds D A King and D P Woodruff (Elsevier, Amsterdam, 1982) p 1
[231] J K Sass, K. Bange, R Dohl, E Piltz and R Unwin, Ber. Bunsenges Phys Chem 88 (1984) 354
[232] J Nørskov, S. Holloway and N Lang, Surface Sci 137 (1984) 65

[233] J.P Lopez, T A Albright and J.A. McCammon, Chem. Phys Letters 125 (1986) 454.
[234] A W. Castleman, Jr., Advan Colloid Interface Sci 10 (1979) 73;
A.W Castleman, Jr., P M. Holland and R G. Keesee, J Chem Phys. 68 (1978) 1760.
[235] I. Dzidić and P Kebarle, J Phys. Chem. 74 (1970) 1466.
[236] M Arshadi, R. Yamdagni and P Kebarle, J Phys Chem 74 (1970) 1475
[237] G C. Bond, Catalysis by Metals (Academic Press, London, 1962)
[238] D M Kolb and D.A Scherson, in Proc 9th Intern Vacuum Congr and 5th Intern. Conf on Solid Surfaces, ASEVA, Madrid, 1983, p. 158
[239] D.L. Rath and D.M Kolb, Surface Sci 109 (1981) 641.
[240] H Neff and R. Kotz, J. Electroanal Chem. 151 (1983) 305
[241] P.A Thiel, F.M Hoffmann and W.H. Weinberg, Phys. Rev Letters 49 (1982) 501
[242] G Blyholder and R.W Sheets, J Catalysis 39 (1975) 152
[243] J.R Creighton and J M White, Surface Sci 122 (1982) L648.
[244] J R Creighton and J M White, Surface Sci. 136 (1984) 499
[245] G B Fisher and C L. DiMaggio, Surface Sci , submitted
[246] G E. Mitchell and J M. White, Chem Phys Letters 135 (1987) 84
[247] Z Miskovic, J Vukanic and T.E. Madey, Surface Sci 169 (1986) 405; 141 (1984) 285
[248] R.C Hilborn, Z Qingshi and D O. Harris, J Mol. Spectrosc 97 (1983) 73.
[249] J Nakagawa, R.F Wormsbecher and D.O Harris, J Mol Spectrosc 97 (1983) 37.
[250] W.B. DeMore, J J. Margitan, M J Molina, R T Watson, D M Golden, R. F. Hampson, M J Kurylo, C.J Howard and A R Ravishankara, Chemical Kinetics and Photochemical Data for Use in Stratospheric Modelling, NASA Evaluation No 7, JPL Publication 85-37 (1985).
[251] H P Bonzel, J Vacuum Sci. Technol A2 (1984) 866
[252] S Semancik, D L. Doering and T.E. Madey, J Vacuum Sci Technol A3 (1985) 1571, Surface Sci. 176 (1986) 165.
[253] E.M. Stuve, R Döhl-Oelze, K Bange and J.K Sass, J. Vacuum Sci. Technol A4 (1986) 1307
[254] G Connell and J A. Dumesic, J Catalysis 92 (1985) 17
[255] M. Hendewerk, M Salmeron and G.A Somorjai, Surface Sci 172 (1986) 544
[256] J.W Ward, in Zeolite Chemistry and Catalysis, Ed J A Rabo (Am. Chem Soc., Washington, DC, 1976) p 118
[257] D G Aitken, P A Cox, R G Egdell, M.D Hill and I. Sach, Vacuum 33 (1983) 753
[258] R.L Kurtz and V E Henrich, Phys. Rev. B26 (1982) 6682
[259] P A Cox, R.G Egdell and P.D. Naylor, J Electron Spectrosc. Related Phenomena 29 (1983) 247
[260] G. Zwicker and K Jacobi, Surface Sci. 131 (1983) 179
[261] V.E. Henrich, Rept Progr. Phys 48 (1985) 1481, Progr. Surface Sci 9 (1979) 143
[262] M.L Knotek, V O Jones and V. Rehn, Phys. Rev Letters 43 (1979) 300.
[263] W.J Lo, Y.W Chung and G.A. Somorjai, Surface Sci 71 (1978) 199
[264] V E Henrich, G Dresselhaus and H J. Zeiger, Solid State Commun 24 (1977) 623.
[265] J M. McKay and V E. Henrich, Phys. Rev. B32 (1985) 6764.
[266] V.E Henrich, H J Zeiger and T B. Reed, Phys Rev B17 (1978) 4121;
V E Henrich, G. Dresselhaus and H J. Zeiger, Phys Rev. B17 (1978) 4908, J. Vacuum Sci Technol. 15 (1978) 534
[267] R G Egdell and P.D Naylor, Chem Phys. Letters 91 (1982) 200.
[268] C Webb and M. Lichtensteiger, Surface. Sci. 107 (1981) L345.
[269] S Ferrer and G A Somorjai, Surface Sci 94 (1980) 41, 97 (1980) L304
[270] F T Wagner and G A. Somorjai, J. Am Chem Soc. 102 (1980) 5494,
F.T Wagner, S. Ferrer and G A Somorjai, Surface Sci. 101 (1980) 462.
[271] M.S. Wrighton, D S Ginley, P T Wolczanski, A.B. Ellis, D.L. Morse and A. Linz, Proc. Natl. Acad. Sci USA 72 (1975) 1518.

[272] A. Fujishima and K Honda, Nature 238 (1972) 37
[273] W Hirschwald, Zinc Oxide, in Current Topics in Materials Science, Vol 7, Ed E. Kaldis (North-Holland, Amsterdam, 1981) ch 3, p. 148
[274] D B Almy, D.C Foyt and J.M. White, J Electron Spectrosc. 11 (1977) 129
[275] J.G Chen, J E Crowell and J T Yates, Jr., J. Chem. Phys 84 (1986) 5906
[276] P R Norton, R.L Tapping and J.W Goodale, Surface Sci 65 (1977) 13
[277] C Leygraf, M Hendewerk and G.A. Somorjai, J. Solid State Chem. 48 (1983) 357, J Catalysis 78 (1982) 341.
[278] G A Somorjai, Absorption of Energy in Photocatalytic Reactors, in: Photoelectrochemistry, Photocatalysis and Photoreactors, Ed M Schiavello (Reidel, Dordrecht, 1985) p 389
[279] R.L. Kurtz and V E Henrich, Phys Rev B, submitted
[280] N. Yamazoe, J Fuchigami, M Kishikawa and T Seiyama, Surface Sci 86 (1979) 335
[281] E W. Thornton and P G Harrison, J Chem Soc Faraday Trans 71 (1975) 461
[282] S Kittaka, S Kanemoto and T. Morimoto, J Chem Soc Faraday Trans. 74 (1978) 676
[283] S. Semancik and D F Cox, in Proc 2nd Intern Meeting on Chemical Sensors, Bordeaux, France, 1986, p 226.
[284] D F Cox, S Semancik and P.D Szuromi, J. Vacuum Sci Technol. A4 (1986) 627
[285] D F Cox, T.B. Fryberger, J W. Erickson and S Semancik, J Vacuum Sci. Technol , in press
[286] J W. Erickson, D F Cox, T B Fryberger and S. Semancik, to be published
[287] M Nishijima, K Edamoto, Y Kubota, S Tanaka and M. Onchi, J Chem Phys 84 (1986) 6458
[288] J A. Schaefer, F Stucki, D.J Frankel, W. Goepel and G.J Lapeyre, J Vacuum Sci Technol B2 (1984) 359
[289] C G Suits, Ed , The Collected Works of Irving Langmuir (Pergamon, New York, 1960–62)
[290] L F Evans, Nature 206 (1965) 822
[291] D.J Elliot, Integrated Circuit Fabrication Technology (McGraw-Hill, New York, 1982)
[292] E.A. Irene, J Electrochem. Soc 125 (1978) 1708
[293] G Ghidini and F W. Smith, J. Electrochem Soc 131 (1984) 2924.
[294] C B. Duke, CRC Crit Rev Solid State Mater Sci 8 (1978) 69.
[295] D.E Eastman, J Vacuum Sci. Technol 17 (1980) 492
[296] A Kahn, Surface Sci Rept 3 (1983) 193
[297] N P Lieske, J Phys. Chem Solids 45 (1984) 821
[298] A L. Robinson, Science 232 (1986) 451
[299] G. Schulze and M Henzler, in Proc. 4th Intern Conf. on Solid Surfaces, Cannes, 1980, Vol 2, p 967
[300] F Meyer, Surface Sci 27 (1971) 107
[301] K Fujiwara and M. Nishijima, Phys. Letters A55 (1975) 211.
[302] K Fujiwara, Surface Sci. 108 (1981) 124, J. Chem Phys 75 (1981) 5172
[303] D. Schmeisser, W Jaegermann and J.E. Demuth, to be published.
[304] Y.J. Chabal, J Vacuum Sci. Technol. A3 (1985) 1448
[305] H. Kobayashi, T. Kubota, M. Onchi and M Nishijima, Phys Letters A95 (1983) 345
[306] S Ciraci and H. Wagner, Phys. Rev. B27 (1983) 5180
[307] D Schmeisser, F J Himpsel and G. Hollinger, Phys Rev B27 (1983) 7813
[308] D. Schmeisser, Surface Sci 137 (1984) 197
[309] W. Ranke and D Schmeisser, Surface Sci 149 (1984) 485.
[310] W Ranke, D Schmeisser and Y R Xing, Surface Sci. 152/153 (1985) 1103
[311] R A Rosenberg, P J. Love, V Rehn, I Owen and G Thornton, J Vacuum Sci Technol A4 (1986) 1451.
[312] J.E Black, P Bopp and M Wolfsberg, Surface Sci 134 (1983) 257
[313] M. Nishijima, K Fujiwara and T Murotani, J. Appl Phys 46 (1975) 3089
[314] W Ranke and Y R Xing, Surface Sci 157 (1985) 339.

[315] C W Kern and M Karplus, in Water: A Comprehensive Treatise, Vol. 1, Ed F Franks (Plenum, New York, 1972) ch. 2, pp 21–92
[316] C.U S Larsson, A L Johnson, A. Flodström and T E Madey, J. Vacuum Sci. Technol., in press
[317] F Meyer and M J. Sparnaay, The Chemical and Physical Properties of Clean Germanium and Silicon Surfaces, in: Surface Physics of Phosphors and Semiconductors, Eds C.G. Scott and C.E Reed (Academic Press, London, 1975) ch 6, p. 321.
[318] R H. Williams and I T. McGovern, Adsorption on Semiconductors, in The Chemical Physics of Solid Surfaces and Heterogeneous Catalysis, Vol. 3, Eds D.A. King and D.P. Woodruff (Elsevier, Amsterdam, 1984) ch 6, p 267
[319] M Green and K H Maxwell, J Phys Chem Solids 11 (1959) 195
[320] M.J Sparnaay, Ann NY Acad Sci 101 (1963) 473
[321] G Ertl and T. Giovanelli, Ber Bunsenges Phys Chem 72 (1968) 74
[322] M Henzler and J Töpler, Surface Sci 40 (1973) 388
[323] J. Töpler and M Henzler, Surface Sci 41 (1974) 377
[324] S. Sinharoy and M Henzler, Surface Sci 51 (1975) 75
[325] J.Q Broughton, J A Schaefer, J.C Bean and H H. Farrell, Phys. Rev. B33 (1986) 6841
[326] A Y Cho and J C Tracy, Jr , US Patent No 3,969,164 (1976)
[327] J Massies and J P Contour, Appl Phys Letters 46 (1985) 1150
[328] C. Webb and M Lichtensteiger, J Vacuum Sci. Technol 21 (1982) 659
[329] M Buchel and H Luth, Surface Sci. 87 (1979) 285
[330] W Mokwa, O Kohl and G Heiland, Surface Sci 139 (1984) 98
[331] J.A Polta, D K Flynn and P A Thiel, J. Catalysis 99 (1986) 88.
[332] E. Spohr and K. Heinzinger, Chem. Phys Letters 123 (1986) 218
[333] P.G. deGennes, Rev Mod. Phys 57 (1985) 827
[334] Committee on Science, Engineering and Public Policy, National Academy of Sciences Research Briefings 1986 (National Academy Press, Washington, DC, 1986). © 1986 by the National Academy of Sciences